ROBUST CONDITION MONITORING AND FAULT DIAGNOSIS OF VARIABLE SPEED INDUCTION MOTOR DRIVES

A Dissertation

by

SEUNGDEOG CHOI

Submitted to the Office of Graduate Studies of
Texas A&M University
in partial fulfillment of the requirements for the degree of

DOCTOR OF PHILOSOPHY

December 2010

Major Subject: Electrical Engineering

ROBUST CONDITION MONITORING AND FAULT DIAGNOSIS OF VARIABLE SPEED INDUCTION MOTOR DRIVES

A Dissertation

by

SEUNGDEOG CHOI

Submitted to the Office of Graduate Studies of
Texas A&M University
in partial fulfillment of the requirements for the degree of

DOCTOR OF PHILOSOPHY

Approved by:

Chair of Committee,	Hamid A. Toliyat
Committee Members,	Shankar P. Bhattacharyya
	Prasad Enjeti
	Won-Jong Kim
Head of Department,	Costas N. Georghiades

December 2010

Major Subject: Electrical Engineering

ABSTRACT

Robust Condition Monitoring and Fault Diagnosis of Variable Speed

Induction Motor Drives.

(December 2010)

Seungdeog Choi, B.S. Chung-Ang University;

M.S., Seoul National University

Chair of Advisory Committee: Dr. Hamid A. Toliyat

The main types of faults studied in the literature are commonly categorized as electrical faults and mechanical faults. In addition to well known faults, the performance of a diagnostic algorithm and its operational reliability in harsh environments has been another concern.

In this work, the reliability of an electric motor diagnosis signal processing algorithm itself is studied in detail under harsh industrial conditions. Reliability and robustness of the diagnosis has especially been investigated under 1) potential motor feedback error; 2) noise interference to a diagnosis-relevant system; 3) ease of implementation; and 4) universal application of diagnostic scheme in industry. Low cost and flexible implementation strategies are also presented.

1) Signature-based diagnosis has been performed utilizing the speed feedback information which is used to determine fault characteristic frequency. Therefore, feedback information is required to maintain high accuracy for precise diagnosis which,

in fact, is not the case in a practical industrial environment due to industrial noise interferences. In this dissertation, the performance under feedback error is analyzed in detail and error compensation algorithms are proposed.

2) Fault signatures are commonly small where the amplitude is continuously being interfered with motor noise. Even though a decision is based on the signature, the detection error will not be negligible if the signature amplitude is within or close to the noise floor because the boundary noise level non-linearly varies and, hence, is quite ambiguous. In this dissertation, the effect of noise interference is analyzed in detail and a threshold design strategy is presented to discriminate potential noise content in diagnosis.

3) The compensating procedure of speed feedback errors and electrical machine current noise, characteristics which are basically non-stationary random variables, requires an exhaustive tracking effort. In this dissertation, the effective diagnosis implementation strategy is precisely presented for digital signal processor (DSP) system application.

4) Most of the diagnosis algorithms in the literature are developed assuming specific detection conditions which makes application difficult for universal diagnosis purposes. In this dissertation, by assuming a sinusoidal fault signal and its Gaussian noise contents, a general diagnosis algorithm is derived which can be applied to any diagnostic scheme as a basic tool.

DEDICATION

To my parents, my wife and my daughters (Yaerim and Enyoung)

ACKNOWLEDGEMENTS

I would like to express my sincere appreciation to Prof. Hamid A. Toliyat. His unlimited patience, constant understanding and support motivated the completion of this thesis. I was truly fortunate to have his valuable guidance throughout my research.

I also would like to thank Prof. Prasad Enjeti, Dr. Shankar P. Bhattacharyya, and Dr. Won-Jong Kim for serving on my graduate committee.

Thanks also to the members of the Advanced Electric Machines and Power Electronics Laboratory (EMPE), Robert Vartanian, Nicolas Frank, Mahshid Amirabadi, Anil Chakali, Anand Balakrishnan, Abdulkadir Bostanci, Steven Campbell, Yateendra Deshpande, Babak Farhangi, Behrooz Nikbakhtian, Siavash Pakdelian, Esra Ozkentli, Vivek M. Sundaram, Dr. Salman Talebi, Dr. Jaehoon Beak, and Dr. Salih Baris Ozturk for their sincere friendship.

I would like to express my gratitude to my research partners, Dr. Akin Bilal, Mina M. Rahimian, and M. Azadpour. Our interesting discussions throughout my study have been truly valuable.

My sincere thanks to Prof. Hoseung Kim, Prof. Tae-Kyung Chung, and Prof. Jaehong Lee for their guidance when I started my study in the USA. I would also like to express my appreciation to Toshiba International Co. for their continuous interest in my research.

Finally, I would like to express my deepest gratitude to my wife, daughters, and parents for their endless love, support, and sacrifice.

TABLE OF CONTENTS

CHAPTER Page

CHAPTER Page

LIST OF FIGURES

FIGURE Page

FIGURE Page

FIGURE Page

LIST OF TABLES

CHAPTER I

INTRODUCTION AND GENERAL DIAGNOSIS*

1.1 Introduction

With the increased demand for sophisticated controls for electric motors in industry, reliability and predictability of motor operations is now a major requirement in many applications. Reliability of a motor operation is especially important where an unexpected shut-down might result in the interruption of critical services such as medical, transportation or military operations where failure potentially could lead to costly maintenance or loss of life.

Those electrical motor faults that potentially lead to the shut down of a system can be classified in two parts (electrical and mechanical) as follows [1][2][3][4]:

This dissertation follows the style of *IEEE Transactions on Industrial Electronics*.

* Reprinted, with permission, from

1. "A robust sensorless fault diagnosis algorithm for low cost motor drive," *In Applied Power Electronics Conference and Exposition (APEC'10)*, by S. Choi, B. Akin, M. Rahimian, H.A. Toliyat, pp. 1190-1994, Copyright 2009 by IEEE.
2. "Fault diagnosis technique of induction machines with ordered harmonic and noise cancellation," *In Industrial Electrical Machine and Drive (IEMDC'09)*, pp. 1333-1339, by S. Choi, B. Akin, M. Rahimian, H.A. Toliyat, and M. Rayner, Copyright 2009 by IEEE.
3. "A generalized condition monitoring method for multi-phase induction motors," *In Industrial Electrical Machine and Drive (IEMDC'09)*, pp. 556-562, by S. Choi, B. Akin, M. Rahimian, H.A. Toliyat, and M. Azadpour, Copyright 2009 by IEEE.
4. "Fault diagnosis implementation of induction machine based on advanced digital signal processing techniques," *In Applied Power Electronics Conference and Exposition (APEC'09)*, pp.957-963, by S. Choi, B. Akin, M. Rahimian, H.A. Toliyat, Copyright 2009 by IEEE.
5. "Implementation of a fault diagnosis algorithm based on advanced digital signal processing techniques," *IEEE Transactions on Industrial Electronics,* by S. Choi, B. Akin, M. Rahimian, and H.A. Toliyat, Copyright 2010 by IEEE.

- Electrical faults

    a) Open or shorts in motor windings (mainly due to insulation failure)

    b) Wrong connection of windings

    c) High resistance contact to conductor

- Mechanical faults

    a) Broken rotor bars

    b) Cracked end-rings

    c) Bent shaft

    d) Bearing failure

    e) Gearbox failure

    f) Air gap irregularity

These fault conditions create specific symptoms during a motor operation which can be described as follows:

a) Motor vibration

b) Temperature increase

c) Irregular air gap torque

d) Instantaneous power variation

e) Audible noise

f) Stator voltage changes

g) Stator current changes

h) Speed variations

Based on monitoring and analyzing these symptoms, a motor fault diagnosis technique might be performed through the following strategies:

- Single symptom analysis
    a) Motor vibration analysis
    b) Temperature measurement
    c) Acoustic noise analysis
    d) Electromagnetic field monitoring through inserted coil
    e) Chemical analysis
    f) Infrared analysis
    g) RF emission monitoring
    h) Partial discharge measurement
    i) Motor current signature analysis (MCSA)
        - FFT analysis
        - Wavelet analysis
        - Complex Park vector analysis
- Multi-symptom analysis
    a) Neural network
    b) Fuggy logic analysis
    c) Statistical analysis of relevant information
- Simulations
    a) Finite element analysis (FEA)
    b) Time step coupled finite element-state space (TSCFE-SS)

1.2 Fault diagnosis of a motor

This section briefly summarizes motor fault conditions and their cause. The considered fault conditions are eccentricity related faults, broken rotor bar faults, bearing faults and stator faults which account for more than 90 % of overall induction motor failures [1][2][3].

A. Eccentricity Faults

The eccentricity fault arises when there is a non-uniform air-gap between rotor and stator [1][2][3][5][6][7][8]. It is usually caused by inaccurate mounting of the rotor with respected to the stator or various other motor defects that result in an unbalance position of a rotor such as bearing wear, rotor shaft deflection, etc. There are two types of eccentricity faults - static eccentricity and dynamic eccentricity. Static eccentricity is shown in Fig. 1.1 where the non-uniform air gap does not vary in time.

The dynamic eccentricity is briefly depicted in Fig. 1.2 and the air gap length changes as the rotor rotates dynamically. Commonly, the two eccentricity types occur si-

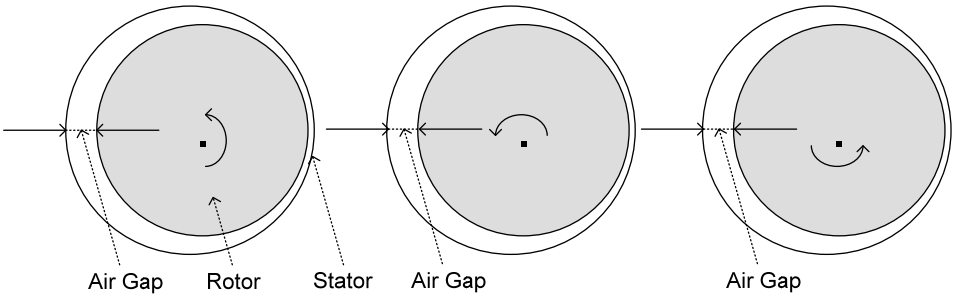

Fig. 1.1. Static eccentricity.

-multaneously in a faulty motor and exist in almost any motor where their severity usually is allowed up to 10% eccentricity. The severe eccentricity fault in a motor induces serious magnetic push force and potentially creates rubs between rotor and stator which eventually results in an unexpected shut-down of the machine [1][3].

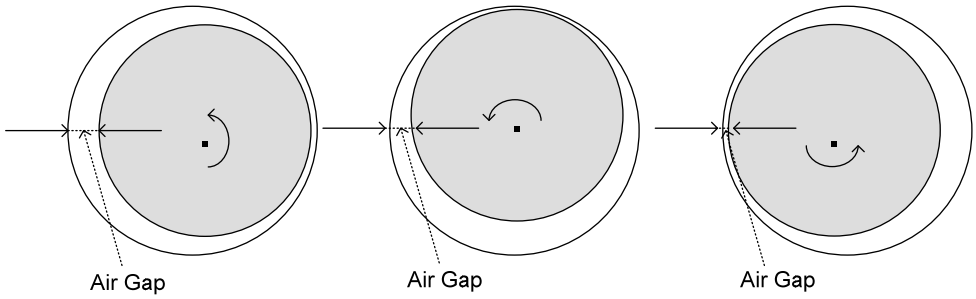

Fig. 1.2. Dynamic eccentricity.

B. Broken Rotor Bar Faults

The broken rotor bar fault condition is shown in Fig. 1.3 which accounts for more than 5% of all the electrical motor failures in industry. A broken rotor bar occurs when a continuous stress is applied to the rotor resulting in increased resistance or breakage of the rotor bar conductor [1][3][9][10][11][12][13]. Those stresses are categorized as magnetic stress (magnetic force), mechanical stress (lamination defect, fatigue parts, etc), thermal stress (thermal overload, cooling system failure), and the residual stress from manufacturing. Commonly, there exists a small broken rotor bar fault symptom in any motor due to inherent resistance difference between rotor bars from manufacturing. Unlike many experimental prototypes in the literature, the broken rotor bar fault

commonly starts inside the bar material which is not visually observable until it becomes severe. An incipient broken rotor bar condition aggravates itself almost exponentially in time as excessive current flow is expected to be concentrated on adjacent bars instead of the broken one which provides propagated electrical stress to adjacent areas.

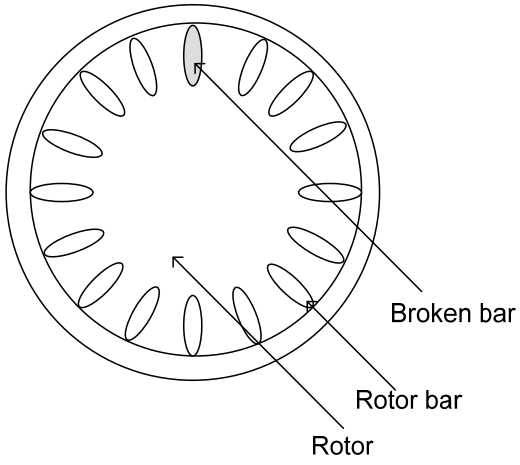

Fig. 1.3. Broken rotor bar.

C. Bearing Faults

Bearing fault accounts for more than 40% of all electrical motor failures [9][13][14] [15][16]. Bearing faults are commonly categorized as outer bearing race defect, inner race defect, ball defect, and train defect. Recently, general roughness has been extensively investigated in the literature as one kind of fault [14]. Bearing faults are caused by iron fatigue due to over life time operation, motor vibrations with non-uniform force on the balls, rotor eccentricity, load unbalance, contamination, corrosion from water or chemicals, improper lubrication, bearing current or residual stress left

from the manufacturing process. As most electrical motors use the ball or rolling elements to cause rotation while supporting the load variation, excessive rotor speed and over load are also the cause of bearing faults. Bearing fault leads to increased motor vibration and acoustic noise during machine operation which at some level results in unexpected system failures.

D. Stator Faults

Stator faults account for 30%-40% of all electrical motor failures [2][17][18]. The stator fault can be broadly classified as the lamination or frame fault (core defect, circulation current, or ground earth, etc.) and the stator winding fault (insulation damage, displacement of conductors, etc.). There are numerous factors that lead to the stator fault such as excessive thermal stress (high winding temperatures and cooling system defects), electrical stress (electrical discharge, short circuits, high resistance contacts), mechanical stress (coil movement or rub between stator and rotor), chemical stress (oil contamination, moisture, and dirt) which are usually related to insulation failure. Due to the destructive nature of electrical fault that occurs in a short time with a large current and, hence, high temperature, these faults are commonly required to be detected during a short diagnosis.

E. Diagnosis Based on Fault Signature

Induction motor design and its operation are fundamentally based on the electro-magnetic coupling between the rotor and the stator. The machine design is commonly intended to have electrical and mechanical symmetry in the rotor and the stator for better

coupling and higher efficiency of motor operation. Fault condition described earlier is expected to damage the symmetrical property where fault dependent motor operation induces an abnormal harmonic modulation in the motor current signal due to its inherent electro-magnetic coupling.

The broken rotor bar and the eccentricity fault result in amplitude modulation in the current signal at characteristic frequencies shown in Fig. 1.4. The broken rotor bar signature is observable two times slip frequency away from fundamental frequency and

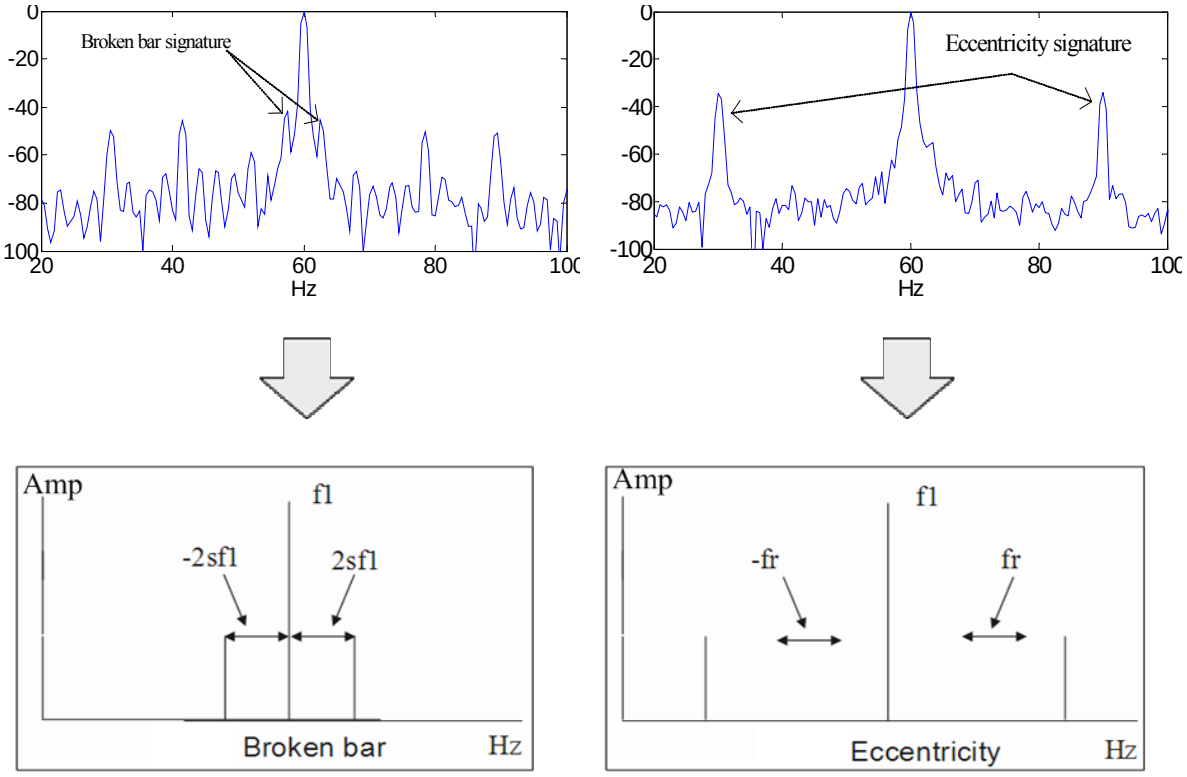

(a) (b)

Fig. 1.4. Harmonic signatures caused by fault conditions: (a) broken rotor bar and (b) eccentricity (s: slip frequency, f1: excitation frequency, and fr: rotor rotating speed).

the eccentricity signature is observable about rotor frequency away from the fundamental frequency. This line current signal harmonic analysis under fault condition has been actively researched and generalized in the literature.

The equation that describes eccentricity characteristic frequency is as follows [1] [19]:

$$f_{eccentricity} = f\left[(mR \pm n_d)\left(\frac{(1-s)}{p}\right) \pm v\right],\ m = 1,2,3,\cdots \tag{1.1}$$

where f is the fundamental frequency, R is the number of rotor slots, $n_d = 1,2,3\cdots$ (n_d=0 in static eccentricity), s is the slip frequency, p is the number of pole pairs, v is the order of harmonics in the power supply.

When static and dynamic eccentricities exist simultaneously, the fault equation can be described as follows:

$$f_{eccentricity} = f \pm f_r,\ m = 1,2,3,\cdots \tag{1.2}$$

The equation that describes broken rotor bar characteristic frequency is as follow:

$$f_{borken\_bar} = ((1-s)\frac{k}{p} \pm s)\, f, k = 1,2,3,\cdots \tag{1.3}$$

The equation that describes bearing fault frequency is given by [66]:

$$f_{brg} = \left| f \pm k f_v \right| \tag{1.4}$$

where

$f_v = (N_b / 2) f_r \left[1 - b_d \cos(\beta) / d_p\right]$ for outer race defect,

$f_v = (N_b / 2) f_r \left[1 + b_d \cos(\beta) / d_p\right]$ for inner race defect,

$$f_v = N_b f_r / b_d \left[1 - \left(b_d \cos(\beta) / d_p \right)^2 \right] \text{ for ball defect,}$$

N_b is the number of balls, b_d is the ball diameter, d_p is the pitch, and β is the contact angle of the ball with race.

Not only with the fault conditions described above, but also most other faults such as bolt loosening and oil whip result in specific frequency signatures in a motor current spectrum [4]. By analyzing the characteristic frequencies where fault signatures are expected in a motor current signal, efficient diagnosis techniques have been suggested and implemented in industry.

1.3 Recent implementation challenges of motor diagnosis on a DSP

In modern industry, as shown in Fig. 1.5, there is increased convergence between energy system and modern network system. The electrical motors in a car, ship, aircraft, building, road, or in power system can be assumed to be mostly connected to committed sensor or wired/wireless sensor network. Those sensed signal such as vibration, current, voltage, speed, etc are forwarded to close or remote microcontroller or digital processor which the controller can performs individual system control, whole system management, or health monitoring.

Many studies have been conducted within the last decade to detect electric machine faults prior to possible catastrophic failure [1][2][19][20][21][22][23][24]. One of the most popular methods for fault diagnosis is motor line current signature analysis (MCSA). Because MCSA techniques usually utilize the parameters and signals obtained

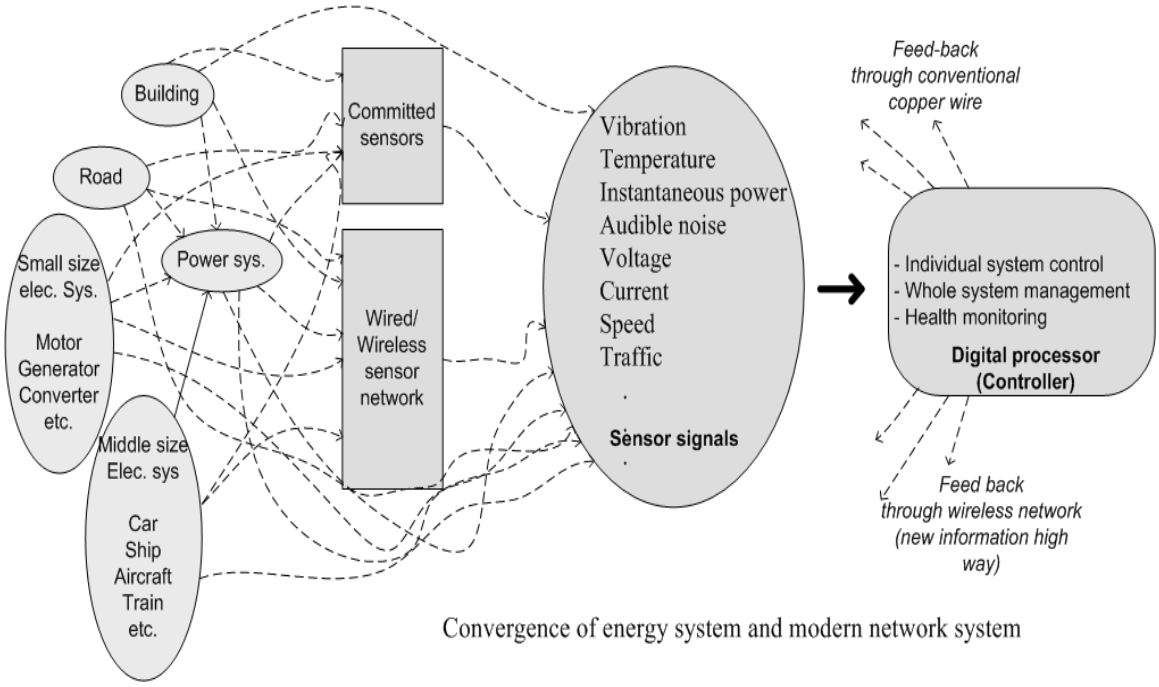

Fig. 1.5. Convergence of energy system and modern network system .

in motor control service routines such as stator current signal, excitation frequency, rotor speed/slip, etc. as briefly shown from (1.1) to (1.4), implementation of motor control and fault diagnosis within a single microcontroller unit can be done at a relatively low cost.

Thanks to recent digital signal processor (DSP) technology developments, motor fault diagnosis can now be done in real time based on the stator line current [9][14][17] [25][26][27][28][29][32][33][34] allowing precise low-cost motor fault detection. Beyond this, once simple and efficient fault detection algorithms are employed, it is possible to control the motor and detect the fault simultaneously at very early stages using the same DSP [17][26][31]. Typically, implementing a comprehensive fault diagnosis algorithm, taking all the details into account like the decision-making stage, is

a long and complicated procedure. Therefore, in order not to violate CPU utilization and degrade motor control performance, the priorities of the DSP-based fault algorithms need to be carefully determined based on practical issues such as noise content, phase unbalance, or frequency errors.

Among widely used traditional algorithms, the Fast Fourier transform (FFT) is one of the most popular signal processing algorithms in motor fault detection applications. However, in realtime applications, (N/2)*log (N) complexity of FFT-radix 2 brings an overwhelming burden to the DSP where significant amounts of data need to be processed in order to produce sufficiently high resolution. Using some recently proposed signal processing algorithms as alternatives to traditional methods [17][29][30] gives good real time performance and satisfactory results when implemented by a DSP. Analysis in [29] describes a generally non-stationary stator current signal with Zhao-Atlas-Marks (ZAM) distribution showing high resolution and practical implementation possibility. In [17], a simple algorithm based on multiple reference frame theory is successfully implemented on a DSP used for direct torque control (DCT) of an induction machine. The Winger Distribution (WD) is used for efficient time-frequency analysis of the signal in an inverter-fed motor especially during a transient condition [30]. On the other hand, a phase locking loop [26] has lower computational complexity for processing a large amount of data. The complexity order of a basic phase locking loop function is N, which is log(N)/2 times less than that of a FFT algorithm. Instead of scanning the whole spectrum, a phase locking loop concentrates only on the expected fault frequencies which improve resolution and noise immunization [26] [31].

In order to implement a full fault detection procedure using DSP, the proposed algorithms should not only detect the fault signatures but also make reliable decisions [61]. An effective algorithm should be able to take variations in fault signature amplitude, line current noise level, frequency offset, and phase offset into consideration to avoid missing or false alarms.

In practical applications, a small frequency offset between the expected and the existing fault frequency can be observed due to inaccurate speed feedback or estimation, slow response of sensing devices, etc. If the detection is performed within a short period, even a small frequency offset can aggravate the overall capability of the detection system. Therefore, it is unlikely to make a reliable decision regarding the fault status until the frequency offset is accurately compensated; this has commonly been neglected in previous studies.

Noise level and its variations must also be considered in a diagnostic system design because the fault signatures are generally observed at a much smaller level than the noise energy level [26][27][28]. One must note that all of the harmonic content in the line current, including the fundamental component, is considered as noise where the main focus is on a very low amplitude fault signature, typically between -40dB to -80dB. Due to the low signal-to-noise ratio (SNR), a robust fault detection method proposed for plants in harsh industrial environments should accurately consider noise content and its variations.

Ignoring these ambiguities might result in erroneous fault indices in industrial applications. Furthermore, to come up with highly reliable fault indices based on fault

references, the thresholds should be updated depending on the motor speed, torque, and control schemes - this will result in further complexity.

1.4 Research objectives

In this dissertation, the fault signature-based MCSA diagnosis has been studied in detail with emphasis on diagnostic reliability, flexible applicability, and low cost implementation.

The first goal of this work is to develop a reliable decision-making scheme using an optimal threshold that discriminates fault signature from potential noise content in the line current signal. For a successful industrial application, the reliability of a suggested threshold scheme needs to be statistically proven in terms of false alarms or missing alarms probability. Since the diagnosis system is expected to operate autonomously when a human is not present, performance should also be statistically fully verified and should be expected, maintained, and controlled under arbitrary noise conditions.

The second objective of this work is to develop a reliable fault signature tracking scheme. The measurement of the characteristic frequency of a fault signature is potentially disturbed by a slip/speed measurement error caused by numerous types of interferences to the motor speed feedback system. The effect of the speed feedback error in a diagnosis is primarily analyzed, measured, and compensated for reliable diagnosis as the fault characteristic frequency is critically dependent on motor shaft speed.

The third objective of this work is to develop an implementation strategy for the proposed diagnostic scheme on a low cost DSP system which is simultaneously used for

motor control. Highly complex frequency tracking and threshold-based decision-making algorithms are usually too overwhelming to be applied in low cost motor control DSP as it requires serious computation complexity which violates CPU utilization. For a successful and flexible implementation, the algorithm should be significantly simplified with efficient computation complexity and memory occupation minimization strategies.

The fourth objective of this work is to mathematically extend the developed algorithms so they will be flexibly applicable to the arbitrary phase system. As high power applications in industry employ multi-phase motors and generators, a generic diagnostic solution is needed for various multi-phase systems which are flexibly extended from existing algorithms with a single philosophy.

The fifth objective of this work is to perform the overall diagnosis independent of the motor's operating points (i.e., motor speed, torque, or fundamental stator current amplitude) and surrounding applications environment. This significantly simplifies the diagnostic consideration and can be flexibly applied to any system. The model's independent nature allows the user to apply it to any kind of motor fault signature detections in any industrial application.

CHAPTER II

PERFORMANCE - ORIENTED THRESHOLD DESIGN FOR FAULT DIAGNOSIS OF INDUCTION MACHINES

2.1 Introduction

This section presents a detailed analysis of a threshold design in the fault diagnosis of induction machines under steady state motor operating conditions. The motor phase currents involve random noise components generated by harsh industrial environments, low and high order harmonics interferences caused by inverters and fast switching devices, and various other design imperfections. Therefore, it is quite challenging to model the overall noise content and eliminate the disturbance while detecting the motor fault signatures. Due to the inherent random variation of motor noise statistics, the noise model and elimination strategy should also be adaptively updated according to the instantaneous noise conditions through which the detection can be done with pre-defined performance expectation. Several successful solutions in the literature have managed to perform a diagnosis under certain noise conditions; however, a detailed performance and adaptability analysis covering arbitrary noise variation in a motor drive has not been satisfactorily addressed. This section mainly deals with performance oriented threshold design strategies for fault signature detection utilizing the noise statistics of a motor phase current signal. The proposed solution is generalized to cover arbitrary noise variations and to derive the optimal form of a threshold that satisfies user's detection quality expectations. The mathematical derivations are proved through statistical theory and the experimental verifications are performed by using a 3-hp motor generator setup.

2.2 Background and previous research work

Modeling the noise contents in a motor phase current signal and eliminating those noise components have been practical issues for a high performance MCSA diagnosis. In [10][28][35][36], the noise disturbance elimination is achieved by simply averaging multiple spectrums. The Zoomed-FFT (ZFFT) [28], the Zoomed-multi signal classification (ZMUSIC) [27], the Eigen-value-based analysis [1][27][36], and the maximum covariance-based frequency tracking (MCMFT) [28] suggest solutions through high noise suppression in a spectral analysis. Recently, in [15], all the components irrelevant to a fault are regarded as noise content and modeled through the Wiener filter. Noise disturbance elimination is performed based on noise modeling. In [14], statistical process control (SPC) achieved high performance and determined the noise level based on the noise-canceled signal which is computationally intensive.

In this dissertation, among many active issues regarding noise management in a diagnosis, the diagnostic decision-making strategy through a threshold for fault signature detection is studied at large. Fig. 2.1 briefly shows the typical risks and reliable decision-making patterns of a signature under the zero mean white Gaussian noise channel [37] [61]. The area under each probability curve is 1 where the noise level determines the variance of the distribution. Here, A is the amplitude of the signal. Two types of decision-making errors with a threshold of $A/2$ in case of equal variance are shaded in the figure. These shaded areas are false and missed detection probability. It is trivial that with a smaller amplitude of signal A and higher noise levels, the overlapped area between the two curves (the shaded error distribution) becomes wider and results in

misleading decisions. In fact, this is the typical condition of decision-making at a very low SNR in the fault diagnosis of electric motors; this has been continuously presented in the literature [14][15][37][61]. One should note that the noise distribution is inherently continuous in a probability curve in the figure. Suggested noise models and disturbance elimination techniques shown in the literature [10][14][15][27][28][35][36] can reduce the noise statistics in a current signal, however the complete elimination of noise content is practically impossible. Decision for small signature detection is expected to be interfered due to residual noise statistics which need further analyses for more precise diagnosis.

Therefore, while determining an active threshold strategy, its adaptability against unexpected residual noise variation should be statistically proven through false or missing alarms probability versus potential noise levels. Since the diagnosis is primarily expected to operate autonomously when there is no human interaction, it should have expectability, maintainability, and controllability features under any noise condition.

Recently, innovative threshold definitions in the literature [26][29][37] have been

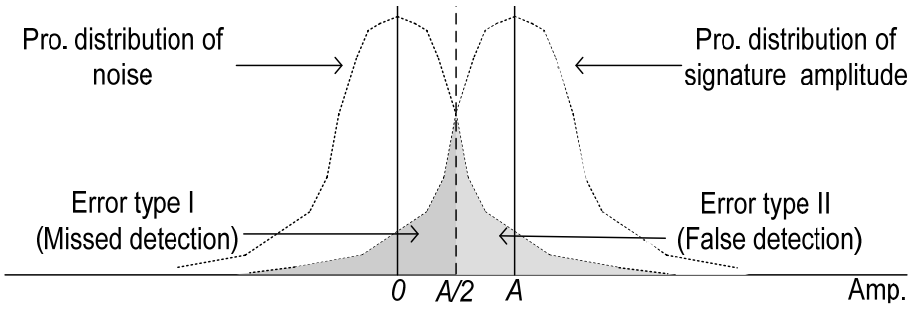

Fig. 2.1. Probability distributions of a fault signature and noise.

adopted for fault decision-making. In [26], the threshold for eccentricity detection is pre-determined based on a rough signature amplitude classification as follows: less than -60dB good, between -60dB to -40dB tolerable and higher than -40dB severe (normalized to fundamental current signal amplitude). In [29], the threshold is adaptively determined as a pre-determined percentage of the fundamental current signal. In [37], the threshold is predetermined based on prior tests before the diagnostic procedure starts. In general, most threshold definitions are determined depending on the applications environment and its expected fault severity. These suggested solutions present an intuitive way to design a threshold for a successful diagnosis.

However, in many threshold schemes, including the aforementioned ones, a statistical performance evaluation has not been sufficiently provided. One should note that it is impossible to suggest a diagnostic technique that guarantees 100% accuracy as non-stationary signals are continuously involved and decision-making is continuously disturbed. The achievable performance should statistically be analyzed to cover arbitrary noise variations. The predetermined threshold definitions in [26][29][37] might be efficiently utilized to measure fault severity but tend to detect sufficiently strong signatures to avoid noise interference. Performance evaluation considering potential noise effects should be performed accurately to determine the critical constraints of proposed diagnostic schemes.

One of the simplest and most common techniques for performing noise suppression in fault diagnostic technology is spectrum analysis through a fast Fourier transform (FFT) [22][40][41]. Since the FFT operation is an effective spectrum averaging process,

it performs a simple de-noising for random noise variations of acquired current signals. Nevertheless, the statistical reliability of the FFT analysis is inherently not guaranteed, especially under low SNR conditions. The FFT provides a relatively short-time analysis of a current spectrum acquired in a limited data window where the small fault signatures are significantly affected by the perturbation of a residual non-stationary noise. The reliability of the FFT-based diagnosis is also known to be affected by its specifications such as FFT size which is limited by the capacity of available memory, computational complexity or implementation cost. Therefore, the FFT efficacy inherently varies depending on the noise environment and size of the FFT implementation system which makes it impractical for diagnostic applications. In fact, not only the FFT technique but also most signal processing algorithms in the literature have inherent performance dependency on the environmental noise or system specification where performance should be accurately identified for a target application system [39][61].

In this study, the derived threshold definition is applied to FFT-based signature detection to prove the basic concept of the performance-oriented decision-making strategy. It is shown that fault detection and decision-making mechanisms can be predictable, maintainable, and controllable. This can be achieved independently from the surrounding noise environment, applications condition, or diagnostic window size, etc. In addition, the model independent feature of the proposed solution allows users to realize the diagnosis with pre-defined performance expectations.

2.3 Threshold derivation and performance analysis

Reliable condition monitoring techniques utilizing motor current signal noise statistics have been studied in the literature but covered only in limited conditions under noise induced in a favorable experimental setup. In order to provide an explicit performance analysis covering arbitrary noise conditions which might be encountered in industry, a common threshold-based diagnostic routine is proposed as shown in Fig. 2.2 where detection accuracy is statistically analyzed in detail. Precision enhancement of the evaluation is managed by measuring the statistics of a motor current signal in advance utilizing a harmonic interference minimization.

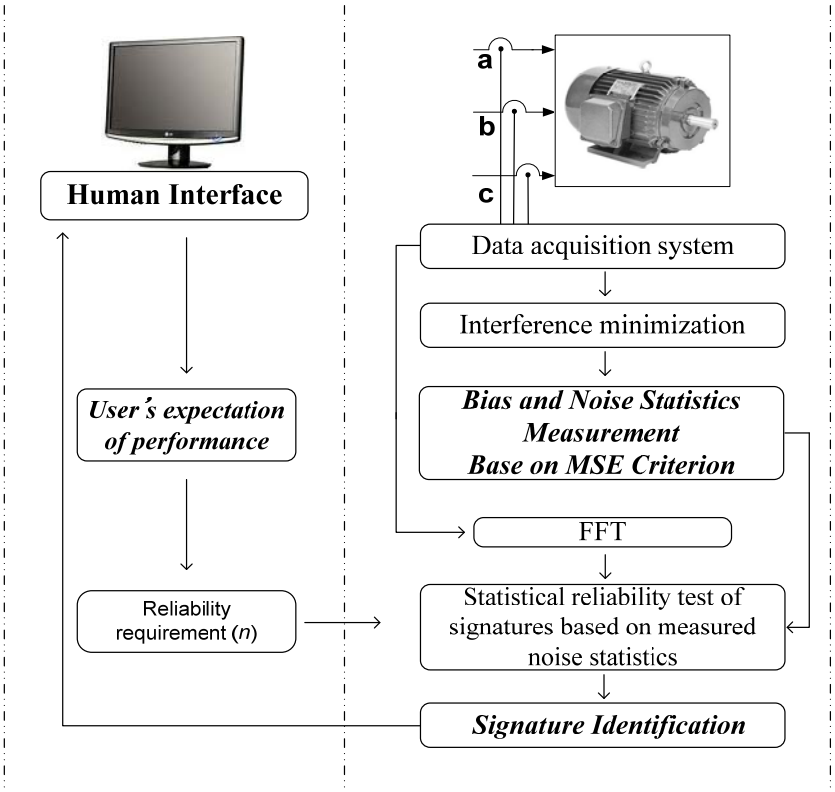

Fig. 2.2. Overall block diagram.

The interference minimized current signals are fed to the bias and noise measurement block which is designed according to a mean square error (MSE) criterion. Afterward, fault signatures in the current spectrum are examined through a reliability test employing an adaptive threshold which is derived from a performance-oriented design strategy utilizing measured noise statistics. User's pre-defined performance of a diagnosis obtained through prior-analysis is fed to the reliability testing block to control the quality of detection.

A. Modeling Motor Current Signal

In order to obtain an accurate fault signature decision, the statistics of a current signal need to be primarily identified. In Fig. 2.3, a single-phase equivalent circuit of an induction motor is shown where the stator current model, including the harmonic signals and bias acquired in the limited data acquisition window W , is described as follows:

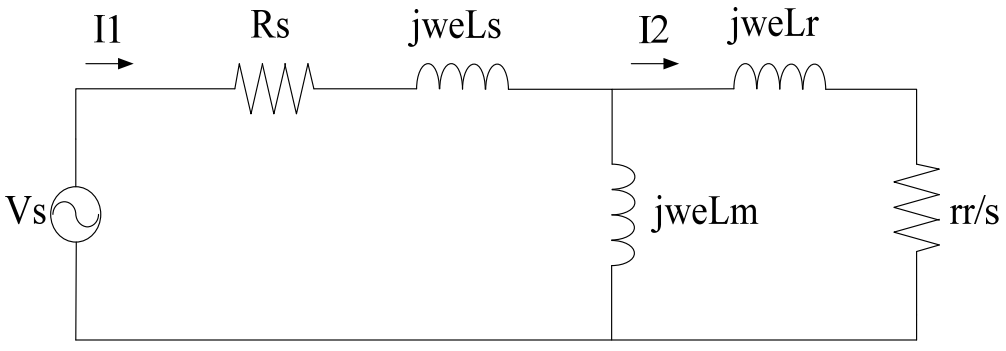

Fig. 2.3. Single phase equivalent circuit of induction motor.

$$a_1(k) = A + \left[I_{fault} \cos\left(w_{fault} k + \varphi_{fault} \right) + \sum_h I_h \left[\cos(w_h k + \varphi_h) \right] + \varpi_k \right] W(d) \quad (2.1)$$

where
$$W(d) = \begin{cases} 1, & d \le k \le d + N - 1 \\ 0, & \text{otherwise} \end{cases} \quad (2.2)$$

where k is the sample index, I_{fault} is the amplitude, w_{fault} is the frequency, φ_{fault} is the phase of the fault signal, ϖ_k is the zero mean white Gaussian noise with a variance of σ^2, d is the start instant of data acquisition window, N is the window size, A is the DC bias, h is the harmonic number, I_h is the amplitude, w_h is the frequency, and φ_h is the phase of harmonic signal.

The orthogonality assumption between the harmonic current signals in (2.1) is made only if $0 \neq w_h \neq w_{fault}$ and N is large enough. Practically, the orthogonality assumption is not maintained and the phase current statistics measurement utilizing signal model in (2.1) is interfered by the non-ideal harmonic signals, especially when an incomplete cycle with limited acquisition time window N as shown in (2.2) results in DC level variations. The non-stationary variations of the DC level in multiple trials are prone to be mistaken as non-stationary noise of motor current statistics as the noise level is inherently small and sensitively affected. Suppression of the negative variation factors (incomplete harmonic interferences) is implemented in advance to accurately estimate the signal statistics from a simpler motor current signal model which is mainly assumed to be distorted by Gaussian noise.

A1. Statistics of Motor Current Signal

In order to obtain a sufficiently precise motor current statistics estimation, eliminating the destructive contribution of non-ideal signal variations within the limited data acquisition window in (2.2) is required. This can be achieved by filtering the dominant harmonics in the machine current signal. The harmonics are first measured through the small signal detection scheme given in [26] and rejected by inserting an opposite phase signal. A notch filter is not employed in this dissertation is to prevent the change of current noise statistics which not only filter the target frequency signal but also inherently affects nearby frequencies due to side band ripples of a filter. The detailed operation of the small signal detection scheme in [26] is out of scope and not elaborated in this dissertation.

The non-stationary variation of the DC level is assumed to be suppressed after the filtering and the residual harmonics in a current signal are assumed sufficiently small, which is approximately described as follows:

$$a_2(k) = A + [\varpi_k] W(d) \tag{2.3}$$

The probability distribution of the modified motor current signal a_2 in the Gaussian noise channel is described as follows:

$$p(\mathbf{a_2}; A) = \frac{1}{\left(\sqrt{2\pi\sigma^2}\right)^N} \exp\left[-\frac{1}{2\sigma^2} \sum^{N} \left(a_2(k) - A\right)^2 \right] \tag{2.4}$$

From (2.4), the statistics of the current signal will be identified if the unknown parameters are measured - the bias A and the noise variance σ^2. The bias and the noise

variance are the parameters which must be accurately identified to obtain a high enough resolution in small fault signature detection.

A2. Bias Estimation in Motor Current Signal

In the motor current spectrum, the DC bias is monitored at 0 Hz which is fundamentally caused by various non-ideal conditions such as inherent current signal distortion, current sensor offset, or noise interference. The minimum variance unbiased estimator (MVUE) is efficiently utilized for a DC signal bias estimation which is derived by using the probability distribution in (2.4) based on the Cramer-Rao theory [61] as follows:

$$\frac{\partial \ln\left(p(\mathbf{a_2};A)\right)}{\partial A} = \frac{1}{\sigma^2}\sum\left(a_2(k)-A\right)^2 = 0 \quad \Rightarrow \quad \hat{A} = \frac{1}{N}\sum a_2(k) \tag{2.5}$$

In (2.5), the derived bias estimator averages a motor current signal. With the assumption of small residual harmonics in (2.3) and sufficient window size N in (2.5), the effect of small harmonics is negligible in the average estimation.

The theoretical performance bound of the DC bias estimator for the current signal in (2.5) measured in variance is derived by:

$$\mathrm{var}(\hat{A}) = \frac{\partial^2 \ln\left(p(\mathbf{a_2};A)\right)}{\partial A^2} = \frac{\sigma^2}{N} \tag{2.6}$$

The performance bound in (2.6) shows the accuracy of the bias estimation which is measured in variance. Assuming the detected bias A, the unknown parameter of the current statistics in (2.4) is the noise variance σ^2.

A3. Noise Estimation in Motor Current Signal

Fig. 2.4 briefly shows bias and the noise statistics measurement procedure for the motor current signal. The interference free motor current signal is fed to the multiple sub-bias estimations which mean bias is observed through the sliding window. The noise statistics of a current signal are measured utilizing bias-compensated signals via mean square error criterion (MSE) [37][39][61]. The noise estimation technique in [42] is modified and applied for this purpose.

The MSE-based noise estimation utilizes the average of the bias-compensated current signal $\hat{\Phi}$ which is defined as follows:

$$\hat{\Phi} = \frac{1}{N}\sum^{N}\left(\varpi_k\right) = \frac{1}{N}\sum^{N}\left(a_2(k) - \hat{A}\right) \tag{2.7}$$

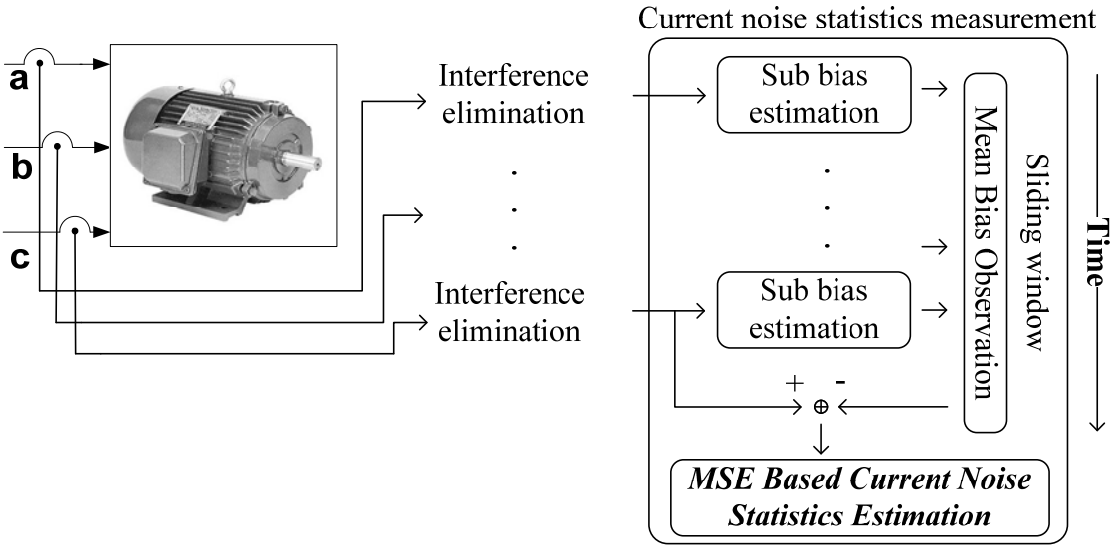

Fig. 2.4. MSE-based current noise statistics measurement.

The mean expectation of $\hat{\Phi}$ is given by,

$$E\left[\hat{\Phi}\right] = E\left[\frac{1}{N}\sum^{N}\left(\varpi_k\right)\right] = 0 \tag{2.8}$$

The noise variance σ^2 of a current signal is derived from the MSE of $\hat{\Phi}$ in (2.7) as follows:

$$mse(\Phi) = E\left[\left(\hat{\Phi}-\Phi\right)^2\right] = E\left[\left(\left(\hat{\Phi}-E\left(\hat{\Phi}\right)\right)+\left(E\left(\hat{\Phi}\right)-\Phi\right)\right)^2\right]$$

$$= Var\left(\hat{\Phi}\right)+\left(\Phi-E\left(\hat{\Phi}\right)\right)^2 = Var(\hat{\Phi})+b^2 = \sigma^2 / N$$

$$\Rightarrow \sigma^2 = NVar(\hat{\Phi}) \tag{2.9}$$

where $b^2 = \left(\Phi - E\left(\hat{\Phi}\right)\right)^2$ is zero.

In (2.9), the noise variance σ^2 of a motor current signal is successfully derived utilizing the bias estimation in (2.5). Finally, the statistics of the motor current signal in (2.4) is fully identified through the bias estimation in (2.5) and the noise estimation in (2.9). Based on the identified statistics, it will be utilized to design a threshold for reliable fault signature detection.

B. Performance-Oriented Threshold Derivation (1)

A Performance-oriented threshold is derived for single fault signature detection in current signal and multi-signature detections in an FFT current spectrum in *section B* and

section C, respectively. The performance of a derived threshold is thoroughly evaluated through statistical theory assuming an arbitrary noise condition in the motor phase current signal.

In order to simplify the threshold derivation, single fault signature detection based on a cross-correlation is analyzed in advance which focuses on the specific fault frequency evaluation in a current signal [26][61][63]. Signature detection can be performed through cross-correlation between pairs of signals which are motor current signal a_1 and fault reference signal s as follows:

$$\mathrm{T} = \sum_{k=1}^{N} a_1(k)s(k) \tag{2.10}$$

where $s(k) = I_{fault}\cos(w_{fault}k + \varphi_{fault})$.

A decision for the existence of a fault signature in a motor current signal can be made on the output of the cross-correlation in (2.10) which is as follows:

$$\mathrm{T} > \gamma \tag{2.11}$$

where γ is the assumed threshold.

To further simplify the latter derivation, the performance of the correlation-based detection through (2.11) is directly adopted from well established statistical theory in [61]. The probability of the detection ($\mathrm{T} > \gamma$) of a fault signature under the Gaussian noise channel is presented as follows [61]:

$$P_D = Q\left(\frac{(\gamma - \mathrm{E})}{\sqrt{\sigma^2 \mathrm{E}}}\right) \tag{2.12}$$

where Q is the *Q*-function. The *Q-function* is defined as follows:

$$Q(z)=\int_z^{\infty}\frac{1}{2\pi}e^{-g^2/2}dg, \qquad z=\frac{(\gamma-E)}{\sqrt{\sigma^2 E}} \tag{2.13}$$

$\mathrm{E}=\sum s^2(k)$ is the energy of fault signal $s(k)$.

The false detection probability when applying the threshold ($\mathrm{T}>\gamma$) is given by

$$P_{FA}=Q\left(\frac{\gamma}{\sqrt{\sigma^2\mathrm{E}}}\right) \tag{2.14}$$

Between false and missing alarm, only the false alarm in (2.14) is analyzed as minimizing the false alarm event under the dominant noise condition is the main concern in small fault signature detection. It is obvious in (2.12) and (2.14) that the diagnostic performance depends on the ratio of fault signal energy to the noise variance. One can note that, by properly choosing the threshold γ to be proportional to $\sqrt{\sigma^2\mathrm{E}}$ in (2.14), a fault signature can be detected independently from signal energy and noise variance $\sigma^2\mathrm{E}$. This provides an intuitive way to design a robust threshold independent of unexpected motor noise variation.

C. Performance-Oriented Threshold Derivation (2)

This section presents a performance-oriented threshold design for multi-fault signatures detection in the motor current spectrum. The amount of disturbances in harmonic signal estimation is expected to be dependent on the average noise floor in a

current spectrum. All the harmonic frequency contents in a spectrum are assumed to be equally disturbed by the noise floor. Based on these assumptions, the noise floor is efficiently measured through the perturbation of a DC signal measurement. From (2.5), the perturbation in the DC measurement is mathematically derived as σ^2 / N, which is measured through (2.9). The noise variance of *N*-point FFT operation is determined as follows:

$$\sigma_1^2 = \frac{\sigma^2}{N} \tag{2.15}$$

The performance evaluation in (2.12) and (2.14) for the fault signature energy detection is modified as the fault signature amplitude detection in a noisy channel follows a similar evaluation philosophy as in section *B* [61].

The performance in the decision-making stage is as follows:

$$P_D = Q\left(\frac{\left(\gamma' - A\right)}{\sqrt{\sigma_1^2}}\right) = Q\left(n - \sqrt{SNR}\right) \tag{2.16}$$

$$P_{FA} = Q\left(\frac{\gamma'}{\sqrt{\sigma_1^2}}\right) = Q\left(n\right) \tag{2.17}$$

where γ' is the threshold chosen to be proportional to $\sqrt{\sigma_1^2}$ in the same way as the previous analysis in (2.14) such as $\gamma' = \sqrt{n^2\sigma_1^2} = n\sqrt{\sigma_1^2}$ where n is the design parameter, $A = \sqrt{\mathrm{E} / N}$ is the fault signature amplitude, and $SNR = \mathrm{E} / \sigma_1^2$.

As can be observed from the false alarm probability in (2.17), the error performance in the detection now becomes independent of noise condition σ_I^2 of a motor current signal. Therefore, the optimal threshold definition with performance independent of the arbitrary noise condition is determined as in the following form:

$$\gamma' = n\sqrt{\sigma_I^2} \tag{2.18}$$

Noise statistics dependency on the number of signal sample *N* used for the estimation is shown in (2.15) which will be the size of *N*-FFT processing in the application. Therefore, even a simple change in the data acquisition window size for an *N*-FFT will potentially alter the noise statistics which, in turn, will potentially challenge the reliability of a small fault signature diagnosis if not sufficiently analyzed. Similar challenges are expected in any type of signal processing technique in the literature since the noise level inherently changes depending on the size of the data acquisition window of a signal processing system which is mainly limited by memory size, computation complexity or industrial implementation cost. It is clearly revealed from the false alarm probability in (2.17) that the error performance of a motor diagnosis can be inherently maintained independently from those variations of the system specifications if the noise variance σ_I^2 of a current signal is properly measured and utilized in the threshold design.

D. Threshold Property

This section presents the detailed property of the derived threshold in fault decision-making and its advantage in industrial application.

According to the derived threshold definition in (2.18), the threshold level is shown to be determined by adjusting the single parameter *n*. From the false alarm probability in (2.17), it can be observed that threshold performance can be completely controlled by simply adjusting the same single parameter *n*. Therefore, threshold performance in fault signature detection can be fully controllable by adjusting *n* as the user expectation of detection quality if the threshold is applied in the special form in (2.18). Utilizing the identified controllability property, a reliability enhancement block can be added to the fault diagnostic service routine in Fig. 2.3 to provide the diagnostic performance as user's expectation.

Fig. 2.5 shows the theoretical performance of the derived threshold in (2.18) which is depicted based on the detection and false alarm probability in (2.16) to (2.17), respectively. As the *n* increases, the false alarm rate becomes suppressed. The false alarm rate is shown less than *0.16, 0.03, 0.002* for each *n=1, n=2, n=3* and constant versus whole SNR axis. Fig. 2.5 shows that the error performance of the scheme is completely predictable by design parameter *n* and maintainable independently from any motor noise condition (SNR conditions) which proves the robustness of the scheme to unexpected noise variation of a motor current signal. The trade-off of the design strategy is that the detection rate loss is reduced with more restriction on the false alarm rate as can be noted in Fig. 2.5. In fact, this is an unavoidable trade-off in most detection and estimation strategies in industry.

A similar diagnostic approach has been done in [37] utilizing noise statistics in a motor current signal for a zero input test when the motor is not operating. It provides the

boundary threshold level of a noise level plus the DC offset of the current sensors. Since the scheme is proposed for a zero input case, it might have limitations in the analysis when the motor operating point changes and the statistics is expected to vary accordingly. More analysis is needed for the property of the suggested scheme in the diagnosis when utilizing noise statistics for detection and decision-making. This will be experimentally verified later.

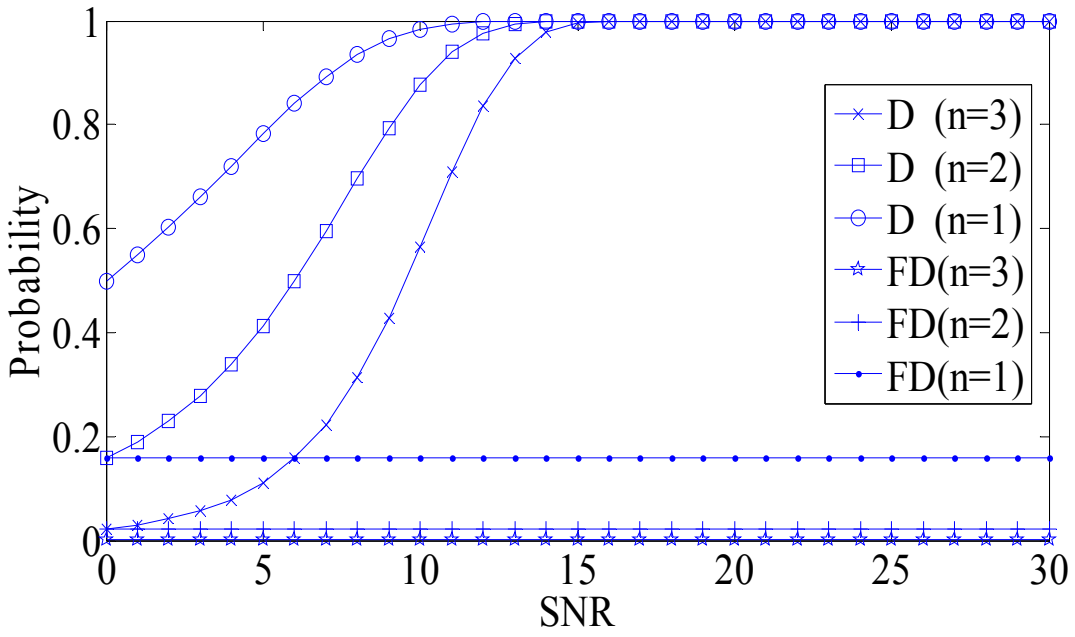

Fig. 2.5. Detection (D) and false detection (FD) probability versus SNR.

2.4 Offline experimental result

Table. 2.1. System Environment 1.

Sampling Hz	25 kHz
ADC	12 bit
Data acquisition board	NI-DAQmx
Motor	3 hp IM
# of pole	4
Supply frequency	60Hz
Full load speed	1760
Input voltage	230V
Threshold design parameter (n)	3
FFT size (N)	50000
Sliding window length	10 seconds
Sub bias estimation time	2 seconds

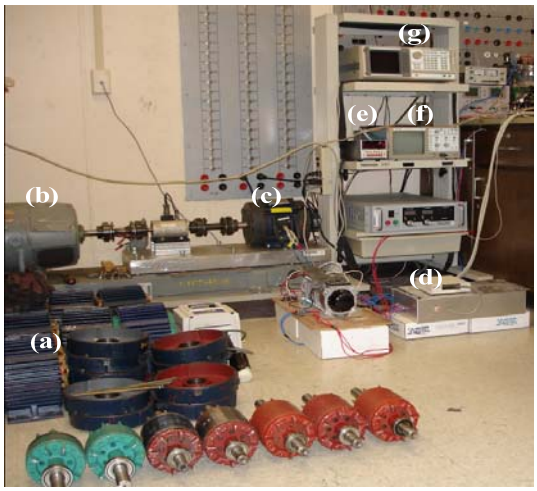

Fig. 2.6. Experimental setup: (a) faulty test motors, (b) DC generator, (c) 3-hp induction motor, (d) data acquisition board, (e) torque monitor, (f) oscilloscope, and (g) spectrum analyzer.

Offline verifications are performed to verify the performance of the threshold-based diagnostic service routine depicted in Fig. 2.2. The derived threshold definition is applied to the raw current signal obtained through a 1.25 MS/s data acquisition system. The 3-hp induction motor is loaded by the DC generator as shown in Fig. 2.6. The test motor bearing houses are artificially modified and re-machined to obtain severe eccentricity and three of the rotor bars are cut using a drilling machine. The name plate of the test motor and the signal processing parameters are shown in Table. 2.1.

A. Noise and Bias Estimation

In this section, based on previous theoretical derivations, estimations of the noise and bias in a motor current signal are performed, which are expected to show the net effect of a current sensor offset, ADC quantization error, inherent motor signal distortion, or applications environment noise. In Figs. 2.7 to 2.9, the normalized result value is the one divided by the fundamental signal amplitude and the absolute value is obtained without normalization.

Fig. 2.7 shows the DC bias measurement in the current signal (2.5) which is observed to change almost in parallel to the load variation. Unlike in [37] where a pre-determined bias level is utilized for the zero input tests, the test result shows that the instantaneous bias under the different motor operating point should be continuously tracked for a reliable diagnosis.

Fig. 2.8 shows the noise statistics measurement of a current signal through (2.9). The normalized result in the figure is effectively the SNR of the fundamental current

signal which is bounded around -72dB. This level of resolution provides good agreement with the range of the SNR specification of the test data acquisition (NI-DAQ) board with 12 bit ADC which provides -72 dB analysis range. If a higher ADC bit is utilized for the estimation, a better SNR boundary can be obtained. A DAQ with a 12 bit ADC is used in this experiment assuming potential application to the motor drive system in industry which popularly adopts 12bit ADC.

Precision of noise estimation can be improved by sufficiently increasing measurement time. Fig. 2.9 shows measured noise variations versus time, which tend to be stabilized as sample time increases, thus verifying the precise derivation in (2.5) to (2.9) of the time dependency. It shows that at least 10 seconds are needed for reliable noise estimation.

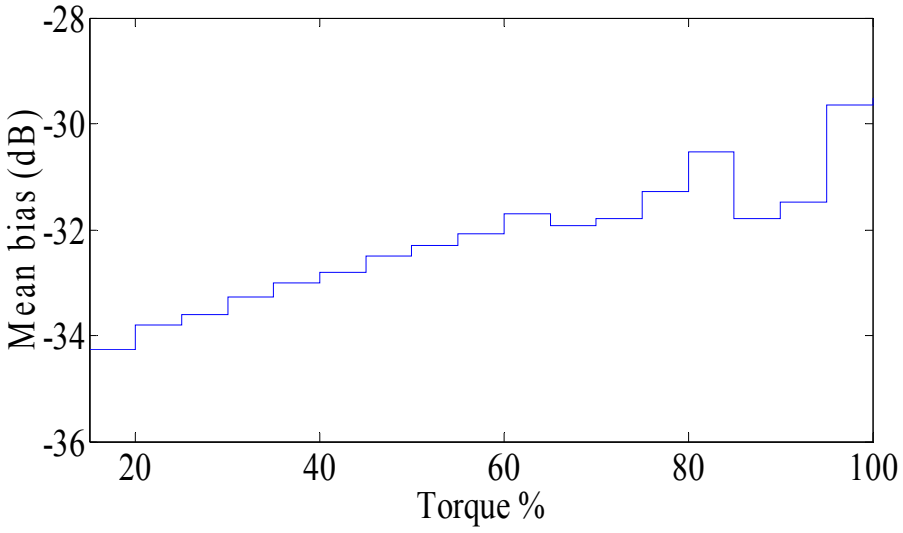

Fig. 2.7. Bias measurement vs torque % (10 sec for each result).

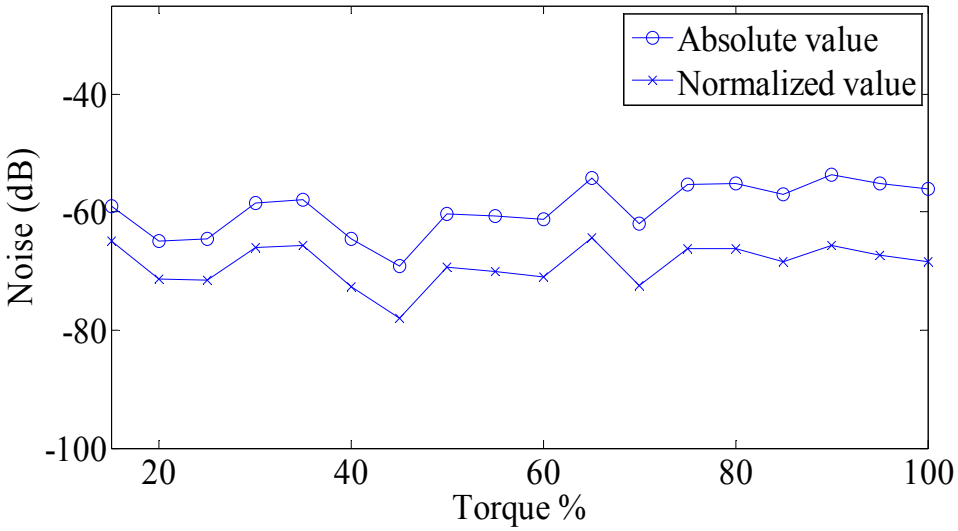

Fig. 2.8. Noise measurement vs torque % (10 sec for each result).

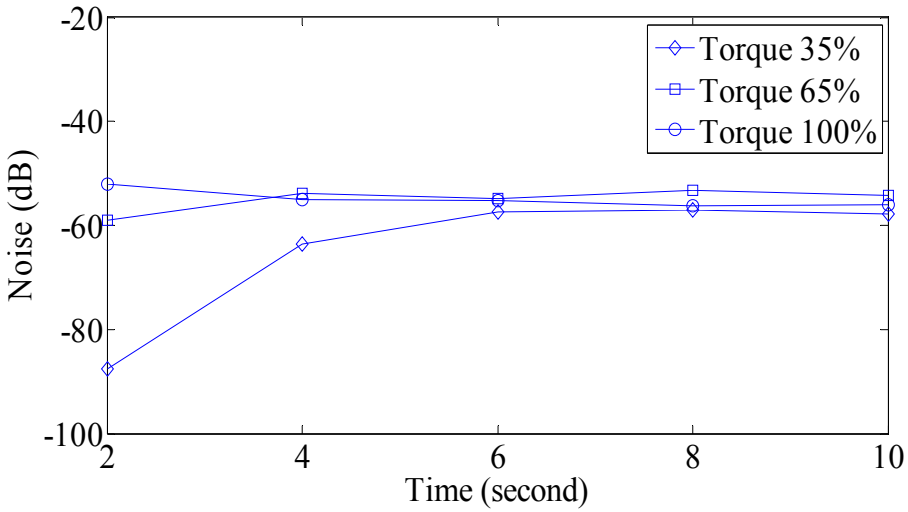

Fig. 2.9. Noise variance measurement vs time (absolute value).

B. Statistical Decision-Making for Signature

All the experiments in this section are performed under 70% motor torque for an easy comparison of decision results which can be extended to any motor condition without loss of generality. Hanning window is applied to the current signal in advance to minimize the leakage effect in the spectral observation. Fig. 2.10 shows the mixed fault signatures in the current spectrum. Statistical decision of those signatures is performed based on the designed threshold in (2.18).

Harmonics elimination based on the PSD in [26] is applied to the fundamental, 3^{rd}, 5^{th}, and 7^{th} harmonics to reliably estimate the bias and, hence, the noise in Figs. 2.7 to 2.10. In Fig. 2.11, the fundamental and the 3^{rd} harmonic shown dotted are suppressed significantly while the statistics of the nearby band are not affected in a manner similar to an ideal notch filter.

Fig. 2.12 shows the current spectrum with the threshold definitions of -72.45dB, -66.4dB, and -62.96dB for $n=1$, 2, and 3, respectively. Each definition is shown to sufficiently make detection of the broken rotor bar and the eccentricity signature. The threshold is shown to provide precise resolution close to -72dB with $n=1$, which is good enough for the noise levels reported in industrial environments.

The effect of noise estimation performance in decision reliability can be explained as an internal change of threshold parameter n. In Fig. 2.8, the instantaneous error about 5.56dB at 45% torque which is measured from -72dB occurs when parameter $n=3$ is internally changed to $n=1.92$. The false alarm rate with $n=1.92$ is still suppressed to be less than 0.028 from (2.17). Taking multiple detection trials will average out the

instantaneous errors. Increasing the measurement time of the noise statistics can be applied as in Fig. 2.9 where the estimation fluctuation is converged to zero after 10 seconds with a marginal effect.

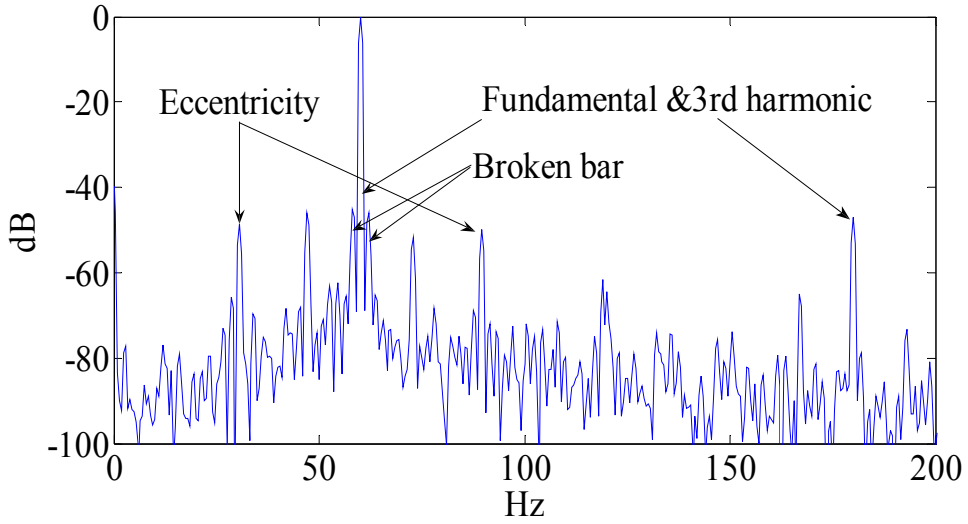

Fig. 2.10. FFT spectrum of the line current (utility driven, 70% torque).

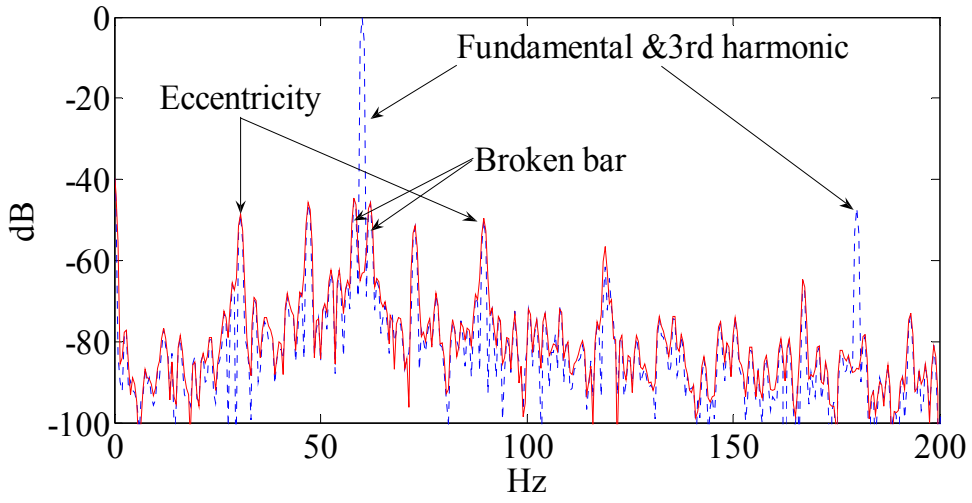

Fig. 2.11. Harmonics elimination.

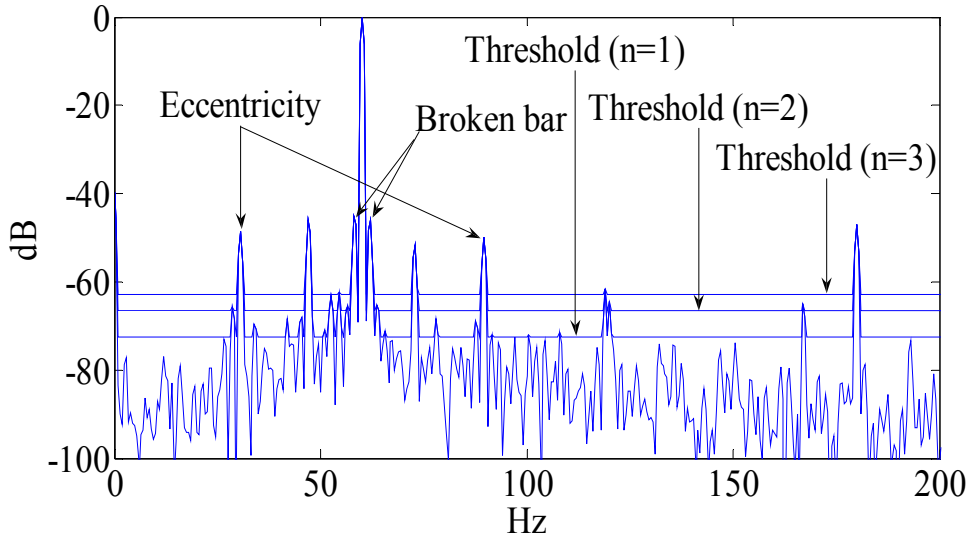

Fig. 2.12. FFT set by noise threshold (utility driven, 70% torque).

B1. Decision-Making in a Different Size System

The size of *N*-FFT is determined depending on the available data acquisition window in an application system (available memory size or computation capacity). Fig. 2.13 simultaneously shows the 50k-FFT spectrum assuming a 25 kHz sampling rate and a 10k-FFT spectrum with a 5 kHz down sampling rate. The eccentricity signature is observed with almost the same amplitude under different sampling strategies. A diagnostic system implementation has been done in the literature with small data memory or less computation time with negligible loss of original signal information of interest which efficiently utilizes the down sampled signal.

Since the FFT is an effective spectrum averaging operation, the reduced FFT size is expected to result in an increased noise floor which is not sufficiently averaged out. An increased noise level results in increased ambiguity in the reliability of small signatures

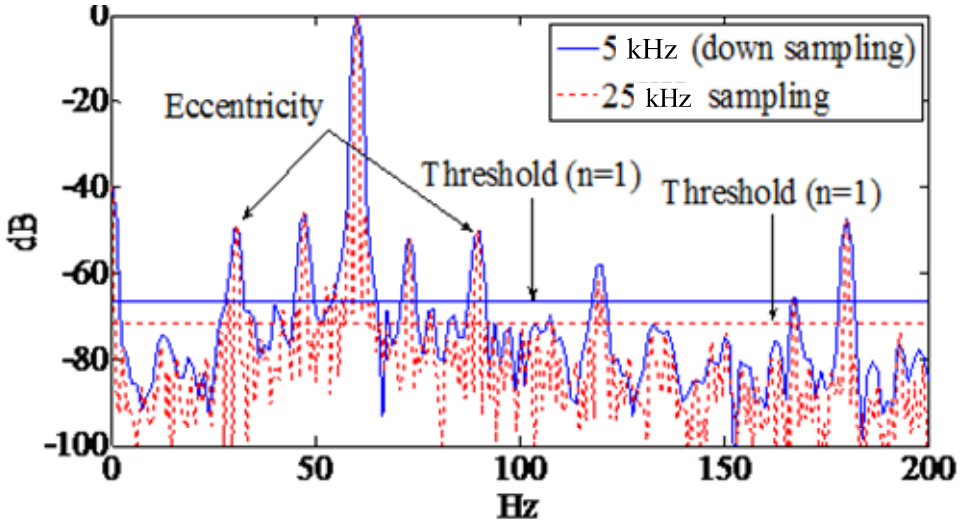

Fig. 2.13. FFT spectrum of the line current with different sampling frequency (utility driven, 70% torque).

detection if not properly analyzed in the applications. In Fig. 2.13, the depicted results are obtained from an acquired current signal under the same motor conditions where noise threshold (*n=1*) is increased from -72.45dB to -67.69dB and FFT size is changed from 50k to 10k, respectively, which result in increased noise floor. Although the threshold level increases depending on the size of data acquisition system window, the performance of the noise threshold in the fault detection is still expected to be maintained. In general, the adaptive scheme can be applied to various systems including the ones under arbitrary noise condition or a different system application if the noise statistics of the input signal to the system are measured to determine the threshold which adaptively changes its level and maintains the performance expectation.

B2. Comparative Evaluation over Existing Schemes

Definition of predetermined thresholds (PT) has been adopted from previous diagnostic studies. The PTs can be determined based on the user's expectation of fault severity which is a simple and efficient way to derive fault severity indication.

In the meantime, PTs in the literature have commonly been designed and applied to diagnosis based on limited analysis and, hence, their performance evaluation has been insufficient. Primarily, detection and decision-making through PTs have been made only based on relative signature amplitude (dB) without consideration of signal statistics, so may not be flexibly applied under the non-stationary noise conditions of a motor current signal in industry. To prevent diagnostic failures in noisy environments, PTs are commonly designed sufficiently higher above the commonly expected current noise level to detect strong fault signatures. Meanwhile, PTs can hardly prevent diagnostic failure in small signature detection which might significantly limit the capability of a diagnostic system in industrial application.

In [27], threshold definitions are derived with a pre-determined percentage of the line current signal amplitude which is a simple and efficient way to initially evaluate the severity of a fault condition in an induction motor. Fig. 2.14 shows one of the adopted PT definitions (1% of the fundamental current signal) to detect severe fault. The PT (-40dB) is effectively the same when $n=42$ in the analysis through the proposed technique. It is shown that all the fault signatures and harmonics detected in Fig. 2.12 are below the PT (-40dB) in Fig. 2.14 which result in critical missing detections due to high n. Reducing a PT close to $n=1$ (-72dB) to detect further smaller signatures will challenge

detection reliability because of non-stationary noise interferences. This can be theoretically predicted in Fig. 2.5; as *n* increases, false detection probability decreases to zero. Meanwhile, detection probability becomes aggravated if *n* is too large and results in serious missing detection.

In [26], threshold definitions (PTs) for the eccentricity signature detection are pre-determined with the following classifications of relative signature amplitude (dB); less than -60dB good, between -60dB to -40dB tolerable, and higher than -40dB severe as shown in Fig. 2.15. The designed threshold in this study shows a much lower level (with *n=1*) which allows signature detection up to -72.45dB which is lower than any PTs in [26]. The conventional PTs have been designed at a relatively higher level to avoid noise interference as the instantaneous noise variation is commonly not reflected in the design stage.

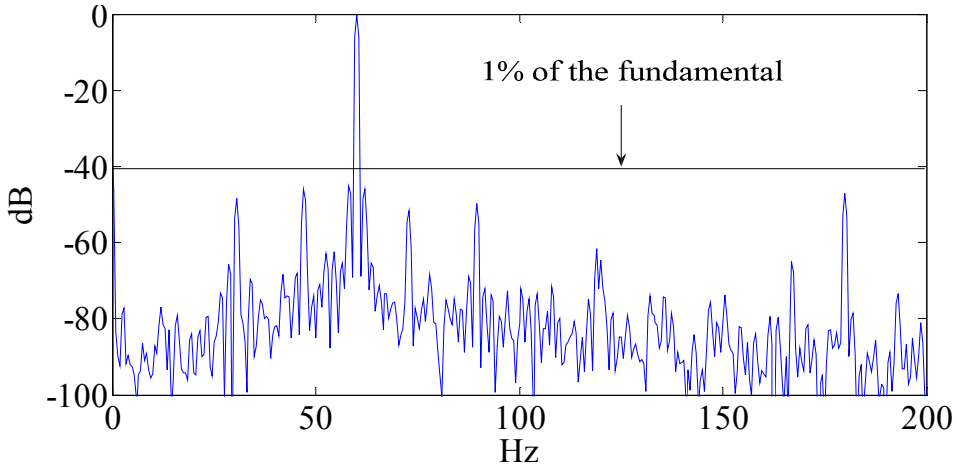

Fig. 2.14. FFT spectrum of the line current (predetermined threshold based the % of fundamental) (utility driven under 70% torque).

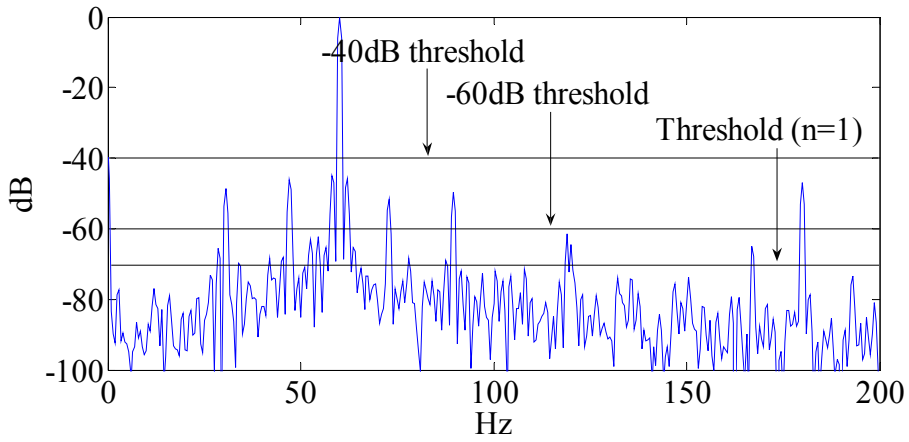

Fig. 2.15. FFT spectrum of the line current (predetermined threshold) (utility driven under 70% torque).

Utilizing the precisely measured noise ambiguity of a current signal and the adaptively determined threshold, the signature detection and the decision-making stages can be reliably performed until the noise-like level in a motor current spectrum.

C. Statistical Decision-Making for Multiple Signatures

The threshold-based diagnostic routine in Fig. 2.2 is applied to the motor current signal to make a reliable decision for multiple signatures in a motor current spectrum. The characteristic frequencies of eccentricity and broken rotor bar fault are utilized in the experiments as follows [38]:

$$f_{eccentricity} = \left[1 \pm m\left((1-s)/(p/2)\right)\right] f = f + mf_r, \;\; m = -1,\, 1,\, 3,\, 5 \tag{2.19}$$

$$f_{borken\_bar} = \begin{cases} (1 \pm 2s) f, \\ (5 - 2(k+1)s) f, \\ (7 - 2(k+1)s) f, \end{cases} \qquad k = 1, 2 \tag{2.20}$$

where s is the per unit slip, f is the fundamental frequency of the stator current , p is the number of poles, and f_r is the mechanical rotation frequency.

For a clear performance analysis without misleading results from the FFT frequency leakage effect [22][40][41], the signatures that are clearly discriminated from the high order fundamental harmonics are considered in (2.19) and (2.20).

Figs. 2.16 to 2.17 show the detection of fault signatures in a motor current spectrum at low torque ranges of 15%~50% and high torque ranges of 55%~100% of the test motor through the proposed threshold. The fault signatures are numbered in an increasing order from low to high frequencies in the x-*axis* based on the characteristic frequencies specified in (2.19) and (2.20). Test results are obtained through 5 independent detection trials for every 5% torque from 15% to 100%. $n=3$ is assumed in the experiment, where a false alarm rate is expected to be less than 0.002 in Fig. 2.5.

In Fig. 2.16, the detection of the eccentricity fault signature is shown high enough with the 1st and 2nd signatures and comparatively low with the 3rd and 4th signatures. The overall detection is degraded at high torque ranges of the motor operation due to the damping effect of the load. The very small 3rd and 4th signatures are assumed to be reliably detected when the instantaneous noise condition is favorable for decision-making which results in a sufficiently low threshold level.

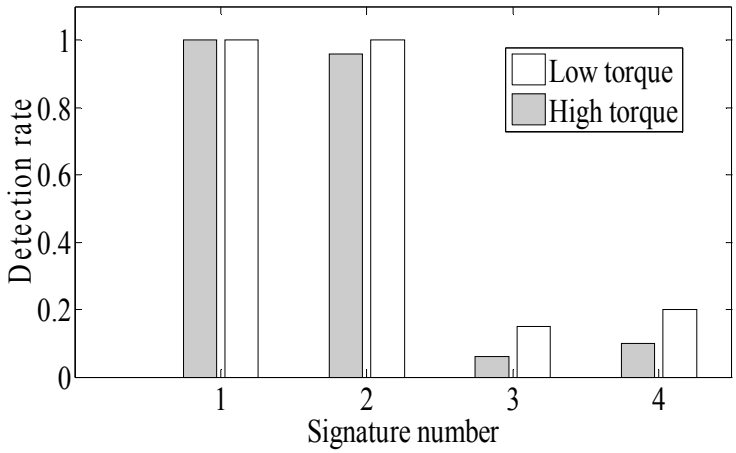

Fig. 2.16 Detection rate of eccentricity signature.

As shown in Fig. 2.17, the detection rate of the dominant 1st and 2nd broken rotor bar fault signatures is lower than the 3rd, 4th, and 5th signatures at low torque range. This is because the 1st and 2nd signatures are easily merged with the fundamental frequency at a light load of the test motor in the FFT current spectrum. Meanwhile, the 3rd, 4th, and 5th signatures are comparatively far away from the nearest fundamental harmonic signal and more reliably detected. Better detection is observed at high torque levels because the broken conductor in a rotor becomes more evident under high rotor current at high load torque.

The results in Figs. 2.16 and 2.17 show similar detection performance as the conventional diagnostic thresholds in the literature. It should be noted that, unlike conventional schemes, the performance of the threshold is precisely controlled from the early design stage. During the whole experiment, the false detection rate is close to zero as the threshold is designed with the false alarm rate of 0.002 which is expected to guarantee detection accuracy of 99.8 %.

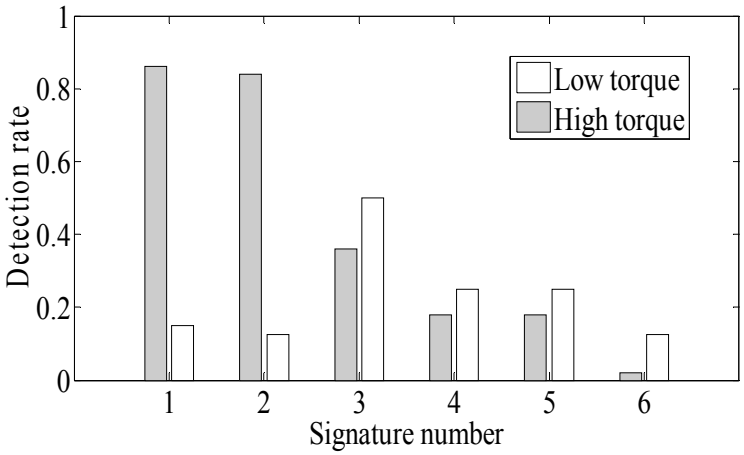

Fig. 2.17. Detection rate of broken rotor bar signature.

Figs. 2.16 and 2.17 show that the detection rate changes depending on the motor operating points when experimented at various torque levels. Even though there is an existing signature at a fault characteristic frequency in a motor current spectrum, the precision of the detection is significantly affected by the motor operating point as the fault signature amplitude and noise statistics varies almost non-linearly under different conditions. Therefore, to maintain the same detection quality, the application of PTs is strictly required to be updated based on a multi-dimensional parameter set such as speed, torque, excitation frequency, motor specification, work environment, etc. which is expected to result in serious computation complexity in industrial applications. The derived threshold in this study is basically designed to perform detection and decision-making adaptively to those instantaneous variations, the net effect of which is measured as noise statistics resulting in independent model detection.

From the one-to-one mapping function between detection probability and SNR value as in Fig. 2.5, the detection rate in Figs. 2.17 to 2.18 can be efficiently utilized to

determine the asymptotic SNR in the experiment. Fig. 2.18 shows the computed SNR for the detections in Figs. 2.17 to 2.18. It is shown that the detections are performed to an extent close to SNR 0 dB. For example, the signatures with SNR=1 dB are shown to be successfully detected through the employed threshold definition which signature amplitude is expected to be too close to the current noise floor to be considered a reliable result in industry. The designed threshold definition in (2.18) is adaptively determined according to the analyzed noise statistics which provide reliable detection, even for small signatures with 1dB SNR, with 99.8 % accuracy.

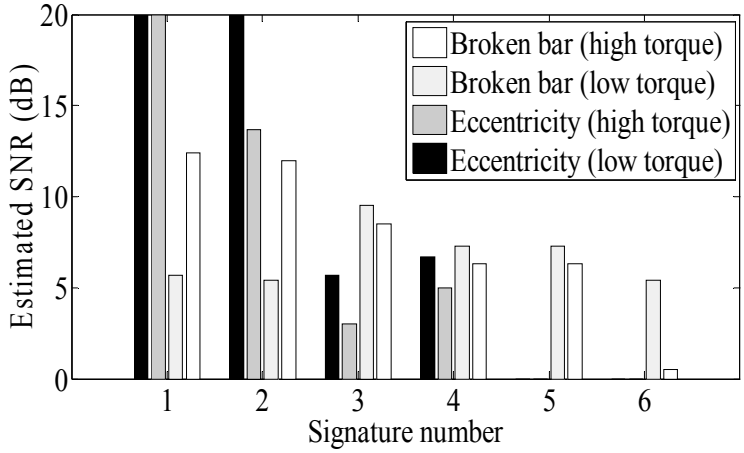

Fig. 2.18. Estimated SNR.

2.5 Conclusion

This section has presented a threshold-based fault signature detection strategy utilizing noise statistics in a motor current spectrum. The results have been verified both mathematically and experimentally. To provide an accurate presentation of the threshold

design under noisy environments, the proposed techniques are supported by detailed statistical theory which is expected to provide clear insight into the exact performance and precise threshold design for industrial applications.

It has been theoretically analyzed and experimentally verified that the designed threshold provides completely predictable, maintainable, and controllable error performance during the decision-making stage which is achieved independently from the signal processing window size, the applications environment, and the operating point of a motor. This becomes possible as the parameters of the threshold definition are obtained through non-stationary noise statistical analysis of the target motor current signal where unexpected variations of a noise have been compensated in the threshold design stage. It is also experimentally demonstrated that the derived threshold provides a higher resolution than any other pre-determined threshold (PT) definition in the literature while maintaining sufficiently higher reliability. The model independency and high resolution features during fault signature detection and decision-making enhance the reliability of diagnostic implementations in harsh and noisy industrial environments.

CHAPTER III

SEMI-BLIND FAULT DETECTION TECHNIQUE THROUGH UNEXPECTED FEEDBACK ERROR MANAGEMENT IN INDUCTION MOTOR DRIVE

3.1 Introduction

This section presents a semi-blind fault detection technique using advanced speed feedback error management for the induction motor drives. Typically, the speed feedback errors can be tolerated by various ac drive systems unless they are above a certain threshold; however, the same error can easily disturb the frequency sensitive diagnosis systems. The speed errors occurring either in sensored or sensorless feedback systems are mainly caused by measurement imperfections, low sensor resolution, noise and parameter deviation adversely affecting the speed observers, or non-stationary interference to the relevant system. The reliability of motor condition monitoring, especially within a short diagnostic time, depends on the instantaneous error management of the feedback system as the characteristic frequency of a fault signal should precisely be determined based on accurate speed measurement and stator excitation frequencies. In this dissertation, the proposed algorithm includes a speed error-immunized diagnostic technique and addresses low cost implementation. It has been theoretically analyzed and experimentally verified that the sensitivity of a fault diagnosis to speed feedback errors can be minimized utilizing a two-step semi-blind diagnostic technique with a coarse-to-fine detection procedure. Implementation of exhaustive coarse-to-fine detection employing a low cost microcontroller is done

through computation complexity and memory occupancy minimization strategies. The proposed algorithm is verified through a 3-hp motor generator setup.

3.2 Background and previous research work

The fundamental assumption of the MCSA-based diagnostic techniques depends mainly on the interaction between the stator current and the electromechanical structure of the motor. Various faults in induction machines are known to create specific signatures in the motor current spectrum due to the inherent coupling. In the literature [1][3][26][31][43], the stator current spectrum exhibits abnormal harmonic modulation where the observed frequencies are generalized as so-called fault characteristic frequencies. By monitoring and analyzing the irregularities of those harmonics, diagnosis has been efficiently performed to determine the fault conditions.

A diagnostic analysis tracking the characteristic frequencies at which only the fault signatures are expected in a current spectrum has been popularly suggested and implemented with reduced computational complexity and low memory occupancy on a microcontroller [1][3][31][26]. One of the most effective noise-immunized detections is also achieved when the analysis focuses on a specific fault frequency tone in a spectrum such as in the Park transform-based analysis (PTA)[22][28], the Phase sensitive detection (PSD) [26], and the related Correlation-based analysis (CA) techniques [31]. The matched filter (MF) theory in [31] has clearly provided the theoretical background showing the low complexity and the high noise suppression of those signature-based diagnostic techniques [26][31][50][65]. Reduced complexity and high performance turns

these techniques into a practical tool which can be directly combined with motor control algorithms without violating the microcontroller utilization.

In alternative signal processing strategies doing whole or partial spectrum analysis [27][49][64], non-fault related frequency tones have been redundantly analyzed requiring additional computation complexity, detection time, and memory occupancy in a microcontroller system. In [64], the multi-signal classification (MUSIC) achieves acceptable noise-immunized detection but takes a relatively long computation time to find fault frequencies of interest through the auto-correlation matrix. To reduce the computational burden, the zoom-MUSIC (ZMUSIC) is proposed to analyze the specific frequency band which acceptably reduces computation time and memory occupancy [27]. Similar work is proposed for the zoom-fast Fourier transform (ZFFT) [49] to principally minimize redundant spectral analysis in the FFT-based diagnosis. Further optimization of those schemes needs to be successfully implemented on a microcontroller with further limited system resources in industry.

Allowing a practical and low complexity implementation, the technical challenge of a specific signature-based diagnosis [1] [3][26][31][50][65] is a serious performance loss even with tolerable speed feedback errors in motor control. With an increased tendency toward sensorless control of AC motor drives in industry, the reliability of a diagnosis under a speed feed\back error has become more practical [43][48][50]. Many sensorless feedback schemes in the literature are known to have an inherent dependency on numerous speed-dependent motor parameters and their estimation accuracy resulting in non-negligible reliability issues as tracking non-linear variations of those parameters is

another challenging task.

The assumption of precise fault frequency information of a fault signal or accurate speed feedback system in an AC drive is not practically valid in industry where an ideality assumption might result in diagnostic failure even with a small amount of error. If a diagnosis is performed in a short time, the detections will become susceptible to instantaneous speed feedback errors resulting in non-negligible reliability issues. In [31], the MF (matched filter)-based detection is analytically derived assuming an ideal condition and is mathematically proven to have an optimal performance maximizing output signal to noise ratio (SNR). However, the MF loses optimality if it is performed with a frequency/phase information error of a fault reference signal. The PSD (phase sensitive detection), PTA (Park transform analysis), and CA (correlation-based detections) in [26][65] that utilize the optimal property of the MF are inherently exposed to performance degradation with a frequency error. The maximum covariance method for a frequency tracking (MCMFT) [28] is a proposed technique with near optimal performance in noise suppression and spectral resolution in the specific frequency band analysis. When the tracking range begins to be reduced while focusing only on a specific frequency band of interest, the computation complexity is reduced maintaining optimality but becomes sensitive to frequency errors or variations resulting in non-negligible reliability. In fact, optimality and reliability are truly important performance features for the diagnostic schemes but practically challenging in real time applications.

Recently, more robust diagnostic techniques are suggested which can minimize speed error sensitivity. Some of these techniques are restricted by motor operating point.

The FFT analysis has been popularly adopted to monitor the current spectrum using the steady state assumption. In [50], the signature-based diagnosis of rotor asymmetry is performed while the vehicle motor is at zero speed. In [12], by disconnecting supply and inducing voltage, rotor flux is utilized for the detection. Without the operating point restriction, some other analyses have been adopted based on more complicated signal processing techniques. In [48], a robust prediction and detection is achieved by utilizing dynamic recurrent neural networks, FFT-based, and wavelet-based analysis. In [14], the general roughness estimation of a bearing is performed through a Wiener filter (WF). In [52], the diagnosis based on the Vienna Monitoring method (VMM) is performed by eliminating its sensitivity to the speed position sensor. In general, a sensorless diagnosis has been performed with a strict restriction on the motor operating point or else serious computation complexity is involved which requires excessive system capacity for industrial application.

For a reliable application in a harsh industrial environment, suggested diagnostic schemes are to be primarily robust to speed feedback errors while maintaining sufficiently low complexity for microcontroller-based real time implementations. This has still been highly challenging. The PTA efficiently performs fault signal tracking by converting the target fault frequency to an equivalent DC signal in a rotating frame similar to vector control reference frame approaches using speed feedback information for motor control. Fig. 3.1 (a) briefly shows the case when the synchronization is lost due to instantaneous speed feedback error in an assumed short diagnosis time which will potentially fail to convert the fault harmonic vector to a DC signal. An error adjustment

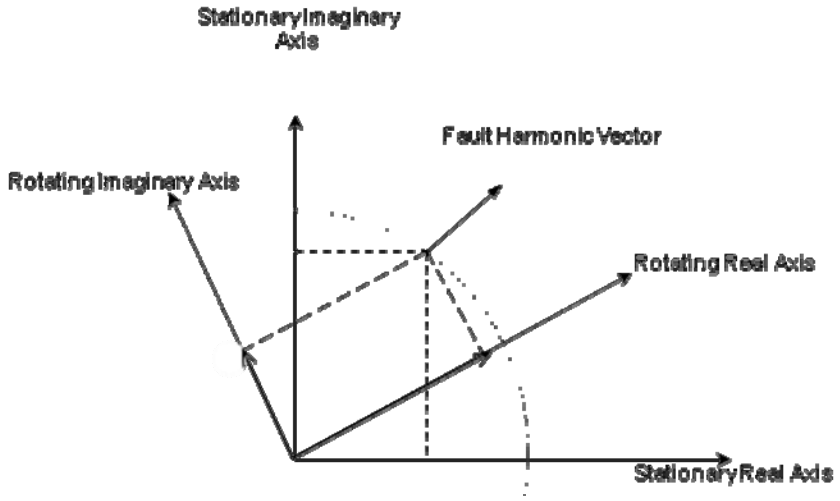

(a)

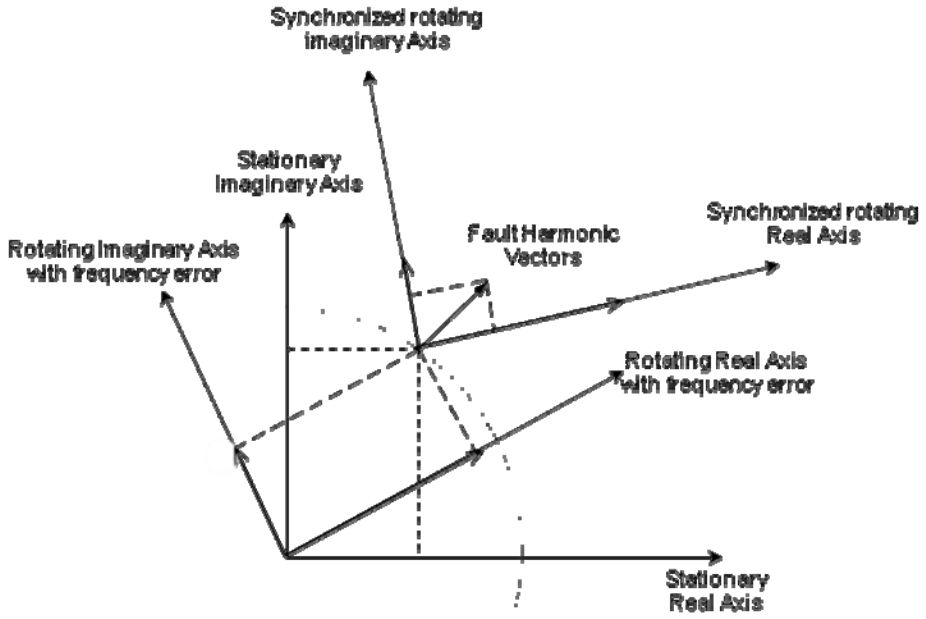

(b)

Fig. 3.1. Park transform-based fault signal tracking: (a) lost synchronization and (b) re-synchronization through error adjustment.

is needed to re-synchronize the rotating frame as shown in Fig. 3.1 (b) which commonly requires exhaustive unknown-error tracking and has been neglected in many diagnostic techniques until recently.

In this dissertation, by assuming non-ideal erroneous speed feedback in an AC drive system, two-step semi-blind detection is proposed which is designed to measure and compensate the unknown speed feedback error parameters during fault diagnosis while maintaining sufficiently low complexity in implementation. The two-step diagnosis consists of the coarse estimation and fine adjustment. The coarse estimation is the conventional fault characteristic frequency prediction assisted by speed feedback information. The fine adjustment for the imperfect measurement in the coarse estimation step is performed through a blind search for potential error parameters without additional signal information input. The semi-blind coarse-to-fine detection technique that commonly requires exhaustive error search computation is significantly simplified in this dissertation. This is achieved by means of the proposed complexity reduction and memory occupancy minimization strategies which allow a direct combination of the speed feedback error-immunized diagnosis with a motor control routine using a single microcontroller.

3.3 Coarse estimation

The proposed diagnostic procedure consists of coarse estimation and fine adjustment. The coarse estimation is presented in this section. During coarse estimation, the speed feedback estimation is considered a part of the coarse estimation procedure by which an

initial prediction of a fault characteristic frequency is achieved. From the dependency of fault frequency estimation on the slip/speed accuracy [1][3][26][31][43], the error range of the coarse estimation is statistically identified and will be used during algorithm optimizations later.

A. Error Range Assumption of Slip/Speed Estimator

The performance evaluation of a diagnostic scheme requires a comprehensive analysis under numerous error conditions. It includes erroneous measurement variables and parameters such as inductances, resistances, current signal, and voltage signal under non-linear motor operating conditions such as iron saturation and temperature variation or unknown interferences to the feedback system [65]. In this study, a performance oriented evaluation of a diagnostic scheme is efficiently done by assuming a zero mean Gaussian distribution model for the statistics of those numerous errors.

Initially, the slip/speed estimation error, which is caused by error conditions with the Gaussian distribution, can be assumed to follow the same distribution as briefly depicted in Fig. 3.2 which will be experimentally validated later. One can note from the figure that the majority of the slip/speed errors are expected to occur within a limited range. The element of the slip/speed error s_{err_j} is initially assumed to be primarily distributed within a certain range as follows:

$$s_{err_j} \in \left[s_{err\,\min}, s_{err\,\max} \right] \tag{3.1}$$

where $j = 1, 2, \cdots$ and $s_{err\,\min} = -s_{err\,\max}$ is assumed.

The probability that error falls in the range in (3.1) is statistically derived as follows:

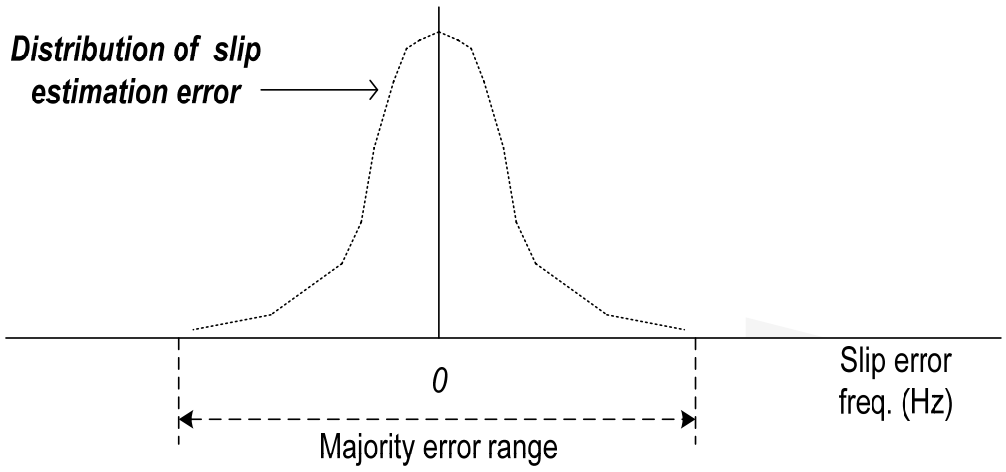

Fig. 3.2. Probability distribution of slip error assuming Gaussian distribution.

$$P = \Pr\{|\, s_{err_j} \,| < s_{err_{\max}}\} = 1 - 2Q(\alpha), \tag{3.2}$$

where $Q(\alpha) = \frac{1}{\sqrt{2\pi}} \int_{\alpha}^{\infty} e^{-x^2/2} dx$, $\alpha = s_{err_{\max}} / \sigma$, and σ is the standard deviation of the distribution.

Fig. 3.3 shows the cumulative probability distribution of feedback errors through (3.1) to (3.2) assuming quite large error statistics of 0.125 Hz, 0.25Hz, and 0.5Hz standard deviation. One can determine from the probability distribution that those errors primarily arise within a limited range with each standard deviation. For example, with a standard deviation of 0.125Hz, most errors (more than 99%) are expected to arise within 0.3Hz. Therefore, the efficient performance evaluations of a diagnostic scheme assuming a limited error range of a speed estimator become a theoretically valid assumption.

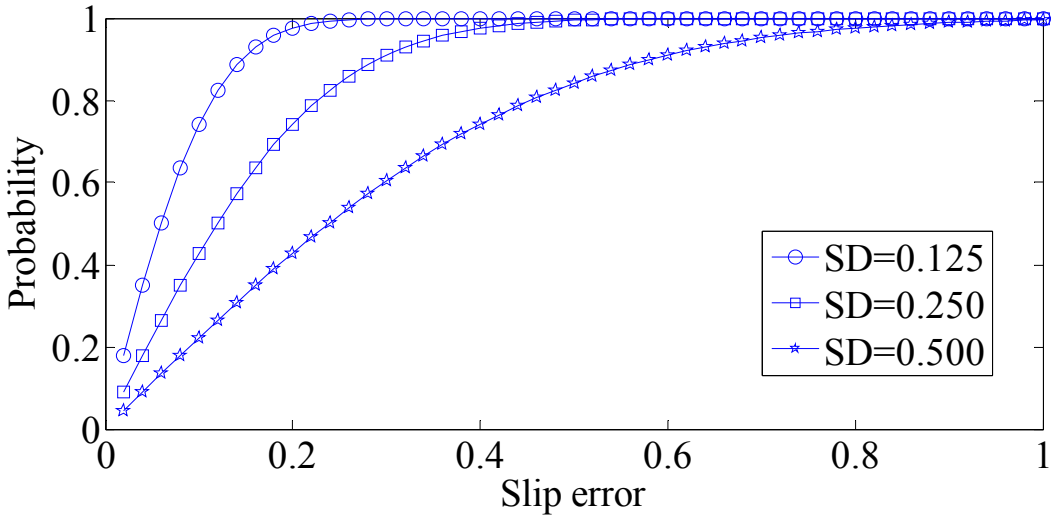

Fig. 3.3. Probability of slip error (Hz) for each standard deviation (SD).

B. Coarse Fault Frequency Estimation and Potential Error Range

Fig. 3.4 briefly shows the proposed two-step diagnostic procedure. In this section, the coarse fault frequency estimation and its potential error range is statistically identified. The eccentricity fault is considered in the analysis which is expected to clearly show the capability of the proposed algorithm for later experiments under a wide amplitude variation of a fault signature versus load. The initial estimation of the dynamic eccentricity characteristic frequency is done based on the fault equations as follows [1] [3][31][26]:

$$f_{eccentricity} = \left[1 \pm m\left(2\frac{(1-s)}{p}\right)\right] f = f \pm m f_r, \;\; m = 1,2,3,\cdots \tag{3.3}$$

where s is the per unit slip, f is the fundamental frequency, f_r is the mechanical rotation frequency, and p is the number of poles.

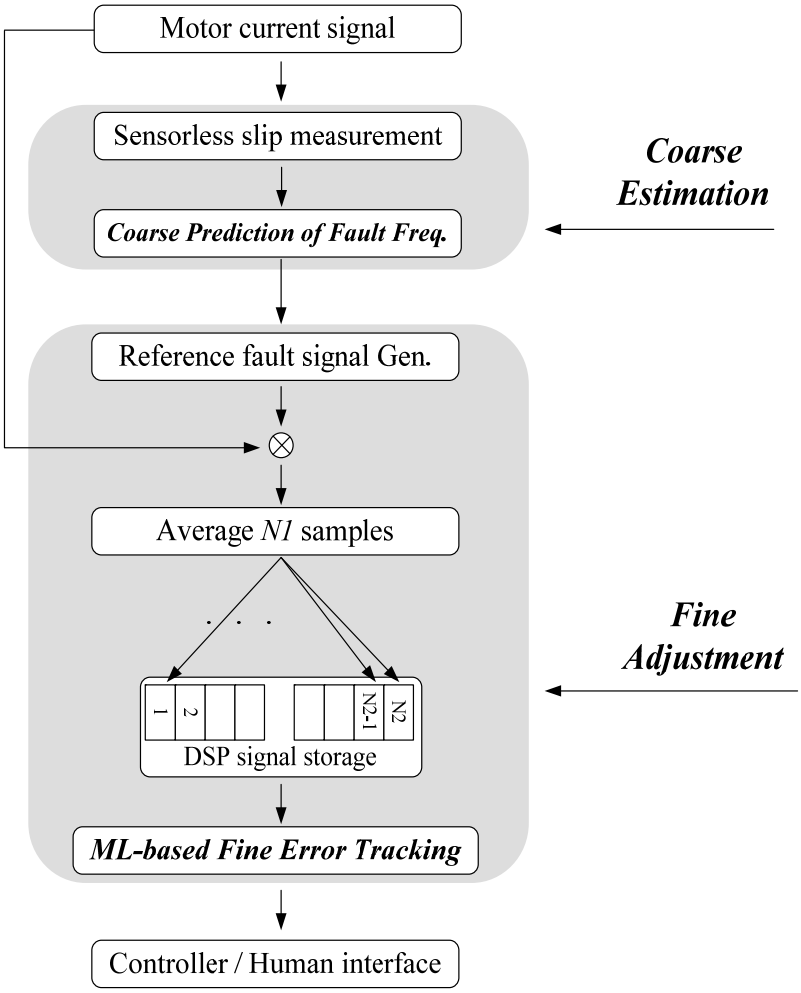

Fig. 3.4. Proposed coarse and fine estimation.

The coarse estimation in (3.3) is the popular fault frequency measurement technique which has been adopted assuming accurate slip/speed estimation in many diagnostic techniques. Depending on the slip/speed feedback information in an AC drive, the coarse estimation in (3.3) becomes susceptible to the instantaneous slip/speed errors resulting in coarse estimation error f_{err} as follows:

$$f_{eccentricity\_err} = \left[1 \pm m\left(\frac{2\left(1-(s+s_{err})\right)}{p}\right)\right] f = f_{\ eccentricity} + f_{err} \tag{3.4}$$

where

$$f_{err} = \mp\left[2m\left(\frac{s_{err}}{p}\right)\right] f \tag{3.5}$$

From the linear operation of the slip error parameter s_{err} in(3.5), the coarse estimation error f_{err} is expected to follow a similar statistical error distribution as in (3.1) which is derived as follows:

$$f_{err_j} \in \mp\left[2m\left(\frac{\left[s_{err\,\min}, s_{err\,\max}\right]}{p}\right)\right] f = \left(\frac{2m}{p}\right)\left[s_{err\,\min}, s_{err\,\max}\right] f \tag{3.6}$$

The error range of the initial coarse estimation of an eccentricity characteristic fault frequency in (3.3) is statistically identified in (3.6). The probability of the error can be calculated in the same way as in (3.2).

3.4 Fine error adjustment

This section presents the fine error adjustment of the initial coarse estimation. The fine adjustment of the potential error in fault frequency in (3.6) will lead to a precise fault diagnosis of an induction machine while minimizing missing or false diagnosis possibility. The proposed fine adjustment procedure consists of three steps: shifting fault information to low frequency (step 1), averaging the low frequency signal (step 2), and ML-based semi-blind error detection for the averaged signal (step 3) which are shown in Fig. 3.3. The three-steps of fine adjustment will be elaborated in the following sections.

A. Shifting Fault Information to Low Frequency

Precision of a diagnostic analysis is commonly limited by the available signal acquisition window within a limited memory capacity in a real time system. Due to the assumed limited resource in an embedded DSP system, the acquired current signal prefers to be processed in a realtime fashion without signal storage as suggested in the literature [26][31]. Realtime processing has a great advantage in a cost effective diagnostic implementation but is inherently sensitive to mis-information or error of a fault signal such as frequency or phase offsets, etc. Once unexpected errors occur, re-evaluation of previous data is no longer available, therefore system robustness is basically limited.

Storing a large amount of data within an embedded DSP system is practically impossible. Data size of a signal needs to be compressed considering limited memory capacity. Here, the suggested compression strategies are realtime signal averaging and signal size reduction which are explained in section *B*. An effective averaging with minimal loss of original signal information of interest is done if, and only if, a fault signal is expected at very low frequency because the averaging is a kind of low pass filtering without interfering with the low frequency signal. This will be mathematically elaborated in the following sections.

To perform successful averaging later in section *B*, a fault signal with frequency determined by the motor operating point as in (3.3) is strategically shifted to a low frequency. The scheme removes carrier frequency in the transmitted communication signal at the signal receiver and sends the signal to the base band (low frequency) for

later fine data processing. In this study, the technique is used to remove excitation frequency f and rotor frequency f_r in (3.3) which eventually shifts the fault signal to zero frequency in an ideal case. By adopting the most simplified procedure, the current signal in (3.9) is multiplied by the expected reference fault signal in (3.8) which is as follows:

$$I_{Stator\_new} \approx I_{fault} + \varpi_1, \qquad if \;\; w_{\exp} = w_{fault} \tag{3.7}$$

where

$$I_{\exp}[n] = 2\cos[w_{\exp} n + \varphi_{fault}] \tag{3.8}$$

$$I_{stator}[n] = I_{fault}\cos[w_{fault} n + \varphi_{fault}] + H_{harmonics}[n] + \varpi[n] \tag{3.9}$$

n is the positive integer, $I_{\exp}[n]$ is the expected fault signal, and $I_{stator}[n]$ is the current signal, $H_{harmonics}[n]$ is the fault irrelevant harmonic signal, I_{fault} is the fault signature amplitude, φ_{fault} is the phase of the fault signal, $w_{\exp}$ is the estimated fault frequency, w_{fault} is the fault frequency, ϖ is the noise, and I_{Stator_new} is the processed signal output between (3.8) and (3.9).

The information of fault signature amplitude I_{fault} is now observable at DC (0 Hz) in (3.7) which is at w_{fault} in the current signal in (3.9). Other harmonics in (3.9) are not considered for diagnosis in (3.7) as they are not in the fault frequency area of interest which is DC (0Hz). The excitation frequency f and rotor speed f_r which determine the fault frequency are no longer considered in (3.7) which later significantly simplifies the fine error adjustment with reduced frequency ambiguity. Here, the fault frequency prediction in (3.4) is now simplified as follows:

$$f'_{eccentricity\_err_j} = f_{err} \tag{3.10}$$

The statistics of the simplified fault frequency in (3.10) are expected to follow the same distribution as the error range in (3.6). The frequency error element f_{err_j} in (3.6) is still effective in a new fault frequency in (3.10) which is a redefined offset as follows:

$$f_{offset} = f_{err_j} \tag{3.11}$$

The majority of error offset in (3.11) is assumed to arise close to 0Hz as shown in Fig. 3.1 and as derived from (3.3) to (3.6).

B. Averaging Low Frequency Signal

By utilizing the fact that the fault signal information is now at a very low frequency range as in (3.11), the averaging is performed in realtime fashion for the signal in (3.7) which will be achieved with minimal loss of target information of interest.

Fig. 3.4 briefly shows the averaging procedure in fine adjustment steps. Realtime averaging is performed for the *N1* consecutive signal sample and then simply stored in time order in *N2* DSP memory as follows:

$$x_i = \frac{1}{N_1}\sum_{d=1}^{N} I_{Stator\_new}[d + (i-1)N_1] \tag{3.12}$$

where $i = 1, 2, \cdots N_2$. The signal averaging technique in [31][53] is modified and elaborately demonstrated for this purpose.

The maximum analysis boundary of the averaged signal in (3.12) is as follows from the Nyquist sampling theorem:

$$B < f_{sampling} / (2N_1) \tag{3.13}$$

The signal averaging with minimal loss of target information of interest is made possible by assuming the fault signal period is much larger than *N1* as follows:

$$f_{sampling} / \left| f_{err_j} \right| >> N_1 \tag{3.14}$$

By assuming that the fault frequency error *ferrj* in (3.11) is close to 0 Hz and the left-hand side is much larger than the right-hand side, the fault frequency information is practically not lost in the averaging while the fault irrelevant signal, in which signal period are much smaller than *N1,* will be removed through an averaging process like the operation of a low pass filtering. This is why complex low pass filtering through convolution operation is not adopted in this algorithm for further computational complexity reduction.

The *N1* size signal is represented with new *N2* samples in (3.12), which is an effectively down sampled version with averaging. The effective down sampling rate (%) in (3.12) is described as follows:

$$\% = (N_2 / N) \times 100 \tag{3.15}$$

Depending on the down sampling rate in (3.15), the memory requirement for signal storage is expected to be reduced and system capacity for the computation is expected to be relieved on a microcontroller with minimal signal processing loss.

A similar implementation strategy, presented in the literature [14][27][51], has reduced computational complexity and minimized memory requirement for signal storage mainly through decimation and low pass filtering for a target fault signal. Those

studies have shown a promising implementation strategy of a complex algorithm in low cost DSP systems utilizing reduced signal size. In this study, it is achieved without the use of complex low pass filtering but with a simple realtime averaging of a signal. The effectiveness of the proposed strategy will be experimentally verified with the precise information of fault signature amplitude in the averaged signal with negligible signal processing loss.

B1. Improving Analysis Resolution of Averaged Signal

The averaged signal shows relatively low resolution, especially around DC (0Hz), since the low frequency signal requires a relatively long signal period to identify its characteristics such as frequency, phase, and amplitude. To improve the analysis resolution during diagnosis, the $w_{\exp}$ in (3.8) is strategically biased as follows:

$$w'_{\exp} = 2\pi \times \left(f_{\exp} + f_{bias} \right) \tag{3.16}$$

The frequency offset in (3.11) can be expressed as follows:

$$f'_{offset} = f_{err_j} + f_{bias} \tag{3.17}$$

The bias frequency f_{bias} can be inserted maintaining the same analysis limits from (3.13) to (3.14).

The bias technique can be applied without loss of generality in the whole algorithm implementation. The error range is the same as the fault frequency ranges in (3.6). Only the error is biased with f_{bias}. With known statistics as in (3.6), similar equations can be

derived and applied as in (3.7) to (3.11). The effectiveness of the technique will be experimentally verified.

C. ML-Based Semi-Blind Fine Error Adjustment

Successful diagnosis of an induction motor largely depends on the efficient unknown offset error management in (3.11) which is fundamentally caused by the imperfection of a speed feedback system in AC drive. Here, by utilizing the fact that most errors expectedly occur in a limited range as in (3.1) to (3.2) and the parameter dependency of fault characteristic frequency in (3.7) is minimum, the blind error adjustment is further simplified and applied only to the statistically expected error range in (3.6). The maximum Likelihood (ML) scheme is efficiently utilized to blindly search for potential errors without any additional information which is the maximum of the periodogram as follows [31] [53][62]:

$$\hat{f}_{ML} = \arg\max_{f} \left| \frac{1}{N_2} \sum_{n=1}^{N_2} x_n e^{-j2\pi fn} \right| \tag{3.18}$$

where x_n is the averaged signal. The maximum of the periodogram in (3.18) is expected to yield the amplitude of the error compensated fault signal I_{fault} and $\hat{f}_{ML}$ is expected to yield the frequency offset error f_{offset_j} defined in (3.11) as follows:

$$\hat{f}_{ML} = f_{offset_j} = \arg \max_{f_{offset_j}} \left| \frac{1}{N_2} \sum_{n=1}^{N_2} I_{fault} e^{-j2\pi f_{offet_j} n} e^{j2\pi f_{offet_j} n} \right| = \arg \max_{f_{offset}} \left| I_{fault} \right| \tag{3.19}$$

where $x_n \approx I_{fault} e^{j2\pi f_{offet_j} n}$ in complex notation for simplicity

The frequency step size in fine adjustment operation is defined as follows:

$$\Delta f = \frac{f_{err_{\max}}}{N_r} \tag{3.20}$$

where N_r is the number of applications of the ML scheme during fine adjustment processing.

Unlike the optimal frequency tracking scheme (MCMFT) in [28] where the tracking step size is chosen depending on motor operating point, which inherently has wide variations, in this study, it is efficiently determined based on the limited fault frequency error range in (3.6) with minimal variation as the frequency variations are primarily suppressed through (3.7) to (3.11).

Similar implementation strategies have been pursued in the literature such as ZFFT and the ZMUSIC techniques [27][28] which have achieved a reduction in computational complexity and memory requirement in the DSP implementation by analyzing a limited frequency range or bandwidth of interest. The analysis range is more efficiently limited and optimized only to the statistically expected error range caused by a feedback system which significantly minimizes redundant tracking complexity in the implementation without violating the CPU utilization.

Therefore, the overall computation complexity and memory occupancy minimization strategies adopted in this study simultaneously utilize an efficient time and frequency domain approach: size compression of time-domain signal in *section B* and minimization of frequency-domain tracking range in *section C*, respectively.

D. Overall Diagnostic Procedure of Coarse-to-Fine Adjustment

Fig. 3.5 shows the proposed two-step diagnostic procedure in the frequency domain. In the coarse estimation step, the prescribed motor current spectrum is shown with the fault frequency interval which is estimated by the coarse estimation equation in (3.3). In the fine adjustment step, for an efficient tracking of expected errors in the coarse estimation, the information of the fault frequency and error content is first shifted to the vicinity of 0Hz through (3.7) to (3.9). The errors, expectedly localized around 0 Hz, are statistically identified and blindly searched through the ML adjustment scheme in (3.18) to (3.20). The coarse-to-fine detection is similar to the strategy in Fig. 3.2 (b) which is expected to adjust the rotating frame synchronization against potential frequency errors.

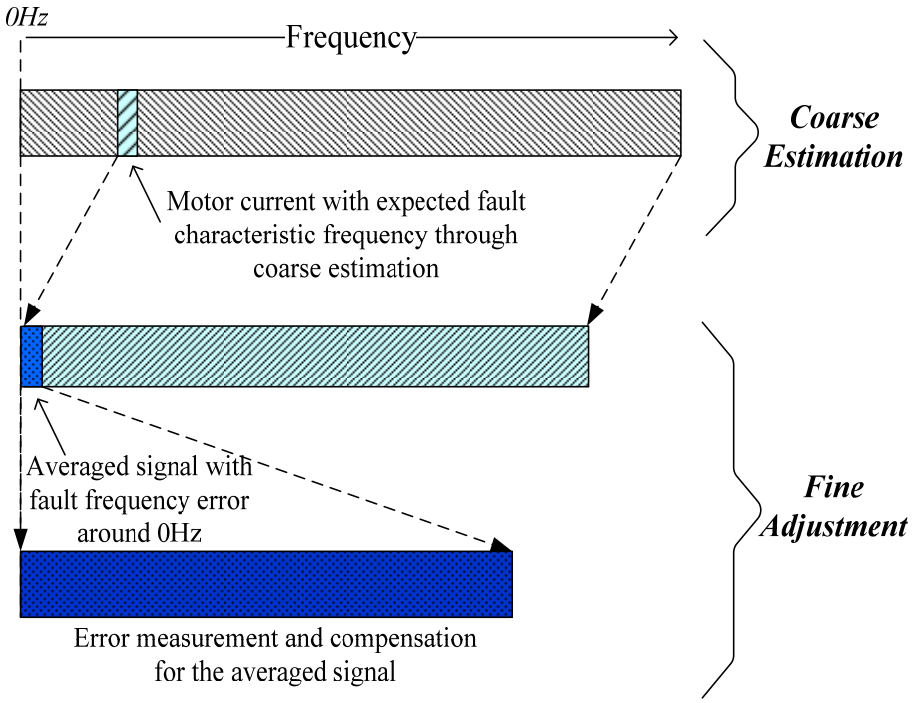

Fig. 3.5. Proposed diagnostic signal processing procedure in frequency domain.

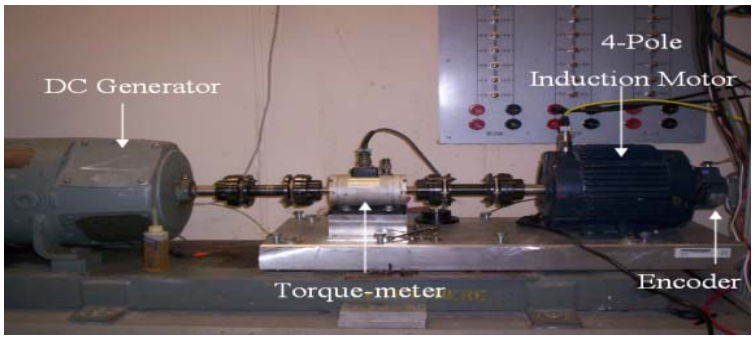

(a)

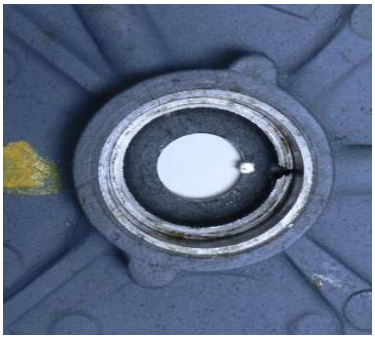

(b) (c)

Fig. 3.6. Experimental setup: (a) 3-hp motor-generator setup, (b) stator of test motor, and (c) stator cover with static eccentricity.

3.5 Offline experimental result

Table 3.1. System Environment 2.

Data acquisition board	NI-DAQmx (12Bit ADC)
Motor/# of pole	3 hp IM / 4
Rr/Ls(=Lr)	0.0727 Ohm/0.079 H
N1	125
N2	200
Δf	0.08 Hz

Offline experiments are performed to demonstrate the performance of proposed diagnostic procedures illustrated in Figs. 3.4 to 3.5, in the time and the frequency domains. The test induction motor is loaded by the DC generator as shown in Fig. 3.6 (a) which is re-machined and has off-centered bearing houses to create artificial eccentricity fault (c). The raw current signal used for the experiment is acquired through the data acquisition setup with the 12 bit analogue digital converter (ADC) and 25 kHz sampling frequency as shown in Table. 3.1.

Fig. 3.7 (a) shows the acquired motor stator current signal in the time domain with signal size 50K samples. Hanning window is applied in advance to the signal to minimize fundamental signal leakage in the diagnostic signal processing which results in an envelop of the signal.

Fig. 3.7 (b) shows the FFT spectrum of the current signal in (a). It clearly shows the existence of eccentricity signatures of the motor with -31.92 dB in the left sideband and -31.55 dB in the right sideband of the fundamental signal. The characteristic frequencies of those fault signatures are monitored around 30Hz and 90Hz in the spectrum.

The time-domain figures in Fig. 3.7 (c) and (d) are obtained by following fine adjustment step 1 and step 2 in Fig. 3.4. In Fig. 3.7 (c), the reference fault signal in (3.8) is generated at 29Hz which has 1Hz error difference from the left sideband signature at 30Hz and which is assumed to verify the effectiveness of the error localization strategy in the proposed diagnostic scheme. The 1Hz error is caused by coarse frequency prediction ambiguity as derived in (3.6). The motor line current signal in (a) is to be multiplied by the fault reference signal in (c) to shift the fault signal information to aro-

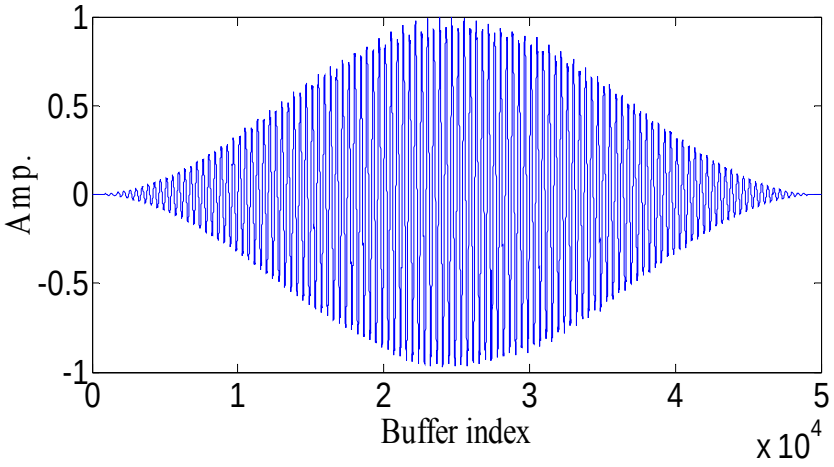

(a)

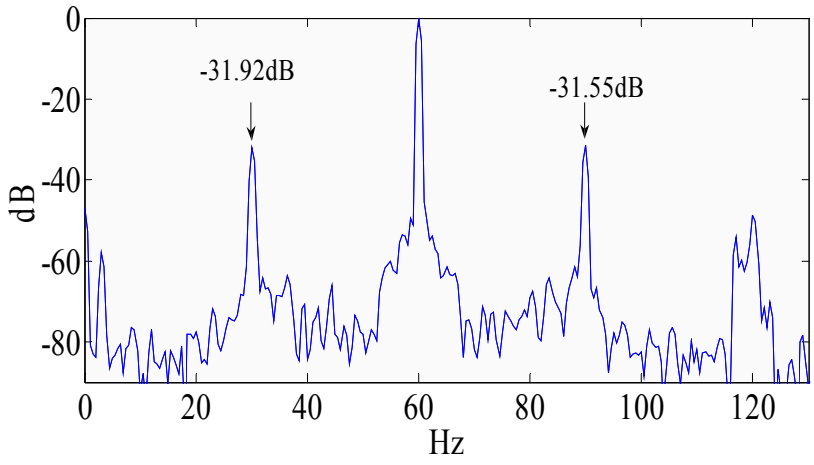

(b)

Fig. 3.7. (a) line current signal, (b) FFT spectrum of current signal, (c) fault reference signal, (d) averaged signal, (e) FFT spectrum of averaged signal for left sideband signature, and (f) FFT spectrum of averaged signal for right sideband signature. (line driven, 15% torque).

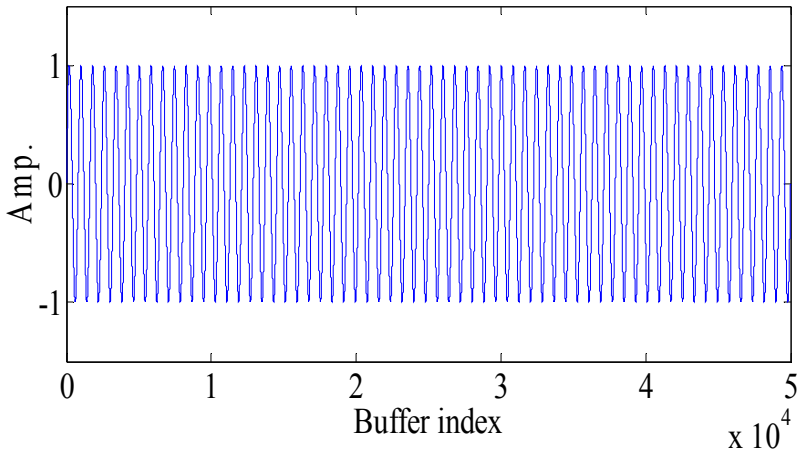

(c)

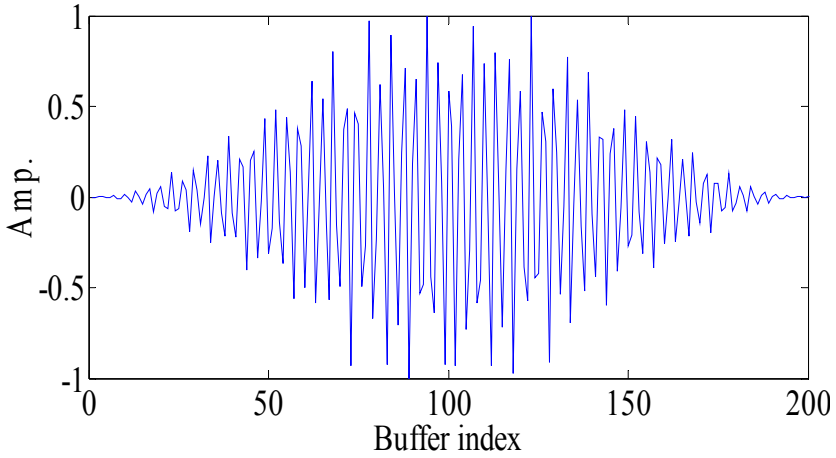

(d)

Fig. 3.7. Continued.

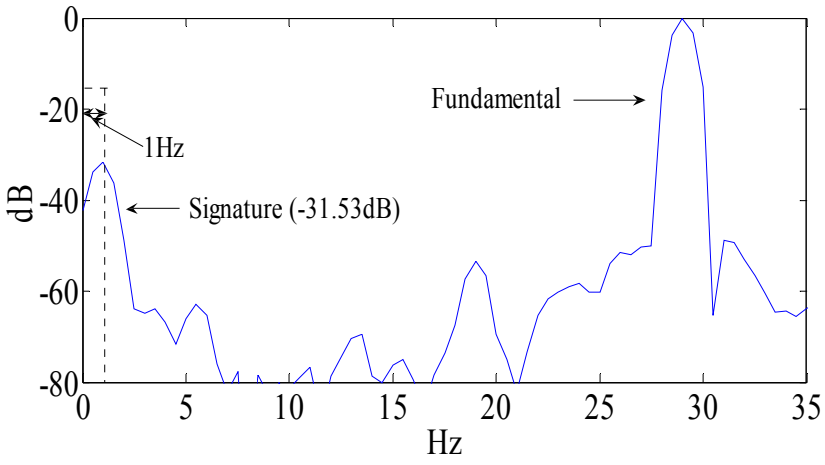

(e)

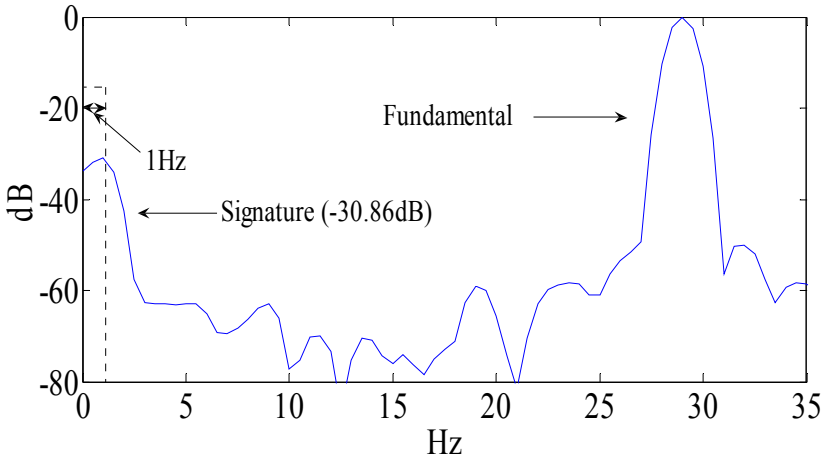

(f)

Fig. 3.7. Continued.

-und 0Hz.

In Fig. 3.7 (d), the product between signal (a) and (c) in realtime fashion is averaged and stored in a buffer ($N_2=200$) as in (3.12) which had 50,000 samples before being averaged. The resultant signal in (d) is shown to be much more simplified when compared with (a).

The frequency-domain spectrum of the time-domain signal in Figs. 3.7 (c) and (d) is depicted in Figs. 3.7 (e) and (f) for detailed explanations. Fig. 3.7 (e) depicts the FFT spectrum of the averaged signal in (d).The relatively low resolution of the spectrum is partially due to the inherent leakage effect of the FFT processing of a small size signal. The eccentricity signature is observed at 1Hz with -31.53dB. The spectrum of the averaged signal in (e) still has the precise information on the left sideband signature amplitude with only 0.39dB difference from the original one in (b). Having almost the same fault signature information in Fig. 3.7 (e) , now the signal is stored with only a 200 size buffer in (d) while the original size is 50K in (a). The complexity / computation time reduction of a diagnostic processing applied to the averaged signal is expected to be significantly reduced up to 99.6 % based on (3.15). The trade-off is the use of additional 200 buffers memory which is assumed to be small enough in the normal DSP system. Implementation of a complex algorithm in a low cost system can be done by utilizing the proposed strategy.

Fig. 3.7 (e) shows that the inserted 1Hz error is expectedly observed around 0Hz with reduced frequency ambiguity. It is shown that the conventional eccentricity frequency in (3.3) and (3.4) is primarily suppressed and only dependent on its error

amount which is mathematically predicted in (3.7) to (3.11). Otherwise, the eccentricity frequency with error will depend on the motor excitation frequency and rotor speed as in (3.3) and (3.4). The direct adjustment will require serious computation effort.

Fig. 3.7 (f) shows the FFT spectrum of the averaged signal for the right sideband at 90Hz, which is derived and plotted in a similar way as described in figures (a) to (e). Compared with the original signal in (b), almost the same signature amplitude information is monitored with only a 0.69dB difference. The 1 Hz in the figure is the error intentionally added to the reference signal to monitor the response in detection. Compared with that in (e), the same error response is expectedly observed.

In Figs. 3.7 (e) and (f), the intentionally inserted frequency error is monitored at exactly the same frequency away from 0 Hz, confirming the precise derivation in (3.7) to (3.10). It shows how the coarse fault frequency estimation error in (3.5) is predictably localized around zero frequency. This predictable error localization provides the advantage of reduced frequency ambiguity and reduction in tracking computation. The semi-blind error search technique in (3.18) can be efficiently applied only to the expected frequency error region for measurement and compensation.

Fig. 3.8 presents offline experimental results to show efficacy of the proposed fine adjustment strategy in step 3 of Fig. 3.4, practical advantage of the signal averaging (a) to (b) and the effectiveness of the fine adjustment with the averaged signal in (c) to (d) .

Fig. 3.8 (a) shows the FFT spectrum for a down sampled (D.S.) signal with the averaging scheme in (3.12) and without averaging (simple decimation) with respect to

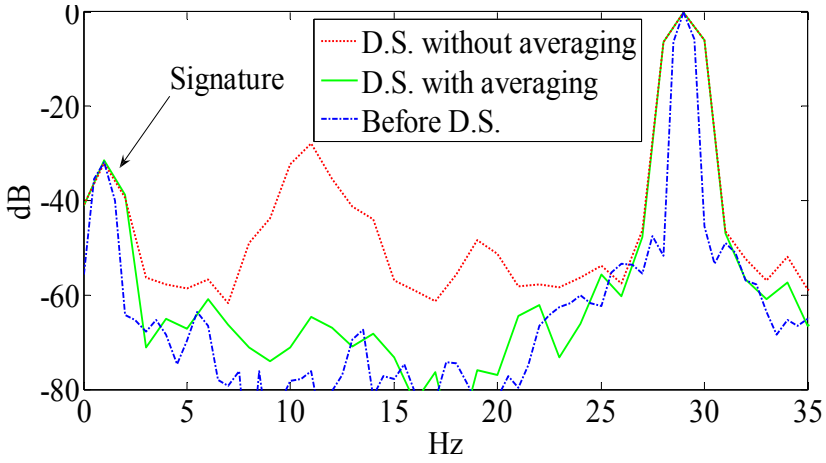

(a)

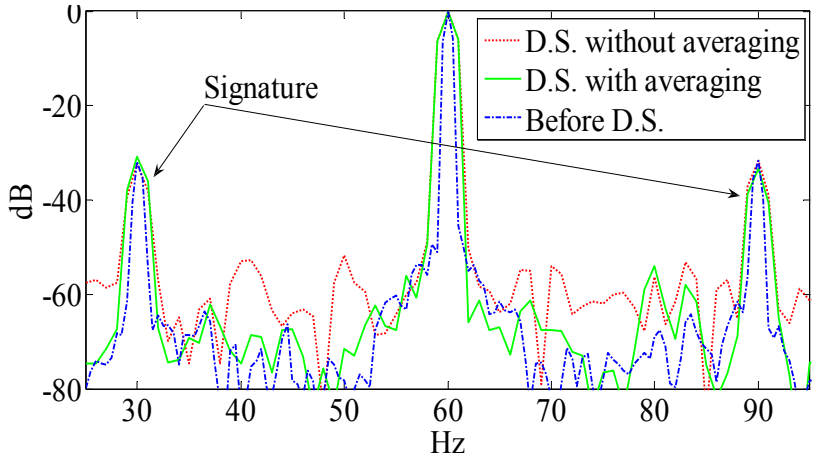

(b)

Fig. 3.8. (a) FFT spectrum of down sampled (D.S.) signal with and without averaging, (b) FFT spectrum of D.S. signal with and without averaging, (c) offline detection with various added error in Hz, and (d) offline detection with added bias in Hz under 1Hz error.

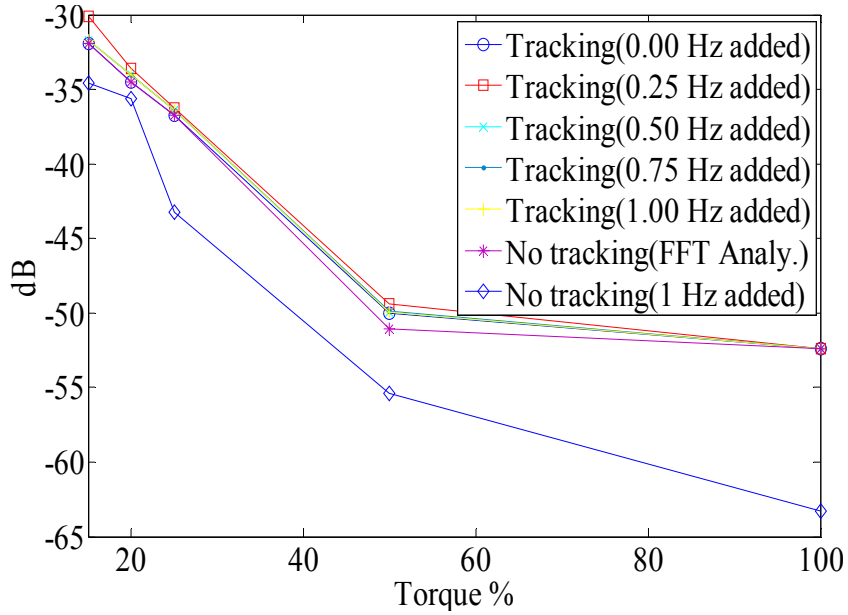

(c)

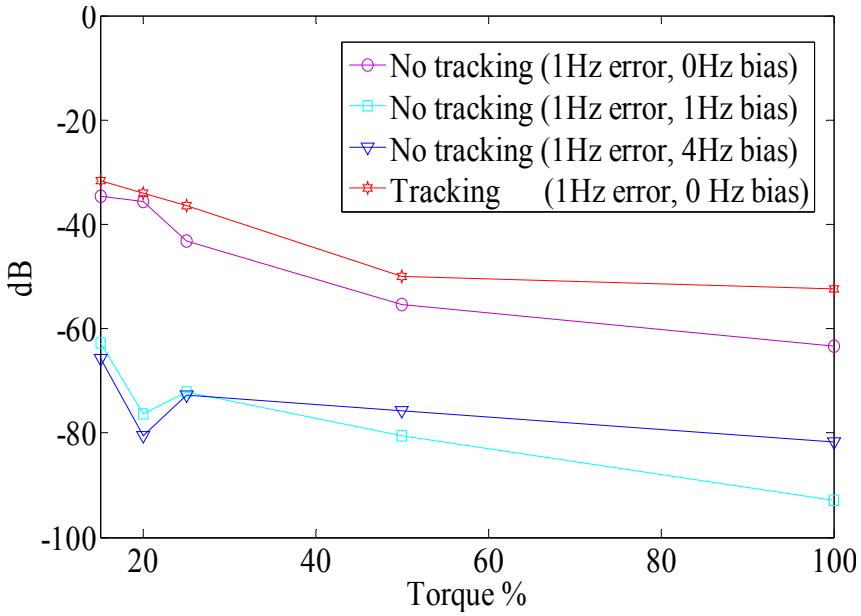

(d)

Fig. 3.8. Continued.

the original signal in (3.7). It shows that noise disturbances are dominant in a spectrum without the averaging while the noise content is acceptably suppressed with the proposed averaging strategy. It is observed that aliasing during the simple down sampling without averaging has resulted in serious disturbances in the analysis. Compared with the reference spectrum of the original signal before down sampling, the spectrum of the averaged signal shows more leakage which is mainly due to the FFT spectrum for a small size signal. The spectrum with an averaged signal shows practically comparable and acceptable signature amplitude identification when compared to the reference spectrum. The simple averaging not only provides an effective low pass filtering as proved in section III *B* but also performs the de-nosing as verified in the figure.

Fig. 3.8 (b) shows the frequency spectrum of the current signal in (3.9) which is plotted in a similar way as described in (a) for comparison. It is shown that the noise contents are suppressed at large through averaging with acceptable resolution in the signature amplitude identification confirming the practical advantage of the simple averaging strategy in this study.

Fig. 3.8 (c) shows signature detections under frequency error conditions to verify the effectiveness of the proposed fine adjustment in (3.18). Bias is assumed as 0 Hz in this experiment. In the figure, the detections with the fine adjustment show almost similar performance under any error conditions. The effectiveness of the fine error adjustment can be confirmed with reference to the precise FFT analysis with almost the same

detection tendency. Detections without the fine adjustment are shown degraded with serious deviation from the reference.

In Fig. 3.8 (d), signature detections are performed to verify the advantage of inserting bias in (3.16). In this figure, detections with the fine adjustment are taken as reference in this experiment. As the bias increases from 0Hz to 1Hz or 4Hz, the detected signature amplitude without the fine error adjustment deviates more severely from the reference detections because of the improved resolution in detection with strategically inserted bias resulting in more precise fault signature identification.

3.6 Online experimental result

The online experiment is performed to verify the effectiveness of the proposed diagnostic procedure. Fig. 3.9 shows the overall implementation of the diagnosis and the motor control routine in the DSP software. The proposed scheme is efficiently combined with motor control software (V/f) within the single DSP system (TI-DSP F2812) without violating CPU utilization. The bias is assumed 0Hz in the online experiment.

During all the experiments, the slip frequency of the motor operation is measured through realtime DSP software utilizing feedback information from a speed sensor or a sensorless speed estimator. The adopted sensorless speed estimation is based on the well-known per-unit (p.u.) slip relation of an induction motor as follows [65]:

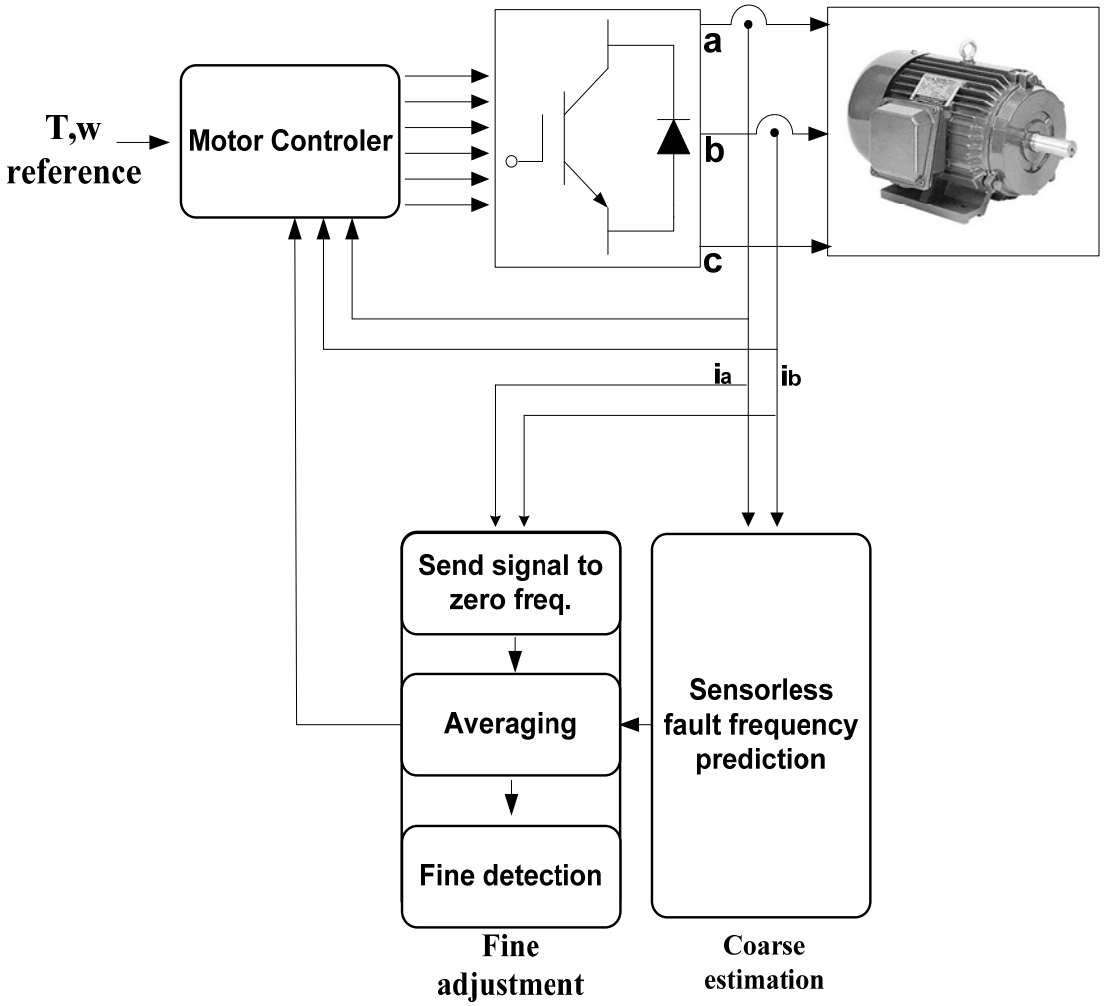

Fig. 3.9. Overall DSP implementation.

$$\omega_{sl}^{pu} = \frac{\left(I_r^{pu}\right)^2 r_r}{T_e^{pu}} \tag{3.21}$$

where T_e^{pu} is the p.u. torque, I_r^{pu} is the p.u. rotor current, and r_r is the rotor resistance.

In the experiment, the measurement errors of the motor parameter are inserted through the DSP software to disturb the speed/slip estimation through (3.21) where

errors are assumed with a rotor resistance offset of 0.035 (Ω) and linearized relation between torque and current relation as $I_r^{pu} \approx T_e^{pu}$. The rotor current I_r^{pu} is approximately measured from stator current by assuming infinite magnetizing inductance in the test motor. Those conditions are expected to induce non-negligible errors in the slip estimation which will eventually perturb the diagnosis. The mis-measurement error of motor parameters in sensorless systems has been the main issue in industry [44][45][46][47][65] as the parameters vary non-linearly depending on motor operating points [65]. Thus, it is challenging to perform precise tracking. Those distortion conditions are assumed unknown during the experiments.

In Fig. 3.10, the slip estimation errors through (3.21) are obtained by taking the speed information from a mechanical sensor as reference. (a) shows continuous errors in the slip estimation versus the entire torque range (%). From the statistically accumulated experimental results with 100 trials, the histogram of the error occurrence is depicted in (b). It is shown that the histogram follows the Gaussian distribution envelop which approximately justifies the fundamental assumption of Gaussian error distribution in this study. The distribution in (b) will come close to an ideal Gaussian distribution with high probability if a sufficient number of experiments are performed. From Fig. 3.10, the instantaneous maximum error that covers more than 99% of those errors is approximately less than 1Hz from which the range of majority slip errors in (3.1) are asymptotically determined as follows:

$$s_{err_j} \in \left[s_{err\,\min}, s_{err\,\max} \right] = [-1Hz, 1Hz] \tag{3.22}$$

From the assumption of the majority error distribution in a limited range, which is

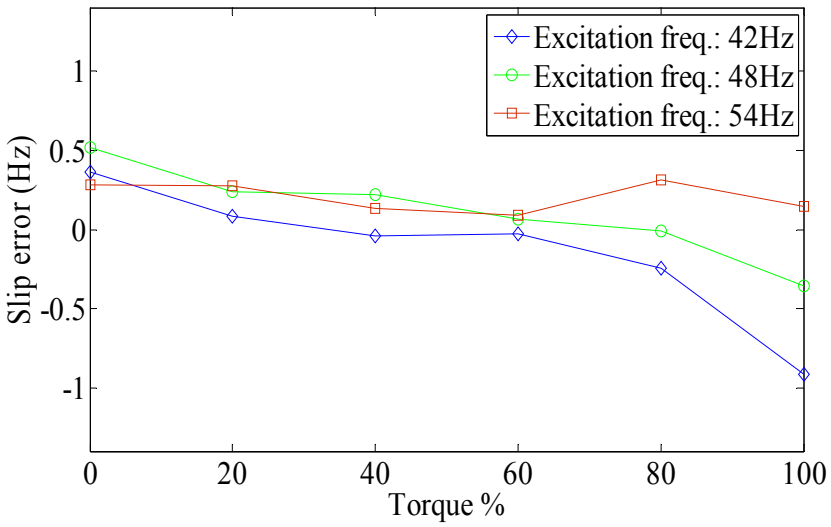

(a)

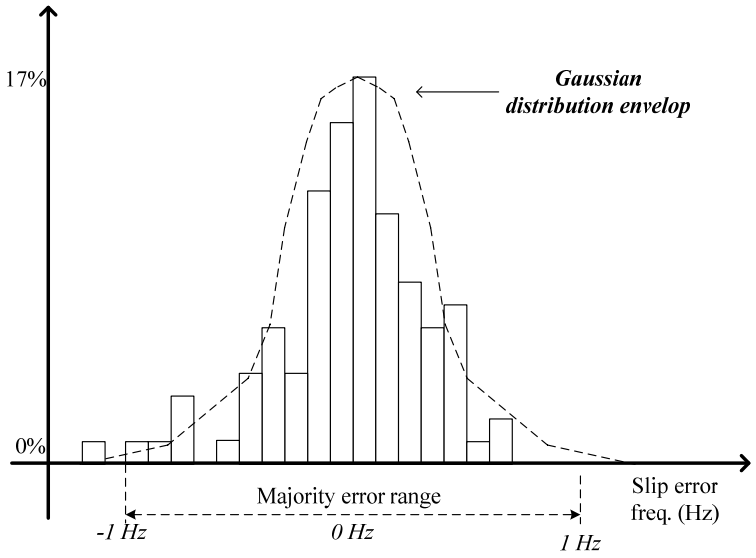

(b)

Fig. 3.10. Slip estimation errors.

theoretically and experimentally validated in Figs. 3.2 to 3.3 and Fig. 3.10 (b), slip errors during this experiment are assumed to arise primarily within the range in (3.22). It is expected to cover more than 99% of error occurrences with high probability.

Based on the slip error distributions in (3.22), the error range in the coarse fault characteristic frequency estimation is determined through (3.6) as follows:

$$f_{err} = \left(\frac{2m}{p}\right)\left[s_{err\,\min}, s_{err\,\max}\right] = \left[-0.5Hz, 0.5Hz\right] \tag{3.23}$$

where *m=1* is assumed and *p=4* from Table. 3.1. The potential error range in the coarse frequency prediction during the experiment is identified through (3.23). The effectiveness of the proposed fine adjustment, which is blindly applied to the limited region in (3.23), will be clearly demonstrated by showing that most errors in the experiment are precisely compensated.

Fig. 3.11 shows the online experiments through the diagnostic service procedure in Fig. 3.9 with fine adjustment with sensorless estimation-based detection, without fine adjustment and with sensorless estimation-based detection, and without fine adjustment for sensor feedback-based detection. Realtime spectrum analysis is taken as a reference in the experiment.

Fig. 3.11 with sensor feedback-based diagnosis at 80% torque, shows instantaneously unreliable results caused by a feedback error from the speed sensor. In fact, such diagnostic distortions with sensor errors have been continuously monitored throughout the experiments at one out of ten detections which are expected to be more serious in a harsh industrial environment resulting in monitoring failure. Most of the in-

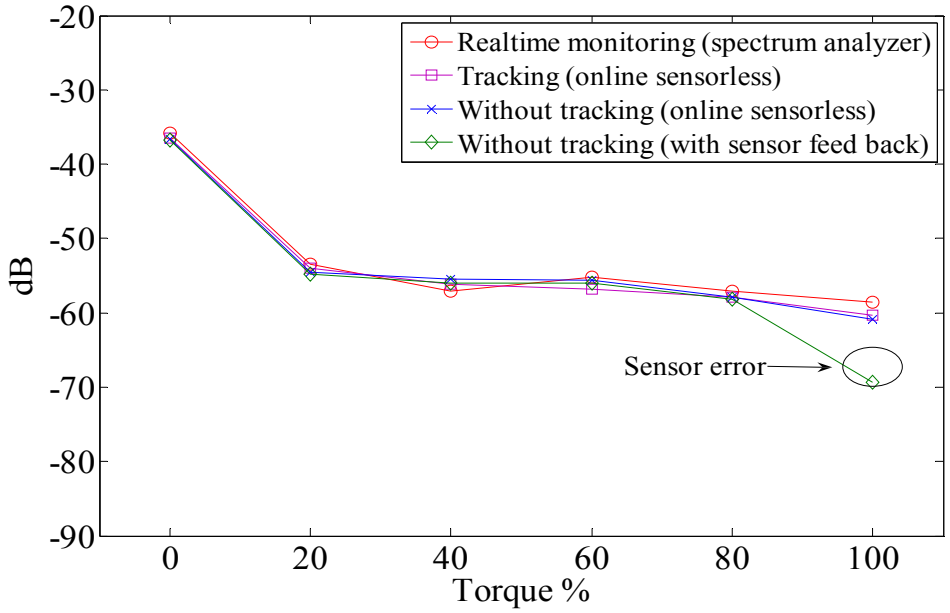

(a)

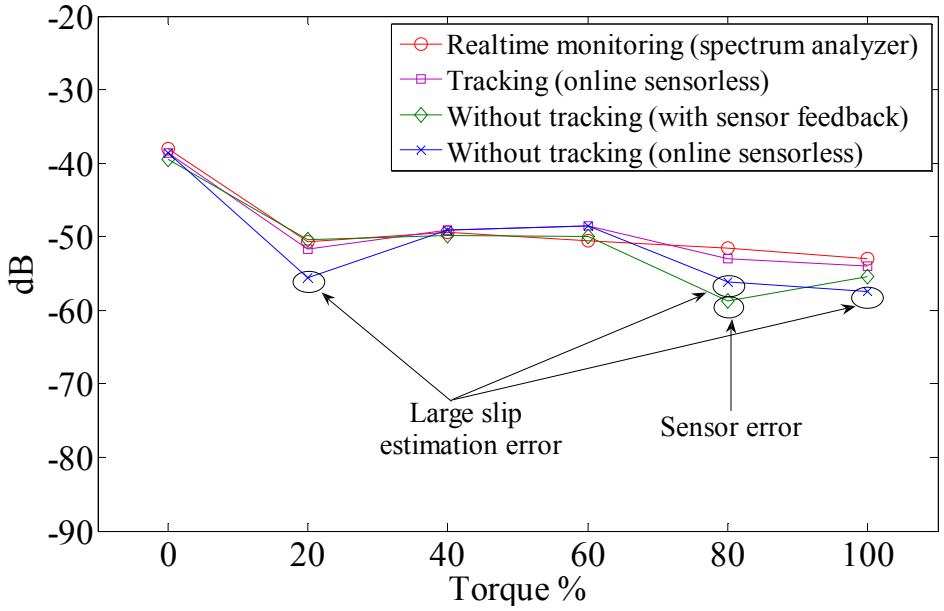

(b)

Fig. 3.11. Signature estimation (a) with excitation of 42Hz and (b) with excitation of 48Hz.

-stantaneous errors might be tolerable in a motor drive due to a relatively long machine time constant, however the errors should be corrected in the diagnosis relying on the speed feedback information in a short time period which is 2 seconds in this experiment. Severe distortions are observed at 20%, 80%, and 100% torques yielded by a sensorless estimation algorithm with the added error conditions in (3.21). The effectiveness of the proposed fine adjustment is verified to compensate for those distortions which can be confirmed from the reference results.

In Fig. 3.12, results are obtained when error is intentionally added in the sensor-based speed estimation through the DSP software. Detections with 0.015 p.u. speed errors are compared with that of 0 p.u as reference. In the figure, the detection with added error shows almost the same detection tendency as that without error when the fine adjustment is effectively applied. Without fine adjustment, severely distorted detections are monitored which can be confirmed from the reference result. The performance degradation under error was predicted in previous offline experiments in Fig. 3.8 (c) and (d).

For industrial applications, the error range in (3.23) can be flexibly derived based on the performance of a speed feedback system in an AC drive. Once the error range is identified, the proposed signature-based diagnosis yields a fairly reliable performance as demonstrated in online/offline experiments.

3.7 Conclusion

A two-step semi-blind diagnosis which consists of coarse estimation and fine

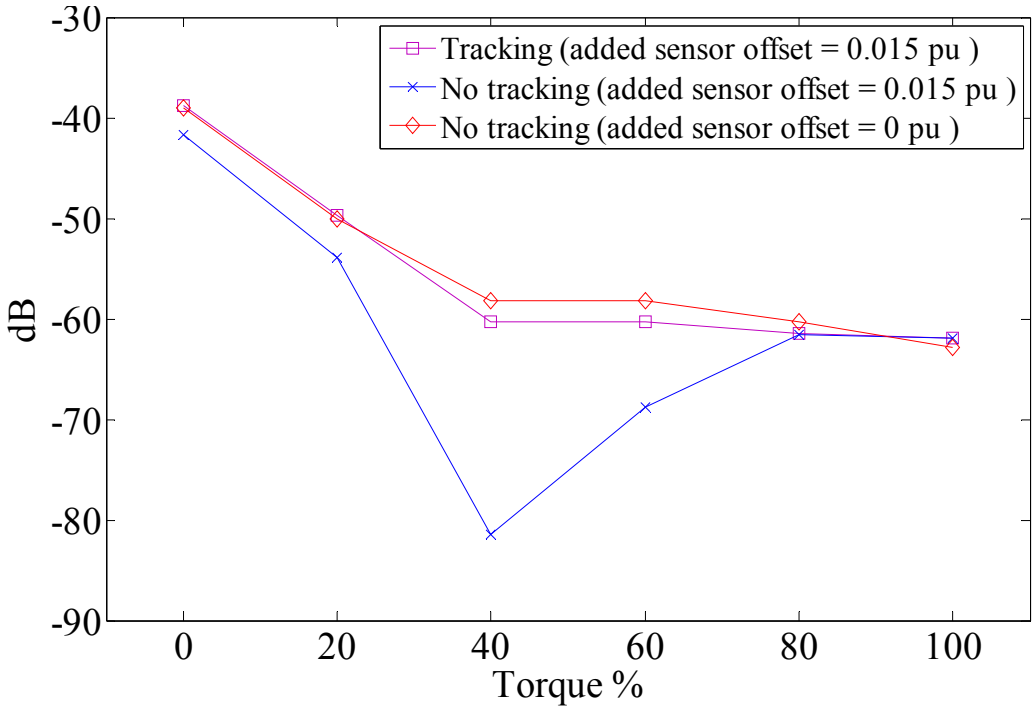

Fig. 3.12. Signature estimation with excitation of 54Hz.

adjustment is proposed through the estimation and compensation of the speed feedback errors in an AC drive. The two-step diagnosis is precisely optimized under the assumption that most speed errors arise within a limited-region which is shown as a theoretically and experimentally valid assumption. Based on the limited error assumption, effective computational complexity and memory occupancy minimizations strategies are derived in this paper through which the implementation of the coarse-to-fine diagnosis on a low cost DSP is successfully achieved. It is theoretically analyzed and experimentally demonstrated that the proposed semi-blind diagnosis provides sufficient robustness against the unexpected speed feedback errors in an induction motor drive. Thanks to low complexity and reduced memory occupancy, features of the

proposed solution make it a sound candidate for low cost and robust motor condition monitoring applications.

CHAPTER IV

SIMULTANEOUS IMPLEMENTATION OF FAULT SIGNATURE DETECTION AND DECISION-MAKING

4.1 Introduction

In this section, a complete cross-correlation–based fault diagnostic method is proposed for realtime DSP applications that cover both the fault monitoring and decision-making stages. In practice, a motor driven by an inverter or utility line is run at various operating points where the frequency, amplitude, and phase of the fault signatures vary unexpectedly. These changes are considered to be one of the common factors that yield erroneous fault tracking and unstable fault detection. In this study, the proposed algorithms deal with the ambiguities of the line current noise or sensor resolution errors and operating point–dependent threshold issues. It is verified that a motor fault can be continuously tracked when the sensor errors are within a limited range through the adaptively determined threshold definition of noise conditions. Offline experiments are performed via Matlab using actual line current data. These results are verified on a DSP-based motor drive in real time where drive sensors and digital signal processor are employed both for motor control and fault diagnostic purposes.

4.2 Cross-correlation-based detection

A. Cross Correlation Scheme Derived from Optimal Detector in Additive White Gaussian Noise (AWGN) Channel

While performing motor fault detection, it is important to have a noise suppression

capability where high energy noise content dominates the low amplitude fault signatures. As an effective tool, the matched filter is often pronounced as one of the best candidates [61] in an AWGN channel. The matched filter is known as an optimal detector which maximizes the SNR in the AWGN channel. A typical filter is expressed by

$$y_n = \sum_{k=1}^{N} h_{n-k} s_k \tag{4.1}$$

where $n = 1, 2, \cdots N$, h_n represent the impulse response of the filter, s_k is the input signal. The output SNR of the filter can be written as

$$SNR = \left(H^T S\right)^2 / E\left[\left(H^T W\right)^2\right] = \left(H^T S\right)^2 / \left(\sigma^2 H^T H\right) \tag{4.2}$$

where $H = [h_N, h_{N-1,}, \ldots h_1]$, $S = [s_1, s_2 \cdots s_N]$, $W = [w_1, w_2, \cdots w_N]$, w_n is the sampled Gaussian noise with variance σ^2, T is the vector transpose. Through the Cauchy-Schwarz inequality, the denominator in (4.2) is maximized as

$$\left(H^T S\right)^2 \le \left(H^T H\right)\left(S^T S\right) \quad when\ H = cS \tag{4.3}$$

where c is constant. It is obvious from (4.3) that the SNR of filtering is maximized when $h_n = s_{N-n}$, which is called the matched filter.

Assuming s_n is the reference signal of the inspected fault signature and x_k is the input current signal; the output of matched filter is rewritten in the form of cross-correlation as given in (4.4) which is expected to suppress noise optimally for signature

diagnosis. Hence, cross-correlation can be proposed as one of the best signal detectors for the systems distorted by Gaussian noise.

$$y_n = \sum_{k=1}^{N} h_{n-k} s_k = \sum_{k=1}^{N} h_{n-k} x_k = \sum_{k=1}^{N} s_{N-(n-k)} x_k \quad \Rightarrow y_N = \sum_{k=1}^{N} s_k x_k \tag{4.4}$$

The analysis of a matched filter in continuous time can be derived in a similar manner through integration instead of summation in (4.1) to (4.4) [61]. The matched filter output in continuous time can also be expressed as the cross-correlation in (4.4) by replacing the summation to integration. The details of continuous-time matched filter are not covered in this study since the implementation is based on discrete time processing.

Implementation of an algorithm on DSP is commonly limited by memory and computing capacity of the system. The memory occupancy for cross-correlation operation is assumed negligible because it is performed in the sample sequence order of the input signal x_k in (4.4) which does not need an additional signal memory buffer. The computing complexity of the cross-correlation is shown as N in (4.4) which is low enough as each multiplication occurs only one time in each interrupt in normal operation of a DSP system. For the FFT-based scheme which has been popularly used in diagnosis, all the signals should be inherently stored in a memory buffer for computation and the number of multiplication required is (N/2)*log(N), which is assumed not acceptable due to the overwhelming burden on DSP, especially for low cost online diagnostic systems. The inherent optimal performance in noise suppression, low memory occupation and low computing complexity makes the cross-correlation based detection an attractive tool for online fault diagnosis of a motor.

In this study, the optimal cross-correlation-based diagnosis is presented assuming stationary operation of a motor in which non-stationary error effects are discussed in the following.

B. Coherent Detection

In signal processing, one of the well known and most widely used detection methods is classified into two parts: coherent detection and non-coherent detection [62]. In this study, simplified cross-correlation based non-coherent detection is adopted for fault detection. The coherent detection basically uses measured frequency and phase distortion of a signal which is compensated in the subsequent stages of the fault detection algorithm in this study. On the other hand, non-coherent detection is applied without knowing the phase information. Since precise measurement of inspected low amplitude fault signatures is a challenging task, non- coherent detection is a more practical tool for diagnostic applications. Indeed, once the necessary information is accurately provided, the coherent detection usually performs better than non-coherent detection as it utilizes more signal information which increases the complexity [62]. The non-coherent detection yields more reliable detection under severely noisy conditions where inaccurate information is available as its performance is not dependent on the distortion factor.

A simplified coherent detection is presented in [26]. As shown in Fig. 4.1, the fault amplitude and phase can be monitored using a phase locking loop procedure. The basic operational functions are defined as follows:

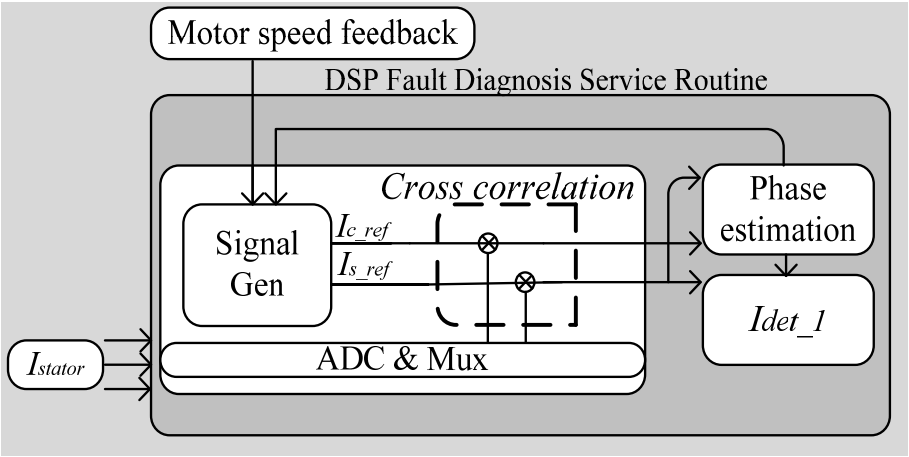

Fig. 4.1. Coherent detection (phase sensitive detection).

$$I_{c\_ref}[n] = I_{ref}\cos[w_{ref}n + \varphi_{ref}] \tag{4.5}$$

$$I_{s\_ref}[n] = I_{ref}\sin[w_{ref}n + \varphi_{ref}] \tag{4.6}$$

$$I_{stator}(t) = I_{fault}\cos(w_{fault}t + \varphi_{fault}) + \varpi(t) \tag{4.7}$$

$$+\sum_{h}\sum[I_{harmonics}(h)\cos(w_{harmonic}(h)t + \varphi_{harmonics}(h)),\ h = 1,2,3,..$$

$$I_{\det\_1} \approx K_1\cos(\varphi_{ref} - \varphi_{fault}) + \varpi_1, \quad if\ \ w_{ref} = w_{fault} \neq w_{harmonic}(h) \tag{4.8}$$

where n is the sample time, h is the harmonic signal number, I_{ref} is the amplitude of reference signal, and $I_{stator}(t)$ is the stator current whose amplitude is the fault signature (I_{fault}) and stator current harmonics ($I_{harmonics}$). φ_{ref} is the reference phase, φ_{fault} is the phase of the fault signature, $\varphi_{harmonics}$ is the harmonic signal phase, w_{ref} is the reference frequency, $w_{harmonic}$ is the harmonic signal frequency, w_{fault} is the frequency

of fault, $I_{\det\_1}$ is the detected value, and $K_1 = I_{ref} I_{fault} / 2$.

The reference signals $I_{c\_ref}[n]$ and $I_{s\_ref}[n]$, can easily be generated by the DSP for the potential fault frequency using the fault equations. The fault signal frequencies depend on the rotor speed and excitation frequency which are updated continuously in a motor control subroutine for control purposes [17][26]. If the phase difference between the reference signal and the fault signature is set to zero and the cosine term is maximized through phase estimation, the fault amplitude can be successfully monitored.

Compared to the algorithms detailed in [25] and [28], phase sensitive detection has remarkably reduced computational complexity and made it possible to perform a large amount of data processing using a low-cost DSP. However, the performance of coherent detection depends on the phase accuracy of the fault signature as depicted in Fig. 4.2.

Therefore, these kinds of algorithms are applicable in conditions where phase ambiguities are negligible.

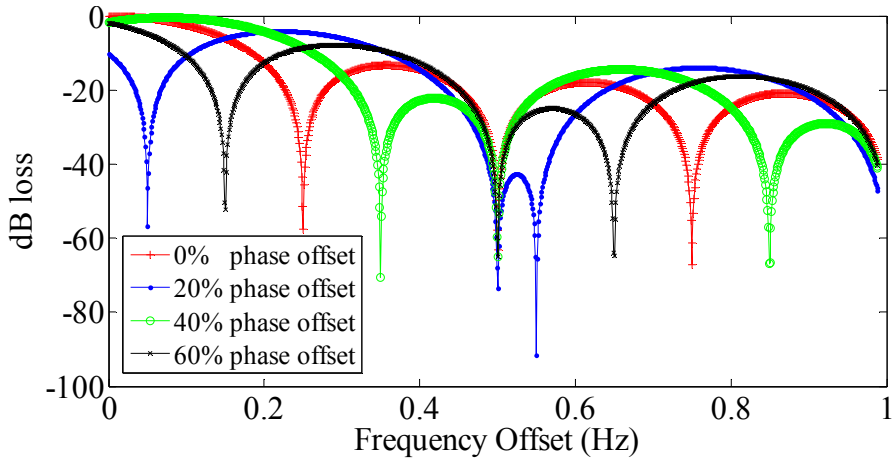

Fig. 4.2. Fault signature detection loss versus frequency.

C. Noncoherent Detection (Phase Ambiguity Compensation)

The basic operational functions are defined as follows:

$$I_{s\_ref}[n] = I_{ref}\ \sin[w_{ref} n + \varphi_{ref}] \tag{4.9}$$

$$I_{c\_ref}[n] = I_{ref}\ \cos[w_{ref} n + \varphi_{ref}] \tag{4.10}$$

$$\begin{aligned} I_{\det\_2} &= \sqrt{\left(K_1 \cos(\varphi_{ref} - \varphi_{fault}) + \varpi_2\right)^2 + \left(K_1 \sin(\varphi_{ref} - \varphi_{fault}) + \varpi_3\right)^2} \\ &= \sqrt{K_1^2(\cos^2(\varphi_{ref} - \varphi_{fault}) + \sin^2(\varphi_{ref} - \varphi_{fault})) + \varpi_4} = \sqrt{K_1^2 + \varpi_4} \approx K_1 + \varpi_5 \end{aligned} \tag{4.11}$$

As shown in (4.11), the amplitude detection procedure is based on phase elimination and hence is inherently immune to the phase ambiguities of fault signatures. The elimination of the phase estimation stage reduces the computational burden of the non-coherent detection algorithm. Even though it shows lower performance than coherent detection at a steady state when the phase information is provided, it allows the user to obtain more reliable detection results under noisy or dynamic system conditions [62]. The block diagram of non-coherent detection is given in Fig. 4.3.

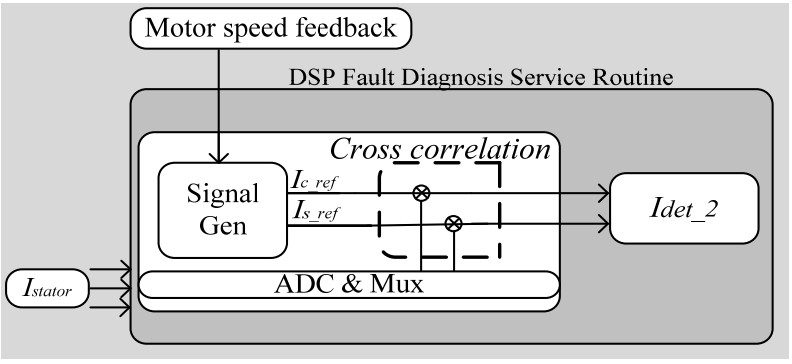

Fig. 4. 3. Noncoherent detection.

D. Frequency Offset Compensation

Rotor speed is one of the most critical variables which needs to be monitored continuously both for motor control and fault detection. The speed feedback is measured either by an encoder or estimated in the code. Unlike the motor control, very precise speed information is needed to identify the severity of the faults. However, in practical applications, a small mismatch between the speed feedback and the actual speed is commonly observed due to encoder resolution, inaccurate speed estimation algorithms or slow response of sensor to unexpected transient condition, etc. In addition to phase ambiguities, even a small amount of frequency offset yields erroneous fault detection results. Assuming the frequency offset $w_{offset} = w_{fault} - w_{ref} \neq 0$ and phase delay $\varphi_{ref} - \varphi_{fault} = \varphi_{offset}$, the cross correlation output signal will be:

$$\begin{aligned} I_{cross} &\approx K_1 \cos[\omega_{ref} n - \omega_{fault} n + \varphi_{ref} - \varphi_{fault}] + \varpi \\ &= K_1 \cos[\omega_{offset} n + \varphi_{offset}] + \varpi \end{aligned} \tag{4.12}$$

In Fig. 4.2, the normalized dB loss of coherent detection versus frequency offset is simulated using Matlab where the phase offset percentage is defined between zero to 2π. It is clearly shown that frequency offset, phase offset or a random combination of these two can truly suppress the fault signature which typically has -40 to -80 dB amplitude. However, great complexity will also be required if all of the expected offsets are monitored. Here, the current signal, $I_{cross}(n)$, is expected to provide high enough resolution for fault detection even if it is averaged in time or down sampled with noise elimination through averaging.

Applying an offset detection algorithm to an averaged signal with small samples will reduce the complexity. In this study, maximum likelihood (ML) detection is used to estimate the sinusoid at offset frequency which is the maximum of the periodogram [61] and is given by

$$\hat{f}_{ML} = \arg\max \left| \frac{1}{N} \sum_{n=1}^{N} x_n e^{j2\pi fn} \right| \tag{4.13}$$

where

$$x_n = \frac{1}{N_1} \sum_{k=1}^{N_1} I_{cross}[k + N_1(n-1)], \;\; n = 1, 2, \cdots N_2 \tag{4.14}$$

is the averaged signal, *N1* is the number of samples averaged, and *N2* is the physical DSP buffer size used for this purpose where the relation between parameters is as follow:

$$N = N_1 N_2 \tag{4.15}$$

The tracking bound without aliasing is given by,

$$Track\_bound \le \frac{N_2}{2} \; Hz \tag{4.16}$$

The maximum bound comes from the Nyquist sampling theorem. If the offset ($w_{offset} = w_{fault} - w_{ref} \neq 0$) is assumed, the aliasing will not be observed, practically.

The computational complexity of ML detection in (4.13) depends on *N* and the frequency range $f_{range} = f_{\max} - f_{\min}$. Since the ML algorithm application in this study has high complexity, it needs modification for realtime DSP applications. In this study, these parameters will be limited through the averaged (effectively down sampled) signal with reduced *N* and limited frequency range where the maximum frequency offset between

the reference signal and the fault signal frequencies is assumed to be less than 1 Hz ($= f_{range} < 1Hz$). In this way, the ML estimator can effectively be utilized in a DSP for online fault diagnosis.

The frequency resolution of ML-based offset detection in (4.13) is determined as follows:

$$f_{\Delta} = \frac{f_{\max} - f_{\min}}{N_{tri}} = \frac{f_{range}}{N_{tri}} \tag{4.17}$$

where N_{tri} is the number of applications of ML trials within f_{range}. The acceptable resolution of f_{Δ} will be determined though simulations and experiments.

4.3 Decision-making scheme

Procedures in diagnostics commonly consist of several steps which are signature detection, decision-making, and final feedback to controller or human interface system. Application of a low cost diagnostic system in the industry is greatly limited by the capability to handle the detection and decision-making process simultaneously within the same microprocessor. Assuming the detection steps shown in previous sections, the applicability of the discussed system further depends on the complexity and reliability of decision-making scheme.

A. Adaptive Threshold Design (*Noise Ambiguity Compensation*)

Reliability is one of the major challenges facing fault diagnostic systems because the decision should be made for a small fault signature in a highly noisy industrial

environment. In fact, the detection algorithm applied at fault frequencies detects noise signatures even with healthy motors, the amplitudes of which are usually hard to discriminate from small fault signature. One of the practical design considerations of the threshold encountered is how the detected signature can be reliably determined to be the existing fault signature. The diagnostic decision-making based on the threshold trained to the motor line current noise variation can evaluate the reliability of detected signature in DSP applications.

Here, the threshold is derived using the statistical decision theory [61] with the hypothesis of *H0* and *H1* for decision tests which are as follows:

$$H_0 : I_{stator} = \varpi$$

$$H_1 : I_{stator} = I_{fault} + \varpi \quad with\ p(\varpi) \sim N(0, \sigma^2) \tag{4.18}$$

where H_0 is the hypothesis of having only noise without any faults, H_1 is the hypothesis of existing fault signature with amplitude I_{fault} in white Gaussian noise, ϖ channel, and $N(0, \sigma^2)$ means zero mean noise with variance σ^2.

A decision rule is made based on the optimal statistical test with Likelihood-ratio test (LRT) of the two distributions of these hypothesis which is as follow:

$$\Phi(I_{stator}) = \frac{P(I_{stator} : H_1)}{P(I_{stator} : H_0)} > \gamma \tag{4.19}$$

where γ is the temporary threshold. With Gaussian distribution of noise, (4.19) is derived as follows:

$$\Phi(I_{stator}) = \frac{\exp\left[-\frac{1}{2\sigma^2}\right]\sum_{n=1}^{N}(I_{stator} - I_{fault})^2}{\exp\left[-\frac{1}{2\sigma^2}\right]\sum_{n=1}^{N}(I_{stator})^2} > \gamma \tag{4.20}$$

$$\Rightarrow \qquad \frac{1}{N}\sum_{n=1}^{N} I_{stator} > \frac{\sigma^2}{NA}\ln\gamma + \frac{I_{fault}}{2} = \gamma' \tag{4.21}$$

where γ' is the threshold and N is the number of samples of current signal used for detection.

Let the left hand side in (4.21) $T = \frac{1}{N}\sum_{n=1}^{N} I_{stator}$.

Then, the statistics of averaged stator current signal, *T,* is calculated as follows:

$$T \sim \begin{cases} N(0, \sigma^2 / N) & Under\ H_0 \\ N(I_{fault}, \sigma^2 / N) & Under\ H_1 \end{cases} \tag{4.22}$$

The performance with threshold γ' applied to the averaged signal T with statistics shown in (4.22) can be derived using the detection probability in (4.23) and false alarm event probability in (4.24) which are as follows:

$$P_D = \Pr\{T > \gamma'; H_1\} = Q\left(\frac{\left(\gamma' - I_{fault}\right)}{\sqrt{\sigma^2 / N}}\right) \tag{4.23}$$

$$P_{FA} = \Pr\{T > \gamma'; H_0\} = Q\left(\frac{\gamma'}{\sqrt{\sigma^2 / N}}\right) \tag{4.24}$$

where Q is the Q-function which is detailed in later section.

With range of allowable error (false alarm), P_{FA}, a threshold is calculated from (4.23) and (4.24),

$$\gamma' = \sqrt{\frac{\sigma^2}{N}} Q^{-1}(P_{FA}) \tag{4.25}$$

The proposed threshold provides a reliable decision-making tool for small signature detection in a noisy channel. Signature-based diagnosis performed with reliably detected signatures through a proposed threshold will lead to more accurate condition monitoring while discriminating its results from random noise interference signatures. From (4.25), the proposed threshold is dependent on the number of samples and the noise variance estimated. These are independently determined from the motor operating point parameters (i.e., the fundamental stator current level, torque, rotor speed, motor specifications). This is a desirable feature of a diagnostic algorithm applicable for general purposes. It becomes possible since the complicated motor environments are generally reflected in line noise which is measured for threshold design in the proposed algorithm. It implies that the diagnostic process is simplified without considering various reference estimations of different motor conditions which will result in increased system complexity and prior knowledge of these variations.

The only unknown parameter in the threshold (4.25) is the noise variance. The instantaneous line noise is effectively measured for the threshold parameter using the method described later in this section.

B. Q-function

Fig. 4.4-1 shows the probability distribution curve of noise and signature amplitude assuming an additive zero mean Gaussian noise channel. The area under each probability curve is one. By assuming an arbitrary threshold, γ_a, applied in decision, the probability distribution of decision-making errors can be identified in the shaded area as a Type I error which is reliability of small signal detection mainly depends on how the type II error (false detection) is suppressed. The *Q- function* is used to measure the error probability of false detection which is the right side of the shaded area in Fig. 4.4-1.

The term $Q^{-1}(P_{FA})$ in (4.25) is effectively a weighting factor. With a greater weighting factor, the threshold in (4.25) is to be increased and the false detection rate is decreased; this relationship is computed through (2.13) and plotted in Fig. 4.4-2. Once the allowable false error rate P_{FA} is determined and, hence, the weighting factor, diagnostic decision-making can be performed with a constant false alarm probability independent from the random noise conditions of the line current signal. This is because

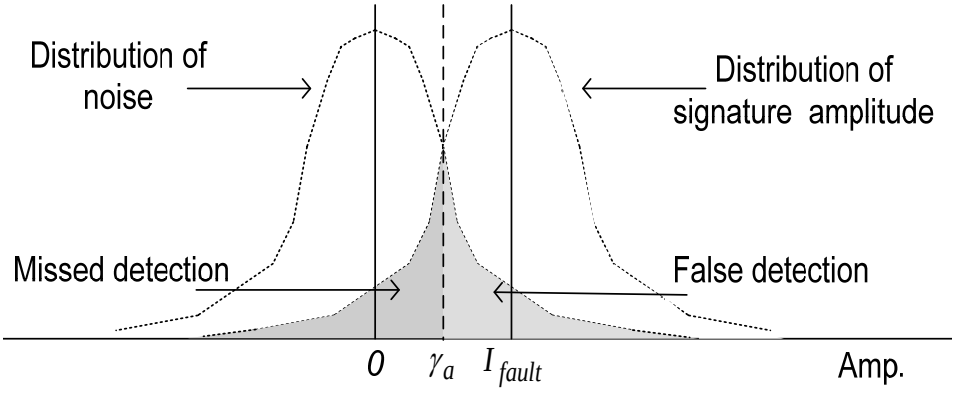

Fig. 4.4-1. Probability distribution of diagnostic decision errors.

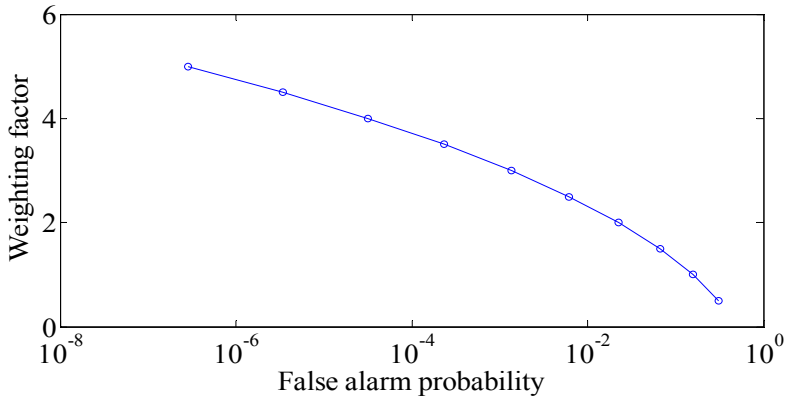

Fig. 4.4-2. Weighting factor vs false alarm probability.

the threshold in (4.25) is adaptively determined based on instantaneous noise condition and decouples the effect of noise on decision-making performance.

The optimization of threshold level and parameter depends on the diagnostic requirement of a specific system. An ideal threshold simultaneously minimizes false detection and missing detection probability. In small signal detections, minimizing the false alarm is commonly of more concern. Based on assumed noise conditions and allowed error probability, threshold parameters can be adaptively designed and optimized for a target system.

C. The Overall Algorithm

Fig. 4.5 shows the proposed diagnostic service routine implemented on DSP used for motor control. In order to prevent signal leakage in diagnostic signal processing, the Hanning window is initially applied. The proposed diagnostic routine starts with correlation-based detection applied to the line current signal which can be processed

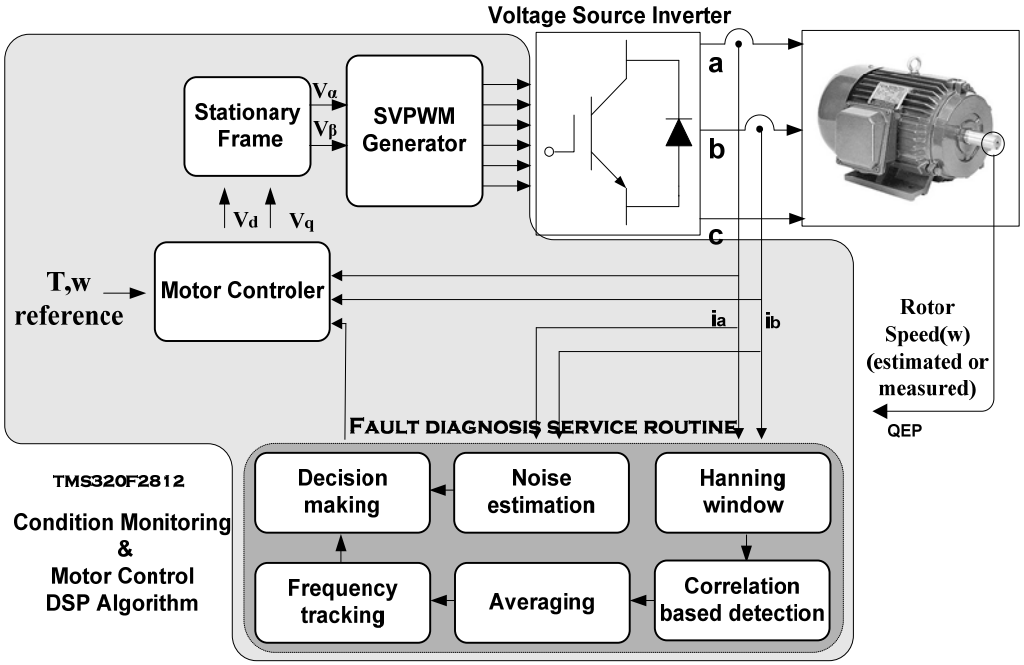

Fig. 4.5. Overall detection scheme.

coherently as shown in Fig. 4.1 or non-coherently as shown in Fig. 4.2. The output of correlations are averaged with (4.14) and fed to an ML-based frequency error tracking block; the operation is carefully derived in (4.13). The signature detections achieved through ML-based error compensation are eventually forwarded to the decision-making step. The decision-making is performed based on the threshold determined through the allowable false alarm requirement, *PFA,* and estimated line current noise in (4.25). The diagnostic service routine is expected to handle major signal processing errors in the proposed procedure for reliable detection which is commonly disturbed by frequency, phase, and noise errors.

4.4 Simulation and experimental results

Table 4.1. Experimental Environment

Sampling Hz	*25 kHz*
Data acquisition board	NI-DAQmx
Motor	3 hp / 4 - pole IM
DSP board	eZ DSP 320F2812
Frequency tracking range	1Hz
PFA	0.00097
# of Buffer (*N2*)	500

A. Modeled Matlab Simulation Result

In order to verify the effectiveness of the proposed diagnostic routine, a typical stator current is modeled with fault conditions of a broken rotor bar. The distorted current signal is established assuming −15 dB noise, and 11% THD with 5th and 7th harmonics. The broken rotor bar signature of -40dB amplitude is inserted based on the fault equation assuming slip s=0.016 pu. The simulation is performed with the modeled signal in Fig. 4.6(a). (All the experiments/simulations are performed assuming stationary operation of a motor.)

In the simulation, *PFA*, frequency tracking range, and available buffer of a DSP are assumed to be the same as shown in Table. 4.1. The signal with 50K samples is utilized for each simulation result. The fundamental signal is assumed filtered for clear presentation of the algorithm in the simulation.

The simulation is performed in the proposed procedure provided in Fig. 4.5. Cross-correlation based detection is applied to the current signal which is processed non-coherently assuming the exact value of the frequency and, hence, phases are practically unknown. The output of cross-correlation is averaged and stored in an assumed DSP buffer in Table. 4.1; this averaged signal is shown in Fig. 4.6(b) with a frequency offset, and (c) without an offset. The relation of the input signal length *N2* and the buffer size *N* is shown in (4.15) where *N=50K, N2=500.*

The averaged signal shows a dominant 1 Hz signal for 250 time samples in (b). It is the inserted frequency offset between the modeled fault signal and the reference signal. The signal without frequency offset is shown in Fig. 4.6(c) for comparison. The averaged signals are fed to a high performance ML-based offset tacking block.

The resolution of the ML algorithm defined in (4.17) is initially assumed as 0.04Hz. The frequency tracked amplitudes and the threshold measured are shown simultaneously in Fig. 4.6(d) with offsets varying from 0 to 1 Hz. In the figure, (–) frequency values are simply replicas of (+) frequency offset results for convenience since non-coherent detection cannot discriminate polarity of frequency. Zero frequency is the point where the tracking scheme is not applied. In the figure, it is shown that the frequency offset inserted is accurately tracked at the frequency of the maximum normalized amplitude in all trials. One can also determine that the maximum points are above threshold while signals are below each threshold at the point without frequency tracking. The assumed resolution 0.04 Hz shows sufficient performance to discriminate maximum points, which is further confirmed in the offline experiment.

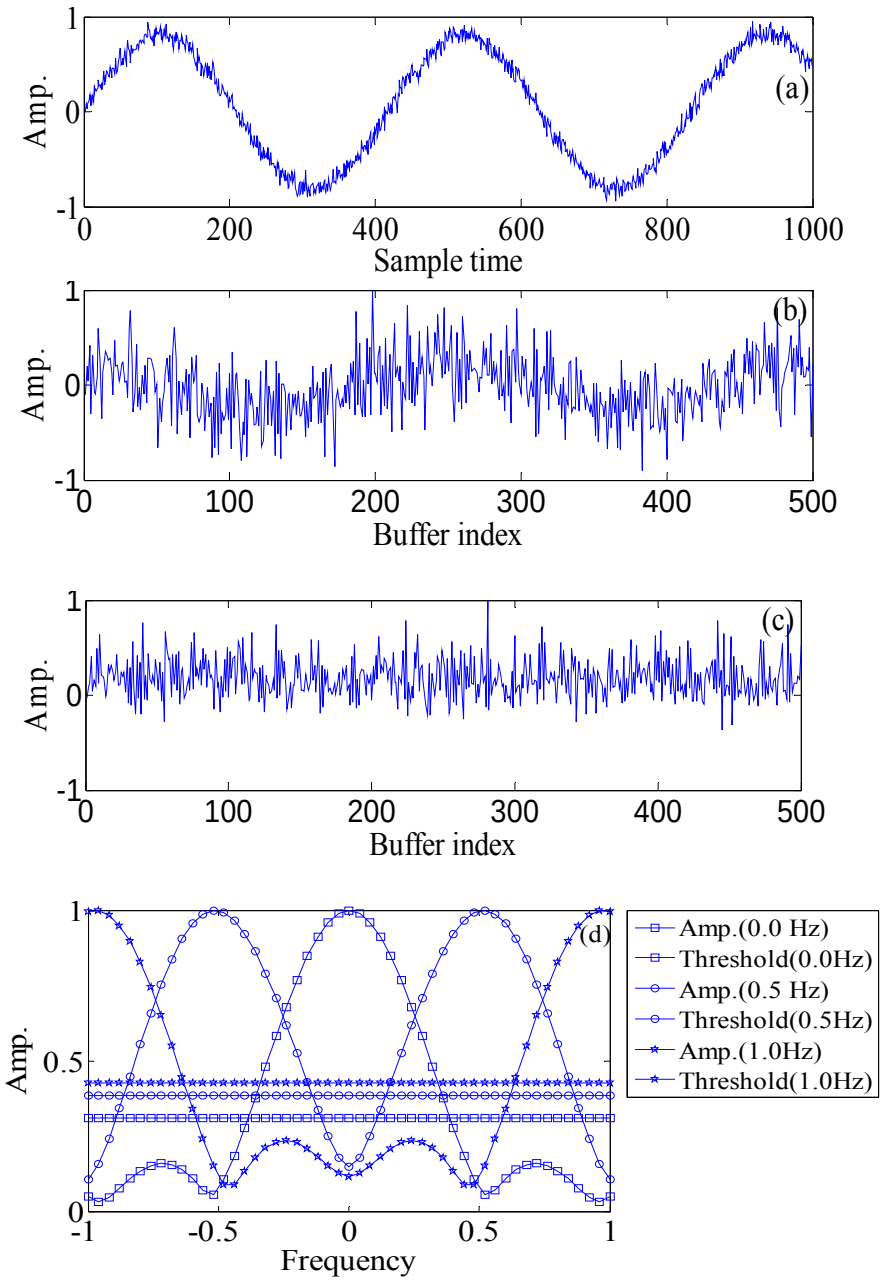

Fig. 4.6. (a) modeled line current signal, (b) averaged correlation output with 1 Hz offset, (c) with 0 Hz offset, and (d) frequency tracking with possible offsets (Resolution = 0.04 Hz).

B. Offline Experimental Result

The verification tests of the proposed algorithm are run utilizing line current data obtained by a 1.25 MS/s, 12-bit resolution data acquisition system which is set to produce a 25kHz sampling frequency. The 3-hp induction motors are loaded by the DC generator which is assumed open loop controlled in all experiments. The acquired offline data are processed using Matlab.

In Fig. 4.7, the stator current from the data acquisition card is shown with (a) eccentricity, (b) mixed fault signatures and unknown signatures simultaneously through FFT analysis. Instantaneous fault frequencies are measured based on the fault equation.

The test motor is designed with mixed fault conditions for performing the experiments in a practical environment. Fault conditions of a test motor are shown in Fig. 4.7. (c) with eccentricity house and (d) with broken bar rotor.

In Tables 4.2 to 4.3, DF is the detection flag, DA is the detected amplitude, TH is the threshold. The definition with subscript T is the result obtained through the frequency tracking operation. All amplitudes are shown in dB.

B1. Fault Signatures of Test Motor

An FFT Spectrum Analyzer is used for realtime investigation of the line current of faulty motor as shown in Fig. 4.7(a) and (b). The eccentricity signature monitored is –41.2 dB at 20% torque which tends to decrease in the high torque range and around

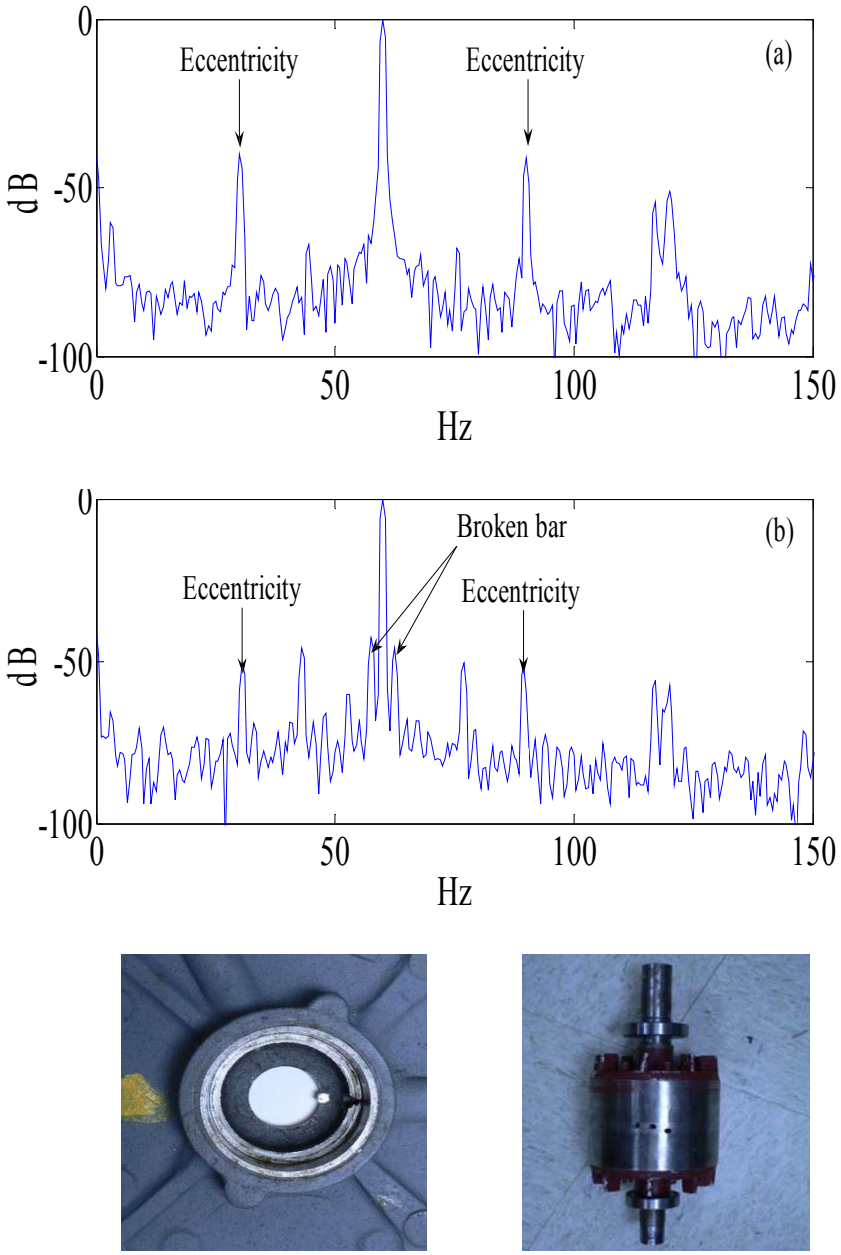

Fig. 4.7. Stator current spectrum: (a) eccentricity signature at 20% torque, (b) mixed signature with broken rotor bar fault at 100% torque (*f*: 60 Hz), (c) eccentricity house, (d) broken rotor bar rotor.

–55.45 dB at 40% ~ 100% torques. For the broken rotor bar signature, it is –45.7 dB at 50% torque. Unlike the eccentricity, the broken rotor bar signatures increases with load and –41.8 dB at 100% torque. These results are taken to evaluate the accuracy of detection in the offline diagnosis.

B2. Offline Results for Eccentricity

Fig. 4.8 shows the averaged correlation output (a) and the frequency tracking result (b). The averaged signal in (a) is rounded due to the applied Hanning window to prevent the effects of the fundamental signal leakages in diagnostic signal processing. In (b), the maximum occurs at zero frequency implying there is negligible frequency offset. The threshold is well placed to decide eccentricity fault. This is further confirmed in Table 4.2. The detected eccentricity signature is determined correctly in both trials of Fig. 4.8(c) shows detection through the PSD scheme in Fig. 4.1. The PSD is one of the algorithms utilizing optimal property of matched filtering in (4), which has been adopted as a high performance low cost diagnostic scheme. With no frequency offset (0Hz) condition, the performance of the PSD is confirmed by the precise detection close to expected -41.2dB as shown in (c). With potential frequency error at + 0.5 Hz or -0.5Hz, the analysis shows the loss of amplitude as expected in Fig. 4.2. In the proposed frequency tracking and without tracking with about 1.04dB error from expected –41.2 dB obtained from the Spectrum Analyzer.

In the proposed scheme in (b), those frequency errors can be tracked and detections

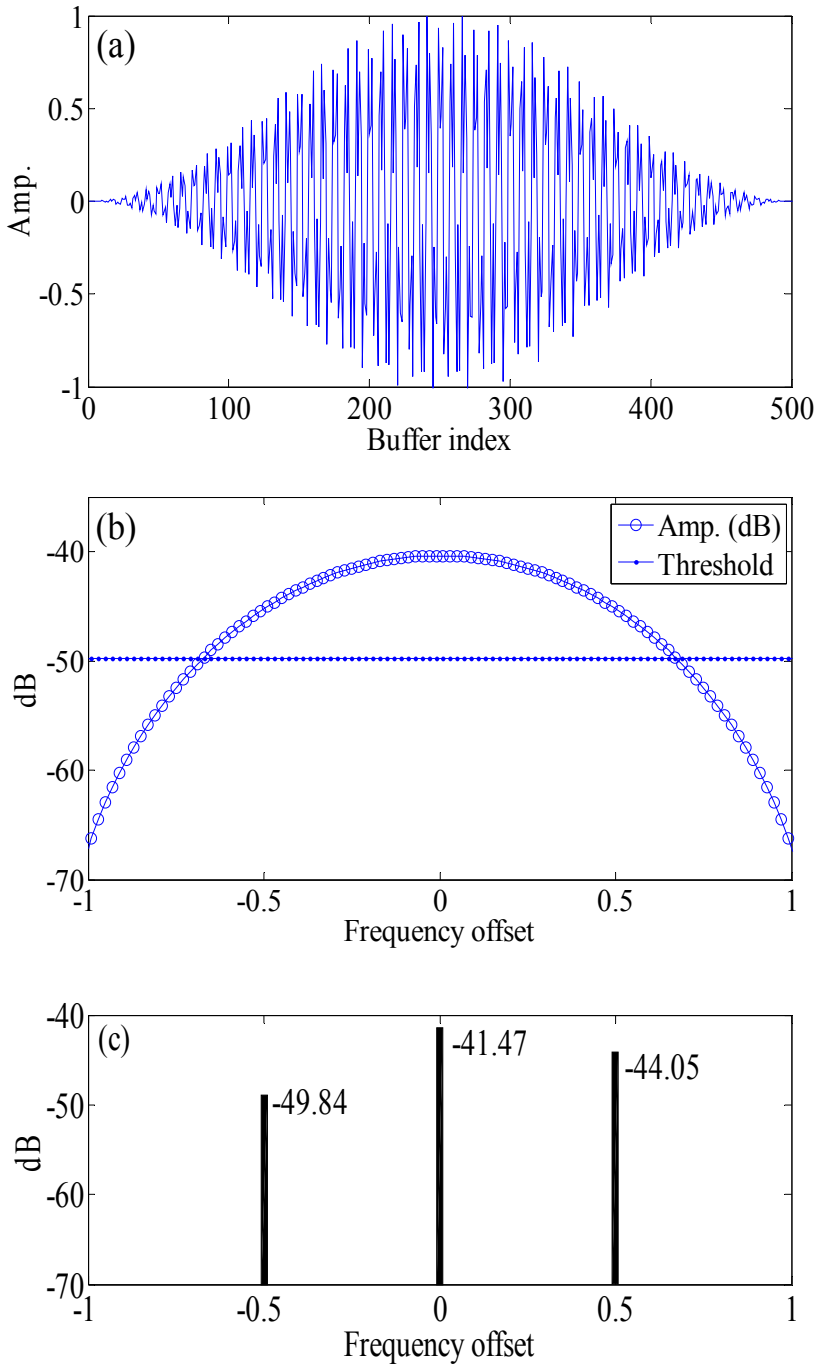

Fig. 4.8. Frequency tracking for eccentricity fault: (a) averaged signal, (b) frequency tracking and decision-making (Resolution = 0.02 Hz), and (c) coherent detection without strategy for frequency offset compensation.

Table. 4.2. Decision-Making 10 Seconds, *f*: 60 Hz, 20 % Torque.

DF	DA	DF_T	DA_T	TH
1	–40.16	1	–40.16	–49.78

are compensated for reliable diagnosis. Because the schemes in [25] [28] are optimized for precise detection in specific frequencies, serious loss of optimality occurs when the frequency/phase information has offsets as in shown in (c). To be adopted in industry, robust performance under error conditions needs to be maintained which is the main assertion of this study.

B3. Offline Results for Broken Rotor Bar

In Fig. 4.9(a), the averaged signal is shown with dominant signal around 1.5 Hz. It is the fundamental stator current signal monitored at about 1.5 Hz away from the broken rotor bar signature (out of tracking range in Table. 4.1). Although the proposed algorithm is effective in small frequency offset tracking, it is interfered if the fundamental signal is within the tracking range. The range needs to be smaller than the difference between the excitation and the expected fault frequencies.

In Fig. 4.9(b), the frequency offset is identified at maximum point with 0.46 Hz. In Table 4.3, the fault is determined correctly only after frequency tracking and detected amplitude is boosted from -49.8 to -41.32 dB. The effectiveness of the proposed ML

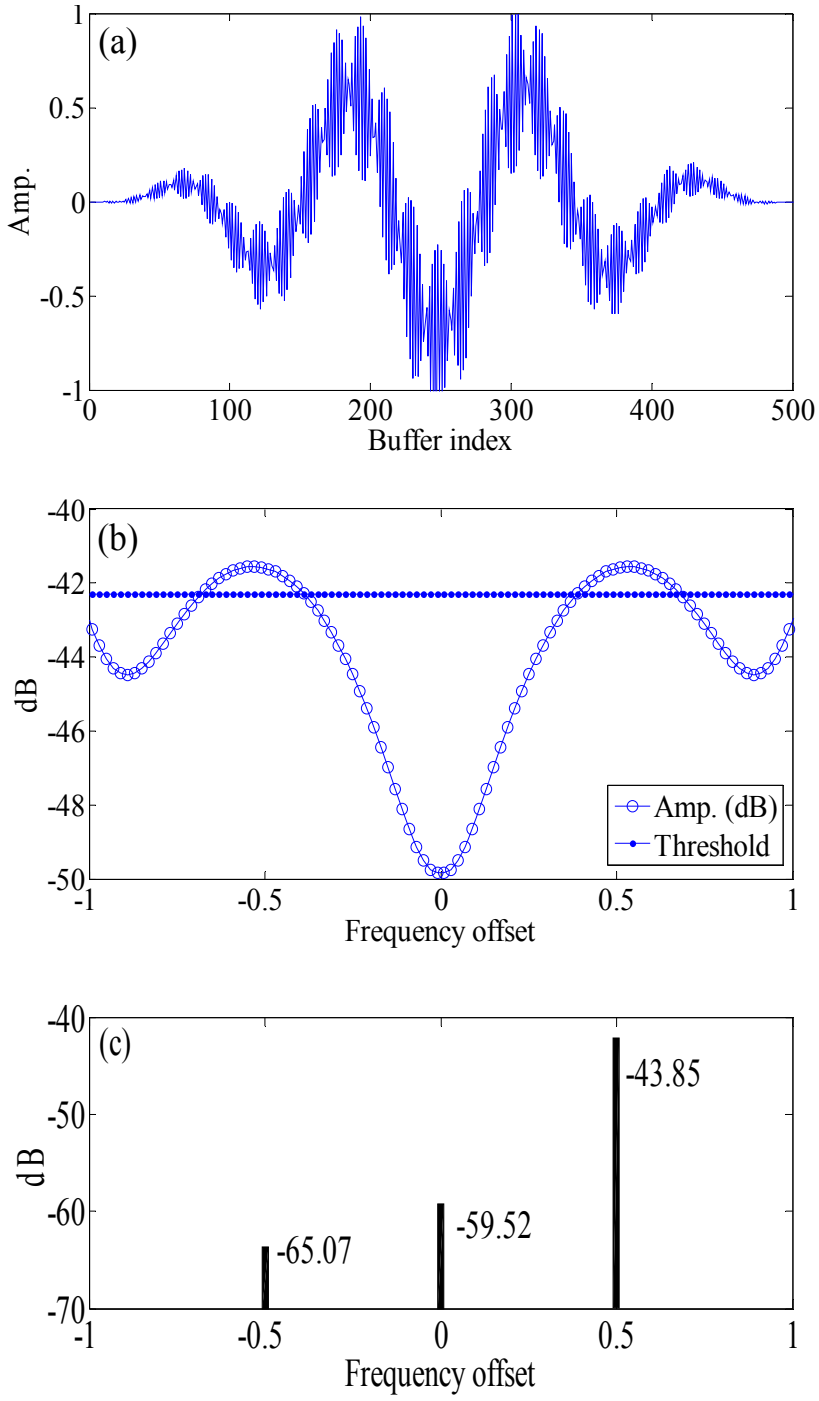

Fig. 4.9. Frequency tracking for broken rotor bar fault: (a) averaged signal, (b) frequency tracking and decision-making (Resolution = 0.02 Hz), and (c) coherent detection without strategy for frequency offset correction.

Table. 4.3. Decision-Making 10 Seconds, f: 60 Hz, 100% Torque.

DF	DA	DF_T	DA_T	TH
0	–49.8	1	–41.32	–42.30

tracking algorithm can be confirmed from amplitude monitored through the Spectrum Analyzer which is –41.8 dB and yields only 0.47dB error from the tracked result.

Fig. 4.9 (c) shows detections through one of the optimal schemes, PSD, to compare the performance with the proposed algorithm in (b) under error conditions. Unlike the zero offset condition in Fig. 4.8, the frequency/phase offsets are completely ambiguous in Fig. 4.9. (c) shows the serious performance degradation of amplitude loss due to frequency/phase ambiguity. Detection at 0Hz, -0.5Hz and 0.5Hz shows unreliable values. Meanwhile, through the use of phase error-immunized detection and frequency tracking in (b), the detection performance almost becomes close to optimal and robustness of detection is maintained under error conditions.

B4. Offline Results for Small Signature Detection

One of the major challenges in diagnostic analysis is the ambiguity between the small fault signature and existing noise. Fig. 4.10 (a) shows the current spectrum with eccentricity signatures with amplitudes ranging -65dB to -52dB. A signature at 210Hz with amplitude -65.29dB is detected below the threshold -59.44dB in Fig. 4.10(b). Based

on Fig. 4.4-2, the adjustment of threshold can be done as -65.73 dB with 0.06681 *PFA* to make a detection of the signature. 0.06681 *PFA* is equivalent to 93.32% accuracy of the detection which practically is high enough. Through the adaptively adjusted threshold definition, performance can be chosen based on user's expectation in small signature detection.

B5. About Threshold Variations and Resolution

The determined thresholds are -59.44dB, -49.78dB, and -42.3dB in Figs. 4.10, 4.8, and 4.9 with load torques 15%, 20%, and 100%, respectively. The thresholds are shown to be increased with more torque but not linearly dependent. More fundamentally, the threshold in (4.25) is determined by measured current noise level which variation is assumed nonlinear. The line current noise is assumed simultaneously reflected from numerous machine conditions such as load variations, speed vibrations, interferences, etc. Incorporating instantaneous noise conditions in the decision-making is assumed to be crucial for the reliability enhancement, especially for small signal detection in a short time.

The resolutions are assumed 0.02 Hz for Figs. 4.8 and. 4.9 and 0.04 Hz for Fig. 4.10. Comparing resolutions at the maximum point in figures, one can determine that there is minimal gain with a higher resolution of 0.02Hz than with 0.04Hz. Even though it is not shown experimentally, the resolution further decreased below 0.04 Hz began to show non-negligible errors. In online experiments, a 0.04Hz resolution is assumed.

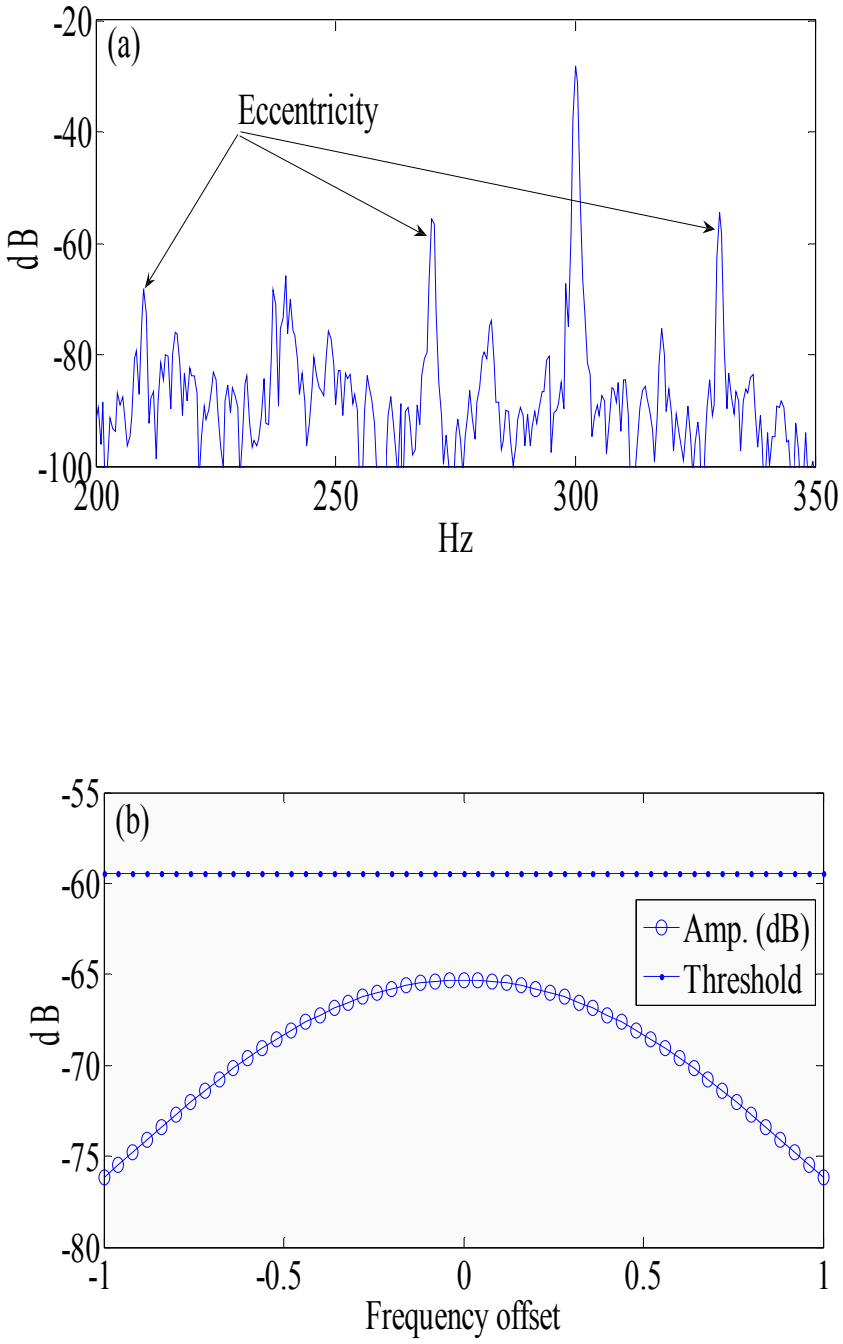

Fig. 4.10. (a) Stator current spectrum with eccentricity signature under 15% torque and (b) frequency tracking and decision-making (Resolution 0.04 Hz).

C. Online Experimental Results

Online experiments are performed to demonstrate the algorithm on a DSP. The test induction motor is driven by the inverter. V/F motor control and online fault diagnostic service routine are simultaneously implemented on a 32-bit fixed-point, 12-bit ADC, 150 MHz DSP of TMS320F2812.

In Figs. 4.11 to 4.12, zero frequency is the fault frequency measured by the DSP from the fault equation. In Fig. 4.11, the DSP measures the fault frequency correctly showing a maximum at zero frequency i.e. -40.2 dB. In Fig. 4.12, 0.24 Hz frequency offset is monitored for the broken rotor bar signature.

The changes in detected amplitude and thresholds in time are shown in Figs. 4.13 to 4.14. In both figures, the detected signature hardly varies after 2 seconds. The threshold measured is unstable initially and becomes stabilized after about 8 seconds. After becoming stabilized, it tends to decrease since one of the threshold parameters, effective noise variance, σ^2 / N, decreases as the number of samples used increases, which confirms careful derivation in (4.25).

The latency time about 10 seconds in diagnosis is assumed to be acceptable because condition monitoring is performed over a relatively long period of time, especially with mechanical type of fault such as broken rotor bar or eccentricity.

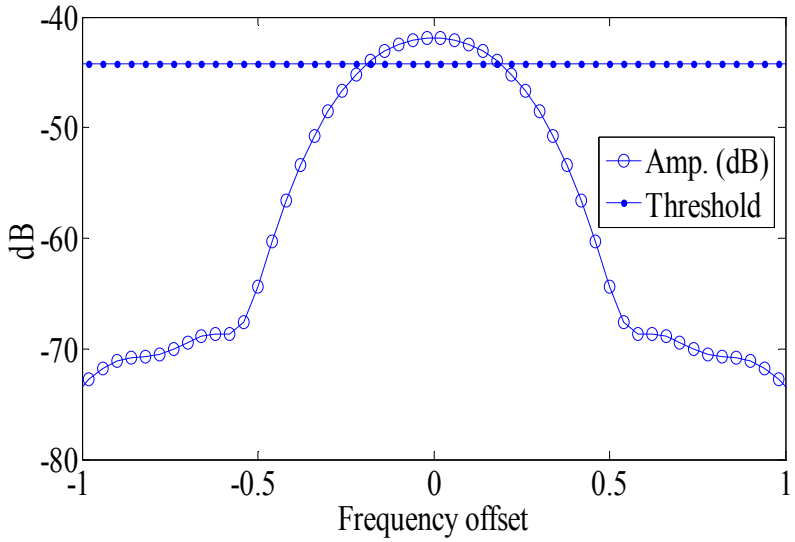

Fig. 4.11. Frequency tracking for eccentricity signature with 20% torque at 10 seconds (*f*: 48.3 Hz, Resolution: 0.04 Hz).

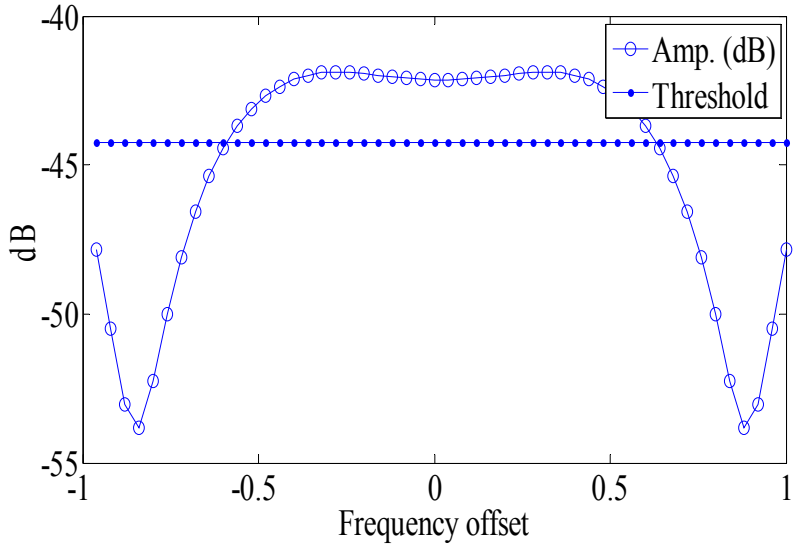

Fig. 4.12. Frequency tracking for broken rotor bar signature with 100% torque at 10 seconds (*f*: 48.3 Hz, Resolution: 0.04 Hz).

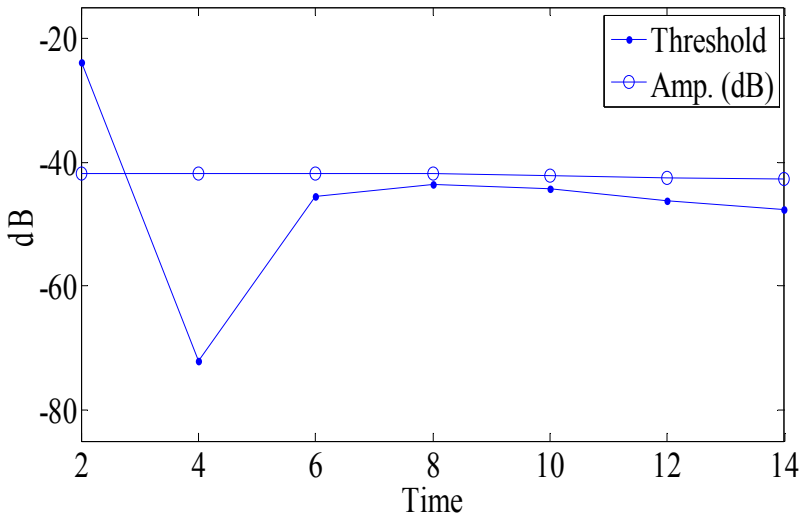

Fig. 4.13. Detection time for eccentricity with 20% torque (*f*: 48.3 Hz).

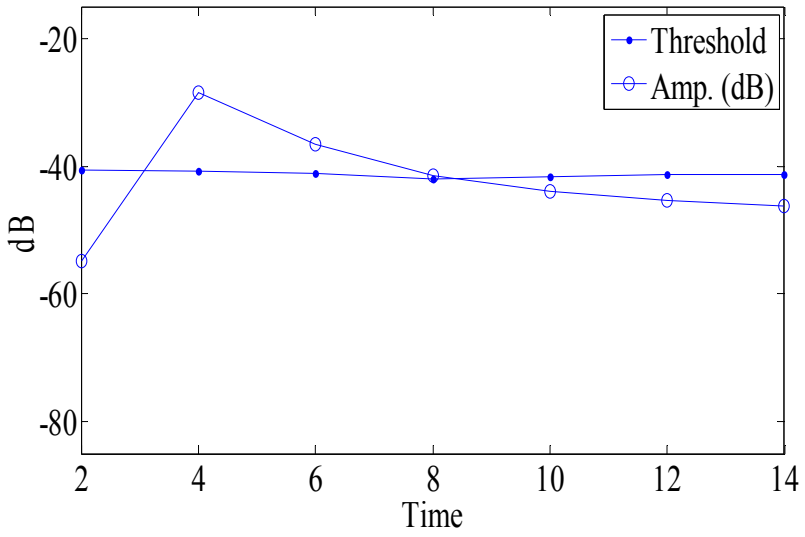

Fig. 4.14. Detection time for broken rotor bar with 100% torque (*f*: 48.3Hz).

The fundamental of the proposed threshold setting and frequency offset tracking algorithm are applied the same in any condition but the result changed in the presented online and offline trial because the error conditions of frequency/phase and noise level are inherently vary randomly. The proposed algorithm is designed to track those error variations resulting in different response. The frequency offsets are monitored 0.46 Hz in Fig. 4.9 in offline and 0.24Hz in Fig. 4.12 in the online experiment. Those offset variations are identified through a proposed tracking scheme showing its robustness to variable offsets. The threshold -49.8dB is shown in Fig. 4.8 in the offline and -44.5dB is observed in Fig. 4.11 in the online experiment which observed differences are usually within 5dB. It is assumed that the instantaneous change of noise level and different environment has effected the decision-making procedure. The threshold measurements are initially labile and become reliably stabilized over time as shown in Figs. 4.13 to 4.14 through multiple trials.

In online experiments, the threshold applied is designed to keep false detection errors strictly within 0.097% as shown in Table. 4.1. That is why the signatures are usually detected close to threshold within 5~10 dB. The thresholds can be further decreased to detect small signatures by reducing the weighting factor in (4.25). This can be done based on the relation shown in Fig. 4.4-2 from the trade-off of detection performance.

4.5 Conclusion

The fault detection and decision-making capability of the proposed algorithms are demonstrated by mathematical verifications, simulations, and offline/online experiments.

It is observed that ambiguities such as fault frequency mismatch, phase of the fault vector, and changes in the noise level and fault signatures can be efficiently handled using a simple algorithm capable of frequency tracking, phase eliminating detection, and adaptive threshold.

Through experiments, the proposed schemes are shown to have robust performance under error conditions while keeping complexity low enough to be applied to DSP for motor control. It is shown to maintain close to optimal performance while conventional optimal schemes result in serious loss of optimality. The proposed threshold has been proved to make decisions for small signatures with theoretically expected performance under any noise conditions.

The established theoretical background can be exploited for development of reliable MCSA algorithms in future studies. A simplified decision-making procedure that is independent of the motor operating is highlighted as a powerful fault monitoring tool to be used as a subroutine in the DSP software.

CHAPTER V

A GENERALIZED FAULT SIGNATURE DETECTION METHOD OF INDUCTION MACHINE BASED ON MULTI-PHASE SIGNAL

5.1 Introduction

As high power applications in industry employ multi-phase motors and generators, a generic diagnostic solution is needed for various multi-phase systems. In this study, a mathematical analysis of the conventional DSP-based diagnostic algorithms is performed, especially with frequency tone detectors. Based on the analysis, it is theoretically generalized and flexibly extended to multiphase machine cases.

5.2 Harmonic interference modeling

Unlike the three phase induction machine, the third harmonic is not canceled out in the current signal of a five phase machine. Suppressing those harmonics commonly requires special control schemes. Even with additional control, there is a high possibility that second and third harmonics and other interferences will appear under iron saturations or machine imperfections which is more probable in a higher phase motor system [54][56].

In this study, the stator current signal is modeled to cover a different noise, I_{noise_a}, I_{noise_b}, I_{noise_c}.... in each line current; different fault signatures, I_{fault_a}, I_{fault_b}, I_{fault_c}, and unbalanced harmonics, $I_{harmonics\_a}$, $I_{harmonics\_b}$, $I_{harmonics\_c}$...., with

different phases $\varphi_{harmonics\_a}$, $\varphi_{harmonics\_b}$, $\varphi_{harmonics\_c}\cdots$

The modeled stator current $I_{stator}(n)$ is as follows

$$I_{stator}(n) = \left(I_{stator\_a}(n), I_{stator\_b}(n), \ldots I_{stator\_K}(n)\right) \tag{5.1}$$

where

$$I_{stator\_a}(n) = I_{fault\_a}\cos(w_{fault}n + \varphi_{fault\_1}) + I_{noise\_a} + \sum_{h}\sum I_{harmonics\_a}(h)\cos(w_{harmonic\_a}(h)n + \varphi_{harmonics\_a}(h))$$

$$I_{stator\_b}(n) = I_{fault\_b}\cos(w_{fault}n + \varphi_{fault\_1} - 2\pi/3) + I_{noise\_b} + \sum_{h}\sum I_{harmonics\_b}(h)\cos(w_{harmonic\_b}(h)n + \varphi_{harmonics\_b}(h))$$

.
.
.

$$I_{stator\_K}(n) = I_{fault\_K}\cos(w_{fault}n + \varphi_{fault\_1} + 2\pi/3) + I_{noise\_K} + \sum_{h}\sum I_{harmonics\_K}(h)\cos(w_{harmonic\_K}(h)n + \varphi_{harmonics\_K}(h))$$

, $h = 1, 2, 3, \cdots$ (5.2)

where h is the harmonic number; $I_{stator}(n)$ is the stator current with amplitude of fault signature (I_{fault}), stator current harmonics ($I_{harmonics}$), and random noise (I_{noise}); φ_{fault} is the phase of the fault signature, $\varphi_{harmonics}$ is the harmonic signal phase, $w_{harmonic}$ is the harmonic signal frequency, w_{fault} is the frequency of a fault, and K is the K^{th} line current signal.

5.3 Detection based on multiphase signal

A. Frequency Tone Detection with Single Phase Signal

From the Fourier series theory, a signal can be decomposed into mean, cosine, and sine terms as follows [63]:

$$s\ (t) = a_0 + \sum_{l=1}^{\infty}\left[a_l \cos(ln) + b_l \sin(ln)\right] \tag{5.3}$$

where a_0 is the mean, and a_l and b_l is the Fourier coefficient for frequency in the interval $[-\pi, \pi]$. Assuming the specific frequency of interest with $k/(2\pi)$, the coefficient detection of the cosine and the sine terms can be made with the averages of a cross-correlation operation. For the cosine coefficient, it is as follows:

$$\begin{aligned}\cos\_coe &= \frac{1}{N}\sum_{n=0}^{N}\cos(kn)s(n) \\ &= \frac{1}{N}\sum_{n=0}^{N}\cos(kn)\left[a_0 + \sum_{l=1}^{\infty}\left[a_l\cos(nl) + b_l\sin(nl)\right]\right] \\ &\approx \frac{1}{N}\sum_{n=0}^{N} a_k \cos(kn)\cos(kn) \approx \frac{a_k}{2}\end{aligned} \tag{5.4}$$

For the sine coefficient, in the same way as in (5.4), it is as follows:

$$\sin\_coe \approx \frac{1}{N}\sum_{n=0}^{N}\sin(kn)s(n) \approx \frac{b_k}{2} \tag{5.5}$$

When the phase information is not available for the signal of interest, (5.4) and (5.5) can be expressed as follows:

$$\cos\_coe = \cos(\theta)\frac{a_k}{2} \tag{5.6}$$

$$\sin\_coe = -\sin(\theta)\frac{b_k}{2} \tag{5.7}$$

The cosine and the sine multiplication in (5.4) and (5.5) used to project the frequency of interest into the orthogonal domain can be defined as a matrix:

$$\Phi_{\text{single}} = \begin{bmatrix} \cos(wn) \\ \sin(wn) \end{bmatrix} \tag{5.8}$$

The strategy to find the frequency coefficient of interest is assumed to be the same as the detecting fault frequency tone in a motor current spectrum.

B. Frequency Tone Detection with Multiphase Signal

The coefficient of a fault signal can be obtained by applying the projecting matrix to the motor current signal; This matrix is obtained through the extension from (5.8) as follows:

$$\Phi_{multi} = \frac{1}{K}\begin{bmatrix} \cos(wn) & \cos(wn-\xi) & ....\cos(wn-(K-1)\xi) \\ \sin(wn) & \sin(wn-\xi) & ....\sin(wn-(K-1)\xi \end{bmatrix} \tag{5.9}$$

The electrical angle between the adjacent magnetic axes of the uniformly distributed *n*-phase windings is represented by ξ.

With (5.9), the coefficient can be obtained through averaging as follows:

$$\cos\_coe \approx \cos(\theta)\frac{a_{k\_averaged}}{2} \tag{5.10}$$

$$\sin\_coe \approx -\sin(\theta)\frac{b_{k\_averaged}}{2} \tag{5.11}$$

From (5.10) and (5.11), the sine and the cosine coefficients of the multiphase system are found, which also looks similar to (5.6) and (5.7).

5.4 Multiphase-based fault signature detection

In the following, detections are derived from an arbitrary multiphase system by applying (5.9) to the modeled line current in (5.1) to determine its operation.

Assuming sufficient averaging time *N*, coefficients are derived as follows.

$$\begin{aligned}\cos\_coe &= \frac{1}{KN}\sum^{N}\begin{pmatrix}\cos(w\ n)I_{stator\_a}(n)+\cos(w\ n-2\pi/K)I_{stator\_b}(n)\\ ....+\cos(w\ n-2\pi(K-1)/K)I_{stator\_c}(n)\end{pmatrix}\\ &\approx \frac{1}{2K}\left(\cos\left(\varphi_{fault}\right)\right)\left(I_{fault\_a}+I_{fault\_b}....+I_{fault\_K}\right)+I_{noise\_x}\end{aligned} \tag{5.12}$$

$$\begin{aligned}\sin\_coe &= \frac{1}{KN}\sum^{N}\begin{pmatrix}\sin(w\ n)I_{stator\_a}(n)+\sin(w\ t-2\pi/K)I_{stator\_b}(n)\\ ....+\sin(w\ n-2\pi(K-1)/K)I_{stator\_K}(n)\end{pmatrix}\\ &\approx -\frac{1}{2K}\left(\sin\left(\varphi_{fault}\right)\right)\left(I_{fault\_a}+I_{fault\_b}....+I_{fault\_k}\right)+I_{noise\_y}\end{aligned} \tag{5.13}$$

where

$$I_{noise\_x} = \frac{1}{KN}\sum^{N}\begin{pmatrix}\cos(w\ n)I_{noise\_a}+\cos(w\ n-2\pi/K)I_{noise\_b}\cdots\\ +\cos(w\ n-2\pi(K-1)/K)I_{noise\_K}\end{pmatrix} \tag{5.14}$$

$$I_{noise\_y} = \frac{1}{KN}\sum^{N}\begin{pmatrix}\sin(w\ n)I_{noise\_a}+\sin(w\ n-2\pi/K)I_{noise\_b}\cdots\\ +\sin(w\ n-2\pi(K-1)/K)I_{noise\_K}\end{pmatrix} \tag{5.15}$$

In (5.12) and (5.13), it is observed that the multiphase-based detection averages existing fault signatures in each line current with 1/*K*. This makes a signature detection more reliable.

In (5.14) and (5.15), it is also shown that the noise is averaged 1/*KN*, which is approximately *N* times more suppressed than the averaged fault signature. It mathematically verifies that the noise can be suppressed more tightly as the amount of phase signal utilization increases.

A. Considerations in Three Phase System

The detection based on the three-phase current signal is analyzed in more detail. From (5.9), the three-phase projecting matrix with *K=3* can be expressed as

$$\Phi_{three} = \frac{1}{3}\begin{bmatrix} \cos(wn) & \cos(wn-2\pi/3) & \cos(wn+2\pi/3) \\ \sin(wn) & \sin(wn-2\pi/3) & \sin(wn+2\pi/3) \end{bmatrix} \tag{5.16}$$

From(5.16), it is similar to the Park transformation matrix in the three-phase system [17][55]. The Park transformation theory is one kind of frequency tone detector used for analysis in the power electronics and motor drive system. If with *K=1*, it explains the conventional low complexity DSP algorithm, a phase sensitive detection where the core step is cosine and sine detection in (5.6) and (5.7).

Meanwhile, Park transform needs further optimization in complexity in diagnosis due to phase approximation in many drive systems which results in redundant computation complexity in diagnosis. In (5.12) and (5.13), it is shown that the fault signature in each line current averages 1/K, which makes detection more convincing.

However, one of the phase signals, which is the third current signal I_c, is commonly not available in the usual three phase system to reduce sensor cost which is commonly approximated from I_a and I_b. The approximation is quite acceptable in many practical control systems since the fundamental current signal is dominant and is supported by a high signal to noise ratio (SNR). In small fault signal detection, the dominancy assumption is not valid, suffering high noise interferences resulting in poor approximation. The fault signature and noise statistics is added multiple times in (5.12) and (5.13) in which the Park transform-based detection builds bias without an increase of detection reliability by additionally utilizing signal I_c.

B. Simple Amplitude Detection

With the frequency tone detection in the previous section, the strategy to find the fault signature amplitude is derived as follows:

$$\begin{aligned} I_{dec} &= \sqrt{\cos\_coe^2 + \sin\_coe^2} \\ &= \sqrt{\left(\frac{1}{2K}\left(I_{fault\_a} + I_{fault\_b} + I_{fault\_c} \cdots\cdots + I_{fault\_K}\right)\right)^2 + I_{noise\_xy}} \\ &\approx \frac{1}{2K}\left(I_{fault\_a} + I_{fault\_b} + I_{fault\_c} \cdots\cdots + .I_{fault\_K}\right) \end{aligned} \tag{5.17}$$

where

$$I_{noise\_xy} = \begin{pmatrix} \frac{1}{K}\left(\cos\left(\varphi_{fault}\right)\right)\left(I_{fault\_a} + I_{fault\_b} + I_{fault\_c} \cdots\cdots + I_{fault\_K}\right) I_{noise\_x} \\ \frac{-1}{K}\left(\sin\left(\varphi_{fault}\right)\right)\left(I_{fault\_a} + I_{fault\_b} + I_{fault\_c} \cdots\cdots + I_{fault\_K}\right) I_{noise\_y} \\ +\left(I_{noise\_x}\right)^2 + \left(I_{noise\_y}\right)^2 \end{pmatrix} \tag{5.18}$$

The averaged fault signature can be approximated as follow:

$$I_{fault\_avg} \approx 2I_{dec} \tag{5.19}$$

where

$$I_{fault\_avg} = \frac{1}{K}\left(I_{fault\_a} + I_{fault\_b} + I_{fault\_c} \ldots\ldots + I_{fault\_K}\right) \tag{5.20}$$

Due to the large noise amplification shown in (5.18), the algorithm shows lower performance than the maximum likelihood-based detection in a steady state which will be compared in the following section.

C. Maximum Likelihood Phase Estimation-Based Detection (MLE)

The MLE of the fault phase is derived as follows, assuming a single phase in the beginning, with the results expanded for multiphase. The line fault signature buried in noise is modeled as follows;

$$I_{stator\_a}(n) = I_{fault\_a}\cos(w_{fault}n + \varphi_{fault\_a}) + I_{noise\_a} \tag{5.21}$$

MLE can be obtained by maximizing the probability function:

$$\begin{aligned} P(I_{stator\_a};\varphi_{fault\_a}) &= \frac{1}{(2\pi\sigma_a^2)^{N/2}} \\ &\exp\left\{-\frac{1}{2\sigma_a^2}\sum_{n=0}^{N-1}\left(I_{stator\_a}(n) - I_{fault}\cos(w_{fault}n + \varphi_{fault\_a})\right)\right\} \end{aligned} \tag{5.22}$$

where σ_a^2 is the noise variance in line current I_a. Then, it is effectively the same when minimized as follows:

$$J(\varphi_{fault\_a}) = \sum_{n=0}^{N-1} (I_{stator\_a}(n) - I_{fault\_a}\cos(w_{fault}n + \varphi_{fault\_a}))^2 \quad (5.23)$$

Through J, the following is derived

$$\begin{aligned} &\sum_{n=0}^{N-1} I_{stator\_a}(n)\sin(w_{fault}n)\cos(\varphi_{fault\_a}) = \\ &-\sum_{n=0}^{N-1} I_{stator\_a}(n)\cos(w_{fault}n)\sin(\varphi_{fault\_a}) \end{aligned} \quad (5.24)$$

The phase of fault signature is obtained from (5.23).

$$\varphi_{fault\_a\_estimated} = -\arctan\frac{\sum_{n=0}^{N-1} I_{stator\_a}(n)\sin(w_{fault}n)}{\sum_{n=0}^{N-1} I_{stator\_a}(n)\cos(w_{fault}n)} \quad (5.25)$$

Expanded to the arbitrary multiphase, the general solution is obtained as follows:

$$\begin{aligned} -\varphi_{fault} &= \\ &\arctan\frac{\sum_{n=0}^{N-1}\begin{pmatrix} I_{stator\_a}(n)\sin(w_{fault}n) + I_{stator\_b}(n)\sin(w_{fault}n - 2\pi/K) \\ .... + I_{stator\_K}(n)\sin(w_{fault}n - 2\pi(K-1)/K) \end{pmatrix}}{\sum_{n=0}^{N-1}\begin{pmatrix} I_{stator\_a}(n)\cos(w_{fault}n) + I_{stator\_b}(n)\cos(w_{fault}n - 2\pi/K) \\ + I_{stator\_K}(n)\cos(w_{fault}n - 2\pi(K-1)/K) \end{pmatrix}} \\ &= \arctan\frac{\sum_{n=0}^{N-1} \sin\_coe}{\sum_{n=0}^{N-1} \cos\_coe} \end{aligned} \quad (5.26)$$

The equation above shows that the MLE of the phase of a fault signal is simply the averaged arctan of the cosine and sine coefficients of the frequency tone in (5.10) and (5.11). The general phase estimation solution can simply be expanded in the same way

from (5.25). Using the equations shown in (5.12) and (5.13) to (5.25), the following results are obtained:

$$\theta_{esti} = -\arctan \frac{\frac{1}{2} I_{fault\_avg} \left(\sin\left(\varphi_{fault} \right) \right) + I_{noise\_y}}{\frac{1}{2} I_{fault\_avg} \left(\cos\left(\varphi_{fault} \right) \right) + I_{noise\_x}}$$

$$= -\arctan(\tan(\varphi_{fault})) \tag{5.27}$$

Based on the phase estimation, the fault signature amplitude can be estimated as follows:

$$I_{fault\_avg} \approx \frac{2\cos\_coe}{\cos(\theta_{esti})} = I_{fault\_avg} + I_{noise\_x\_1} \tag{5.28}$$

$$I_{fault\_avg} \approx \frac{2\sin\_coe}{\sin(\theta_{esti})} = I_{fault\_avg} + I_{noise\_y\_1} \tag{5.29}$$

where

$$I_{noise\_x\_1} = \frac{\frac{2}{KN} \left(\sum^{N} \begin{pmatrix} \cos(w_e t) I_{noise\_a} + \cos(w_e t - 2\pi / K) I_{noise\_b} \\ .... + \cos(w_e t - 2\pi(K-1)/K) I_{noise\_n} \end{pmatrix} \right)}{\cos(\theta_{esti})} \tag{5.30}$$

$$I_{noise\_y\_1} = \frac{\frac{2}{KN} \left(\sum^{N} \begin{pmatrix} \sin(w_e t) I_{noise\_a} + \sin(w_e t - 2\pi / K) I_{noise\_b} \\ .... + \sin(w_e t - 2\pi(K-1)/K) I_{noise\_n} \end{pmatrix} \right)}{\sin(\theta_{esti})} \tag{5.31}$$

In (5.30) and (5.31), the noise term shall be divided by the cosine or the sine term utilizing the estimated fault phase. If the noise average in the numerator is assumed to be almost zero and the phase estimation is exact, then the noise term is expected to be approximately zero. There appears to be a lower amplification of the noise than that

obtained with the method shown in (5.18) where the noise amplification is fixed. However, in a condition in which the phase estimation has errors, division by the sinusoidal estimation will result in a great amplification of a noise. This method, therefore, should be avoided when requiring fast detection under an extremely noisy condition. It is appropriate, though, for a high-performance diagnostic algorithm for the system with a continuous steady state condition. On the other hand, the scheme in section B has been known to show reliable detection even in a noisy system.

5.5 Theoretical performance limit of a detector

The Cramer-Rao lower bound (CRLB) is theoretically known as the maximum possible performance of a detector in a given condition measured with MSE [61]. Since the phase estimation in the ML method is crucial in fault diagnosis, theoretical maximum detection capability is derived to evaluate its detection performance.

Assuming that w_{fault} is known and I_{noise_a} is Gaussian noise with noise variance σ_a^2 and the ideal mean = 0, the following is obtained

$$I_{stator\_a}(n) = I_{fault\_a}\cos(w_{fault}n + \varphi_{fault\_a}) + I_{noise\_a} \tag{5.32}$$

Through the probability function and statistics theory [61], detection variance is obtained as follows

$$Var(\varphi_{fault\_a\_estimated}) \geq \frac{2\sigma_a^2}{NI_{fault\_a}^2} \tag{5.33}$$

In(5.33), the approximated CRLB is obtained.

Expanding the general multiphase system

$$Var(\varphi_{fault\_a\_estimated}) \geq \frac{2(\sigma_a^2 + \sigma_b^2 + ...\sigma_K^2)}{K^2 N I_{fault\_avg}^2} \tag{5.34}$$

where σ_b^2 is the noise variance in line b, and σ_K^2 is the noise variance in line K.

From (5.34), the CRLB of a multiphase system is obtained, which is the theoretical maximum performance that a fault detection algorithm can achieve. It has been verified that the maximum performance is dependent on the noise of each line and inversely dependent on the number of samples and fault amplitude which are also reasonably intuitive. It is also inferred that suppressing the noise in the detection can be done by considering more signal samples, which is determined by detection time or sampling rate.

5.6 Statistical threshold derivation

To perform a more complete diagnosis, the threshold design is required to make a decision for the detected fault signature. The derivation of a threshold is based on the method in [31][61] which is expanded to multiphase detection in this study.

The threshold is derived based on the following hypothesis:

$$H_0 : I_{stator\_a} = I_{noise\_a} \tag{5.35}$$

$$\begin{aligned} H_1 : I_{stator\_a} &= I_{fault} \cos(w_{fault} n + \varphi_{fault\_a}) \\ &\quad + I_{noise\_a} \quad with\ p(I_{noise\_a}) \sim N(0, \sigma_a^2) \end{aligned} \tag{5.36}$$

where H_0 is only noise hypothesis, H_1 is the hypothesis of fault signal with additive noise I_{noise_a}, and $N(0, \sigma_a^2)$ is the zero mean noise with variance σ_a^2.

For the sake of simplicity, The detailed derivation of the statistical threshold is not presented here. For the generalized multiphase threshold in a multiphase system, the statistical threshold is derived as follows:

$$Threshold = \sqrt{\frac{(\sigma_a^2 + \sigma_b^2 ..... + \sigma_K^2)}{K^2 N}} Q^{-1}(P_{FA\_ref}) \tag{5.37}$$

where Q is the Q function and PFA_ref.

It is shown that the threshold applied is dependent simply on the number of samples and noise estimation. These are independently determined or measured from the motor's operating point (i.e., fundamental stator current level, torque, rotor speed, control strategy). This is expected to simplify the fault decision-making process since various reference estimations of non-stationary motor conditions are not needed.

From (5.37), it is observed that the threshold is dependent on the summation of the noise variance in each line current. The noise of a motor current signal can be derived by assuming an all harmonics signal except for the noise which is as follows:

$$Var(\cdot) \approx \frac{\sigma_a^2 + \sigma_b^2 ..... + \sigma_K^2}{K^2 N} \tag{5.38}$$

$$-> \sigma_{avg}^2 \approx K^2 N Var(E_N) = K^2 N (E_N)^2 \tag{5.39}$$

where

$$E_N = \frac{1}{KN} \sum_{k=1}^{N} \left[I_{stator\_a}(t) + I_{stator\_b}(t) ... + I_{stator\_K}(t) \right]$$

$$\approx \frac{1}{KN} \sum_{l=1}^{N} \sum_{k=a}^{K} n_{l\_k} \tag{5.40}$$

In (5.39), it is shown that noise variance is obtained. The estimation consists of mainly summation operations which make possible decision-making adaptively in every instant needed by DSP.

5.7 Conclusion

The algorithms derived in this chapter are the extension of previous diagnostic techniques which can further be flexibly utilized for arbitrary phase motor diagnosis in industry.

CHAPTER VI

CONCLUSION AND FUTURE WORK

This chapter presents the summary of research work in earlier chapters, plus conclusions and suggestions for future potential work. Fault symptoms of an induction motor have been extensively researched based on machine design theory and control theory in the literature. Recently, advanced signal processing techniques have been applied to detect those fault conditions for industrial application but most of them have assumed almost ideal signal processing conditions without detailed analysis. In this dissertation, diagnostic strategies are analyzed which consider non-ideal industry conditions. Potential error compensation schemes are proposed which can be flexibly applied with low cost to industry.

6.1. Summary of research and conclusion

A complete diagnosis is presented that covers fault detection and decision-making in industry. Commonly, fault signature detection is performed by estimating fault characteristic frequency which is critically determined depending on motor shaft speed. Therefore, fault signature detections are inherently exposed to potential error in motor speed feedback information. The decision-making of detected fault signatures is also continuously interfered by instantaneous motor noises.

In Chapter I, the classification of induction motor faults, its symptoms and conventional detection methods are presented. The recent implementation challenge of

those diagnostic strategies on DSP systems is described assuming harsh industrial environments for which the research objective in this dissertation is directed.

Chapter II analyzes the performance of fault decision-making with a threshold under harsh industrial noise environments. The precise performance-oriented design strategy of a threshold is presented and its exact performance is analyzed for industrial application. It is clearly proved that the performance of the threshold is predictable, maintainable, and controllable independently from the surrounding environment.

Chapter III derives a fault signature tracking scheme that is robust to motor speed feedback errors. For efficient tracking purposes, it is shown that rotor fault can be assumed to occur within statistically limited regions from which assumption a low cost and high performance diagnostic scheme is effectively derived. It is shown that commonly exhaustive error tracking can be significantly simplified and implemented on a DSP used for motor control without violating CPU utilization.

The work in Chapter IV deals with the simultaneous implementation of detection and decision-making on a DSP system used for an AC motor drive. Precise experiment and simulation of those detections and decision-making steps are presented with a detailed theoretical analysis which is compared to an optimal diagnostic scheme.

Section V deals with generalized diagnostic detection and decision-making that can be flexibly extended to multiphase system applications. With increased industrial demand for multiphase motors with high power, high performance, and better reliability, a diagnostic scheme needs to be modified to be applicable to arbitrary phase systems. The

algorithms are derived based on previous signal processing schemes in the literature which are carefully and flexibly expanded to multiphase diagnostic systems.

In all sections, the derivations are done to make the algorithm operation independent from the non-ideal and harsh industrial environments and relevant system conditions.

In this dissertation, a signature-based MCSA diagnosis is studied in detail with emphasis on diagnostic signal processing reliability, flexible applicability and their low cost implementation. It is expected that the analysis in this dissertation can be further utilized toward creating powerful diagnostic tool for industrial application.

6.2. Future potential work

A. Stationary Fault Diagnosis

In this dissertation, the analyzed diagnostic schemes have primarily been studied under the stationary operation of a motor. Therefore, the steady state fault diagnosis assumes that the current signal is in a stationary condition.

Commonly, the steady state fault diagnosis has been developed assuming the open loop control of a motor in the literature. In a closed loop control system, the controller inherently tries to control the current signal variation resulting in an unreliable MCSA diagnosis. For example, the eccentricity signature amplitude varies depending on the motor controller bandwidth. Therefore, in closed loop control, the fault characteristic frequency-based diagnosis needs to take the controller operation into account. Some of the algorithms in the literature need to be verified if applied to closed-loop control systems.

B. Transient Fault Diagnosis

Transient fault diagnosis assumes that the motor current signal is in a non-stationary condition. In an adjustable speed drive (ASD) application, the mechanical speed of a motor and the current frequency presents time varying behavior. This makes the application of conventional diagnostic analysis techniques impossible.

The transient fault diagnosis is expected to follow the routine as shown in Fig. 5.1-1. Innovative research in the literature has primarily focused on the monitoring method with a new time-frequency analysis to improve the resolution even under transient conditions. Recently, a plethora of new time-frequency algorithms has been reported in many papers [13][29][57][58][59][60].

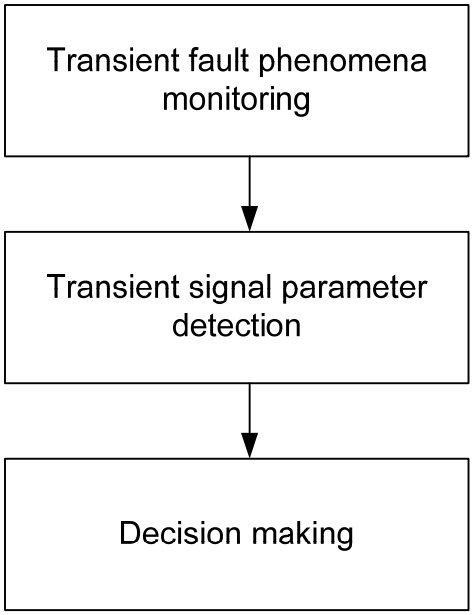

Fig. 5.1-1. Transient fault diagnosis.

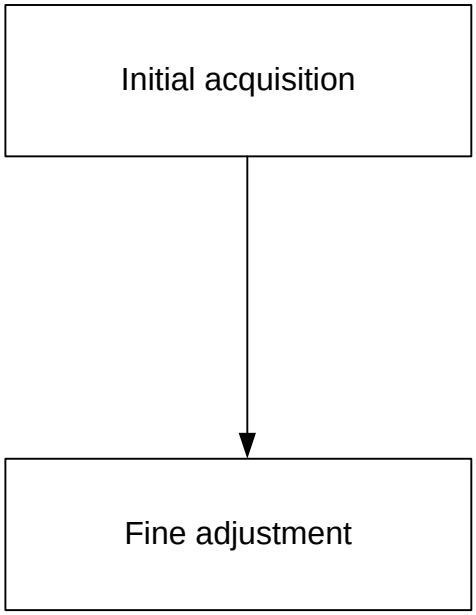

Fig. 5.1-2. Common signal detection.

Few papers are dealing with transient fault signal parameter detection (precise amplitude or energy etc.). Since the amount of signal distortion is dependent on the severity of a motor operating transition, the exact detection of parameters is a highly challenging issue which needs further study.

For decision-making, generally, the evaluation of statistically accumulated data is necessary. The amount of data in a time-frequency analysis approach is commonly too overwhelming to be processed by a low cost DSP system. Therefore, transient fault diagnosis may not be economical for a low cost application but applicable for a middle power or high power system.

Fig. 5.1-2 shows a common signal detection procedure applied to a commercialized communication system, especially in synchronization-signal detection. It consists of two stages of the initial acquisition and its fine adjustment. In the figure, the signal that is detected in initial acquisition is forwarded to fine adjustment through which the usage of the CPU is efficiently reduced. Recently, suggested time-frequency analysis methods reported in the literature are more suitable for fine adjustment applications. Direct application of time-frequency analysis without the initial acquisition will redundantly increase diagnostic complexity which is a subject to be further studied in future research.

C. New Fault Signature

In a conventional MCSA diagnosis, the fault condition of a motor has been popularly analyzed based on the abnormal harmonic modulation at characteristic fault frequency in a current spectrum. For simplicity, those signatures are defined as conventional fault signatures.

Fundamentally, since fault signatures are created by the effect of electromagnetic couplings between stator and rotor in a faulty motor, it is more appropriate that those fault signatures are defined at all frequency in a motor current spectrum not at just a conventional fault frequency. The new signatures that will be studied are defined as non-conventional fault signatures.

Utilizing both conventional and non-conventional signatures for the condition monitoring of a motor will lead to a more reliable diagnosis.

D. Robust Diagnosis under Unstable Power Electronics System

The diagnosis algorithm presented in this dissertation is focused on the reliability and robustness of diagnostic signal processing technique itself by assuming ideal operation of motor drive power electronics system. In industry, reliability and robustness issue of MCSA is also encountered under non-ideality of power electronics system operation such as source current distortion, unexpectedly injected harmonic signal from inverter, DC bus ripple in the rectifier, or any partial failure of the motor drive power electronics system. There is a need for further research effort to derive a reliable diagnosis technique under those non-ideal system environments.

REFERENCES

[1] S. Nandi, H.A. Toliyat, and X. Li, "Condition monitoring and fault diagnosis of electrical machines-a review," *IEEE Trans. on Energy Convers.,* vol. 20, issue. 4, pp. 719-729, Dec. 2005.

[2] A. Siddique, G.S. Yadava, and B. Singh, "A review of stator fault monitoring techn. -iques of induction motors," *IEEE Trans. on Energy Convers.*, vol. 20, issue 1, pp. 106– 114, Mar. 2005.

[3] M. El Hachemi Benbouzid, "A review of induction motors signature analysis as a medium for faults detection," *IEEE Trans. on Industrial Electronics*, vol. 47, issue 5, pp. 984 – 993, Oct. 2000.

[4] Y.E. Zhongming and W.U. Bin, "A review on induction motor online fault diag- -nosis," *IEEE Power Electronics and Motion Control Conference (IPEMC'00)* vol. 3, pp.1353-1358, Aug. 2000.

[5] S. Nandi, T. Ilamparithi, S.B. Lee, and D. Hyun, "Pole pair and rotor slot number independent frequency domain based detection of eccentricity faults in induction machines using a semi on-line technique," *IEEE International Symposium, Diagnostics for Electric Machines, Power Electronics and Drives* (*SDEMPED'09)*, pp. 1-7, Aug. 31 - Sept. 31, 2009.

[6] S. Nandi, M. Bharadwaj, and H. A. Toliyat, "Performance analysis of a three phase induction motor under mixed eccentricity condition," *IEEE Trans. on Energy Convers*., vol. 17, issue 4, pp. 392-399, Sep. 2002.

[7] H. Xianghui, T.G. Habetler, and R.G. Harley, "Detection of rotor eccentricity faults in a closed-loop drive-connected induction motor using an artificial neural network," *IEEE Trans. on Power Electron.*, vol. 22, issue 4, pp. 1552 - 1559, Jul. 2007.

[8] S. Nandi, M. Bharadwaj and H. A. Toliyat, "Performance analysis of a three-phase induction motor under mixed eccentricity condition," *IEEE Trans. on Energy Convers.*, vol. 17, issue. 3, pp. 392–399, Sep. 2002.

[9] B. Yazici and G..B. Kliman, "An adaptive statistical time-frequency method for detection of broken bars and bearing faults in motors using stator current," *IEEE Trans. on Ind. Appl.,* vol. 35, issue 2, pp. 442-452, Mar. 1999.

[10] G. Didier, E. Ternisien, O. Caspary, and H. Razik, "Fault detection of broken rotor bars in induction motor using a global fault index," *IEEE Trans. Ind.Appl.,* vol. 42, issue 1, pp. 79–88, Jan./Feb. 2006.

[11] G.Y. Sizov, A. Sayed-Ahmed, Y. Chia-Chou, and N.A.O. Demerdash, "Analysis and diagnostics of adjacent and nonadjacent broken-rotor-bar faults in squirrel-cage induction machines," *IEEE Trans. on Ind. Electron.*, vol. 56, issue 11, pp. 4627–44641, Nov. 2009.

[12] J. Milimonfared, H. M. Kelk, S. Nandi, A. D. Minassians, and H. A. Toliyat, "A novel approach for broken-rotor-bar detection in cage induction motors," *IEEE Trans. on Ind. Appl*., vol. 35, issue 5, pp. 1000-10006, Sept./Oct. 1999.

[13] B. Yazici and G. B. Kliman, "An adaptive statistical time–frequency method for detection of broken bars and bearing faults in motors using stator current," *IEEE*

Trans. Ind. Appl., vol. 35, issue. 2, pp. 442–452,Mar./Apr. 1999.

[14] W. Zhou, T.G. Habetler, and R.G. Harley, "Incipient bearing fault detection via motor stator current noise cancellation using Wiener filter," *IEEE Trans. on Ind. Appl.*, vol. 45, issue 4, pp. 1309 - 1317, Jul.-Aug. 2009.

[15] W. Zhou, T.G. Habetler, and R.G. Harley, "Bearing fault dete*ction* via stator current noise cancellation and statistical control," *IEEE Trans. on Ind. Electron.*, vol. 55, issue. 12, pp. 4260–4469, Dec. *2008.*

[16] J. Liu, W. Wang, F. Golnaraghi, "An extended wavelet spectrum for bearing fault diagnostics," *IEEE Trans. on Instrumentation and Measurement,* vol. 57, issue 12, pp. 2801-2812, Dec. 2008

[17] S.M.A. Cruz, H. A. Toliyat, and A.J.M. Cardoso, "DSP implementation of the multiple reference frames theory for the diagnosis of stator faults in a DTC induction motor drive," *IEEE Trans. on Energy Convers*, vol. 20, issue. 2, pp. 329–335, Jun. 2005

[18] D. Shah, S. Nandi, and P. Neti, "Stator inter-turn fault detection of doubly-fed induction generators using rotor current and search coil voltage signature analysis," *IEEE Trans. Ind. Appl.*, vol. 45, issue 5, pp. 1831-1842, Sept. 2009.

[19] A. Bellini, F. Filippetti, and C. Tassoni, G.A. Capolino, "Advances in diagnostic techniques for induction machines," *IEEE Trans. on Ind. Electron.*, vol. 55, issue 12, pp. 4109 – 4126, Dec. 2008

[20] A. Stefani, A. Bellini, and F. Filippetti, "Diagnosis of induction machines' rotor faults in time-varying conditions," *IEEE Trans. on Ind. Electron.,* vol. 56, issue

11, pp. 4548 – 4556, Nov., 2009.

[21] A. Bellini, A. Yazidi, F. Filippetti, C. Rossi, and G.A. Capolino, ”High frequency resolution techniques for rotor fault detection of induction machines,” *IEEE Trans. on Ind. Electron.*, vol.55, issue 12, pp. 4200 – 4209, Dec. 2008

[22] A. Khezzar, M.E. Oumaamar, M. Hadjami, M. Boucherma, and H. Razik, ”Induction motor diagnosis using line neutral voltage signatures,” *IEEE Trans. on Ind. Electron.*, vol. 56, issue 11, pp. 4581–4591, Nov. 2009.

[23] O. Poncelas, J.A. Rosero, J. Cusido, J.A. Ortega, and L. Romeral, “Motor fault detection using a Rogowski sensor without an integrator,” *IEEE Trans. on Ind. Electron.*, vol. 56, issue 10, pp. 4062–4070, Oct. 2009.

[24] T.M. Wolbank, P. Nussbaumer, C. Hao, and P.E. Macheiner, “Non-invasive detection of rotor cage faults in inverter fed induction machines at no load and low speed,” *IEEE International Symposium, Diagnostics for Electric Machines, Power Electronics and Drives (SDEMPED’09)*, pp. 1-7, Aug. 31 to Sept. 3, 2009.

[25] M. Benbouzid, M. Vieira, and C. Theys, “Induction motors' faults detection and localization using stator current advanced signal processing techniques,” *IEEE Trans. on Power Electron,* vol. 14, issue 1, pp. 14-22, Jan. 1999.

[26] B. Akin, H. Toliyat, U. Orguner, and M. Rayner, “Phase sensitive detection of motor fault signatures in the presence of noise,” *IEEE Trans. on Ind. Electron.*, vol. 55, issue 6, pp. 2539-2550, June, 2008.

[27] S.H. Kia, H. Henao, and G. Capolino, "A high-resolution frequency estimation method for three-phase induction machine fault detection," *IEEE Trans. on Ind.*

Electron.., vol.54, issue. 4, Aug. 2007.

[28] A. Bellini, G. Franceschini, and C. Tassoni, "Monitoring of induction machines by maximum covariance method for frequency tracking," *IEEE Trans. on Ind. Appl.*, vol. 42, issue. 1, pp. 69-78, Jan./Feb. 2006.

[29] S. Rajagopalan, T.G. Habetler, R.G. Harley, J.A. Restrepo, and J.M. Aller, "Non-stationary motor fault detection using recent quadratic time-frequency represent--tations," *Ind. Appl. conference,* vol. 5, pp. 2333-2339, Oct. 2006.

[30] M. Blodt, D. Bonacci, J. Regnier, M. Chabert, and J. Faucher, "On-line monitoring of mechanical faults in variable-speed induction motor drives using the Wigner distribution," *IEEE Trans. on Ind. Electron.*, vol. 55, issue. 2, pp. 522–533, Feb. 2008.

[31] S.D. Choi, B. Akin, M.M. Rahimian, and H.A. Toliyat, "Fault diagnosis implementation of induction machine based on advanced digital signal processing techniques," *Proceedings of Applied Power Electronics Conference and Exposition (APEC'09)*, pp. 957-963, Feb. 2009.

[32] S.D. Choi, B. Akin, M. Rahimian, H. A. Toliyat, and M. Rayner, "Fault monitoring technique of a induction machine with ordered harmonic and noise cancelation," *Electrical Machine and Drive (IEMDC'09)*, pp. 1333-1339, May 2009.

[33] S.D. Choi, B. Akin, M. Rahimian, H. A. Toliyat, and M. Azadpour, "A generalized condition monitoring method for multi-phase induction motors," *Electrical Machine and Drive (IEMDC'09)*, pp. 556-562, May, 2009.

[34] B. Akin, S.D. Choi, M. Rahimian, and H.A. Toliyat, "DSP based continuous multi-fault signature monitoring implementation," *Applied Power Electronics Conference and Exposition (APEC'09)*, pp. 938-944, Feb. 2009.

[35] W. T. Thomson and M. Fenger, "Current signature analysis to detect induction motor faults," *IEEE Ind. Appl.. Mag.*, vol. 7, issue. 4, pp. 26–34, Jul./Aug. 2001.

[36] M. E. H. Benbouzid, M. Vieira, and C. Theys, "Induction motors' faults detection and localization using stator current advanced signal processing techniques," *IEEE Trans. Power Electron.*, vol. 14, issue. 1, pp. 14–22, Jan. 1999.

[37] J. Jung, J. Lee, and B. Kwon, "Online diagnosis of induction motors using MCSA," *IEEE Trans. on Ind. Appl.*, vol. 53, issue 6, pp. 1842-1852, Dec. 2006.

[38] B. Akin, U. Orguner, H.A. Toliyat, and M. Rayner, "Low order PWM inverter harmonics contributions to the inverter-fed induction machine fault diagnosis," *IEEE Trans. on Ind. Electron.,* vol 55, issue. 2, Feb. 2008.

[39] S.D. Choi, B. Akin, M.M. Rahimian, and H.A. Toliyat, "Fault diagnosis technique of induction machines with ordered harmonic and noise cancellation," *Proceedings of Electrical Machine and Drive (IEMDC'09)*, pp. 1333-1339, Feb. 2009.

[40] M. Puche-Panadero, M. Riera-Guasp, J. Roger-Folch, E. Hurtado-Perez, and J. Perez-Cruz, "Improved resolution of the MCSA method via Hilbert Transform, enabling the diagnosis of rotor asymmetries at very low slip," *IEEE Trans. on Energy Conver.*, vol. 24, issue 1, pp. 52-59, Mar. 2009.

[41] M. Heideman, D. Johnson, and C. Burrus, "Gauss and the history of the fast

Fourier transform," *IEEE ASSP Magazine*, vol. 1, issue 4, pp. 14-21, Oct. 1984.

[42] S.D. Choi, B. Akin, M.M. Rahimian, and H.A. Toliyat, "Implementation of a fault diagnosis algorithm for induction machines based on advanced digital signal processing techniques," *IEEE Trans. on Ind. Appl.*, 2010.

[43] G.B. Kliman, W.J. Premerlani, B. Yazici, R.A. Koegl, and J. Mazereeuw, "Sensorless online motor diagnostics," *IEEE Computer Applications in Power*, vol. 10, Issue 2, pp. 39 – 43, Apr. 1997.

[44] J. Guzinski, H. Abu-Rub, and H.A. Toliyat, "An advanced low-cost sensorless induction motor drive," *IEEE Trans. Ind. Appl.*, vol. 39, issue 6, pp. 1757–1764, Nov.-Dec. 2003.

[45] M.S. Zaky, M.M. Khater, S.S. Shokralla, and H.A. Yasin, " Wide-speed-range estimation with online parameter identification schemes of sensorless induction motor drives," *IEEE Trans. on Ind. Electron.*, vol. 56, issue 5, pp. 1699 – 1707, May 2009.

[46] D.G. Forchetti, G.O. GarcIa, and M.I. Valla, "Adaptive observer for sensorless control of stand-alone doubly fed induction generator," *IEEE Trans. on Ind. Electron.*, vol. 56, issue 10, pp. 4174 – 4180, Oct. 2009.

[47] S.M. Gadoue, D. Giaouris, and J.W. Finch, "Sensorless control of induction motor drives at very low and zero speeds using neural network flux observers," *IEEE Trans. on Ind. Electron.*, vol. 56, issue 8, pp. 3029 – 3039, Aug. 2009.

[48] K. Kim, A.G. Parlos, and B.R. Mohan, "Sensorless fault diagnosis of induction motors," *IEEE Trans. Ind. Appl.*, vol. 50, issue 5, pp. 1038 – 1051, Oct. 2003.

[49] A. Yazidi, H. Henao, G.A. Capolino, M. Artioli, and F. Filippetti, “Improvement of frequency resolution for three-phase induction machine fault diagnosis,” In *Proc. 40th IAS Annual Meeting*, vol. 1, pp. 20–25. 2005

[50] B. Akin, S.B. Ozturk, H.A. Toliyat, and M. Rayner, ”DSP-based sensorless electric motor fault diagnosis tools for electric and hybrid electric vehicle power train applications,” *IEEE Trans. Vehicular Technology,* vol. 58, pp. 2150 – 2159, Jun. 2009.

[51] B. Ayhan, H.J. Trussell, M. Chow, and M. Song, “On the use of a lower sampling rate for broken rotor bar detection with DTFT and AR-based spectrum methods,” *IEEE Trans. on Ind. Electron.*, vol. 55, issue 3, pp. 1421-1434, Mar. 2008.

[52] C. Kral, F. Pirker, and G. Pascoli, “Model-based detection of rotor faults without rotor position sensor-the sensorless Vienna monitoring method,” *IEEE Trans. on Ind. Appl.*, vol. 41, issue 3, pp. 784-789, May/Jun. 2005.

[53] S. Choi, B. Akin, M.M. Rahimian, and H.A. Toliyat, “A robust sensorless fault diagnosis algorithm for low cost motor drives,” *Proceedings of Applied Power Electronics Conference and Exposition (APEC’10)*, pp. 1990-1994, Feb. 2010.

[54] Gerada, C., Bradley, K.J., Sumner, M., Wheeler, P., Pickering, S., Clare, J. Whitley, C., and Towers, G., “The results do mesh,” *IEEE Ind. Appl. Mag.*, vol 13, issue 2, pp. 62-72, Mar.-Apr. 2007.

[55] B. Akin, S.B. Ozturk, H. Toliyat, and M. Rayner, “On–board fault diagnosis of HEV induction motor drive at start-up and during idle-mode,” *IEEE Trans. Vehicular Technology*, vol. 58, issue 5, pp. 2150-2159, June 2009.

[56] E. Levi, R. Bojoi, F. Profumo, H. A. Toliyat, and S. Williamson, "Multiphase induction motor drives – A technology status review," *IET – Electric Power Appl.*, vol. 1, issue. 4, pp. 489-516, July 2007

[57] S. Rajagopalan, J. M. Aller, J. A. Restrepo, T. G. Habetler, andR. G. Harley, "Diagnosis of rotor faults in brushless DC (BLDC) motors operating under non-stationary conditions using windowed Fourier ridges," *40th IEEE IAS Annu. Meeting*, vol. 1, pp. 26–33, 2005.

[58] S. Rajagopalan, J. A. Restrepo, J. M. Aller, T. G. Habetler, and R. G. Harley, "Wigner–Ville distributions for detection of rotor faults inbrushless DC (BLDC) motors operating under non-stationary conditions," in Proc. *Diagnostics for Electric Machines, Power Electronics and Drives, (SDEMPED'05)*, vol. 1, pp. 26-33, Oct., 2005.

[59] M. Blodt, M. Chabert, J. Regnier, and J. Faucher, "Mechanical load fault detection in induction motors by stator current time–frequency analysis," *IEEE Trans. Ind. Appl.*, vol. 42, issue 6, pp. 1454 1463, Nov./Dec. 2006.

[60] F. Auger, P. Flandrin, P. Goncalvès, O. Lemoine, Time–Frequency Toolboxfor use with MATLAB reference guide. CNRS France/Rice University,1996. [Online].Available: http://tftb.nongnu.org/refguide.pdf

[61] S.M. Kay, *Fundamentals of Statistical Signal Processing: Estimation and Detection Theory,* Englewood Cliffs, NJ. Prentice-Hall, 1993.

[62] A.J. Viterbi, *Principles of Coherent Communication,* McGraw-Hill, New York, 1966.

[63] A.V. Oppenheim and R.W. Schafer, *Discrete-time Signal Processing*, Prentice-Hall, 1989.

[64] S.M. Kay, *Modern Spectral Estimation*, Englewood Cliffs, NJ:Prentice-Hall, 1988.

[65] D.W. Noyotny and T.A. Lipo, *Vector Control and Dynamics of AC Drives*: Oxford University Press, New York, 1996.

[66] P. Vas, *Parameter Estimation, Condition Monitoring, and Diagnosis of Electrical Machines*, Oxford University Press, New York, 1993.

VITA

Seungdeog Choi received his B.S. degree from Chung-Ang University, South Korea in 2004, and his M.S. degree from Seoul National University, South Korea in 2006. Both degrees are in electrical engineering. He joined the doctoral program of the Department of Electrical Engineering at Texas A&M University and received his Ph.D. in Dec. 2010.

He was an R&D engineer with LG Electronics, South Korea, from 2006 to 2007, and worked with Toshiba International Cooperation, Houston, TX from 2008. He can be reached through Dr. Hamid A. Toliyat, Department of Electrical and Computer Engineering, Texas A&M University, College Station, Texas 77843-3128.